QUAGGA MUSSEL INDUCED PHOSPHORUS CYCLING CHANGES IN LAKE MICHIGAN

by

Rae-Ann MacLellan-Hurd

A Thesis Submitted in
Partial Fulfillment of the
Requirements for the Degree of

Master of Science
in Freshwater Sciences and Technology

at
The University of Wisconsin-Milwaukee
August 2020

ABSTRACT

QUAGGA MUSSEL INDUCED PHOSPHORUS CYCLING CHANGES IN LAKE MICHIGAN

by

Rae-Ann MacLellan-Hurd

The University of Wisconsin-Milwaukee, 2020
Under the Supervision of Professor Harvey Bootsma

Quagga mussels (*Dreissena rostriformis bugensis*) are an invasive ecosystem engineer that have successfully colonized both profundal and nearshore regions in Southern Lake Michigan. Quagga mussels directly altered the flow of nutrients by filtering particles, excretion of soluble forms of nutrients in the benthos, and through the production of biodeposits. Mussel excretion, egestion, and capture rates of P were compared between a 25 meter and a 55 meter deep site near Milwaukee Harbor to determine the retention of nutrients in these regions. The capture rate of particulate phosphorus at the 25m site (278 ± 388 μmol m^{-2}) was similar to that at the 55m site (324 ± 245 μmol m^{-2}). When these values are compared with estimates for 10m depth nearshore Milwaukee (Bootsma et al. 2012), the highest capture rates occur nearshore but remain relatively high through mid-depth regions compared to phytoplankton growth meaning the benthos in this region has a high capacity to retain nutrients. However, a large portion of captured phosphorus is recycled in the dissolved form and in the form of biodeposits.

Approximately 40-50% of recycled phosphorus was in the form of biodeposits. However, there is limited understanding if biodeposits represent a sink or source of nutrients. A series of incubations were conducted to determine the fate of biodeposits and their effect on dissolved nutrients over time scales of 2-3 weeks. Biodeposits promoted bacteria growth, which in turn led to an uptake of dissolved forms of C, N, and P. The bacteria depleted dissolved phosphorus

concentration to below detection limit, 0.016 μmol/L, within ten days of incubation. After 12-15 days, dissolved P concentration increased to levels higher than the starting conditions, indicating that biodeposits were a net source of dissolve P over longer time scales.

Mussels may further alter phosphorus cycles through indirect processes such as interfering with apatite dissolution, the promotion of bacterial growth, and increasing the effective settling rate of phosphorus by filtering small particles. The passive settling rates of phosphorus was determined at the 55 meter site using sediment traps. Sediment cores were also taken from the 55 meter site as well as a 100 meter site offshore of Muskegon, MI to determine the phosphorus burial rate. By comparing sedimentation and sediment burial rates, approximately 60% of recently deposited phosphorus at the sediment-water interface is recycled back into the water column. Measurements of sediment fluxes, including sedimentation, accumulation, and permanent burial rate, were combined with mussel fluxes to create a new conceptual model of internal P cycling in Lake Michigan. Before the mussel invasion, zooplankton within the water column were responsible for the bulk of phosphorus recycling. In the new model, the majority of phosphorus cycling occurs in the benthos with heterotrophic bacteria playing a larger role.

TABLE OF CONTENTS

LIST OF FIGURES

LIST OF TABLES

ACKNOWLEDGMENTS

I am very grateful for my advisor, Dr. Harvey Bootsma, who provided me with this research opportunity. He was a wonderful mentor who was always willing to help in whatever way possible, including spending many days trying to fix a liquid waveguide. I would also like to recognize my committee member Dr. Qian Liao and Dr. Laodong Guo, as well as my CIGLR advisor Dr. Hank Vanderploeg, for their advice and expertise. I also need to thank Will Stacey and Jeff Houghton for their many hours of help in the field. I would like to extend a thank you to all of the Bootsma lab members as well as the *R/V Neeskay* crew. I am also grateful for Pat Anderson and Randy Metzger's time. Pat was patient with all of the inevitable "hiccups" that occur when using the IRMS. Randy was always willing to help me design and build new contraptions. I also need to thank Dr. Ryan Newton and Lou Lamartina for their work on the bacterial count data and their knowledge of microbial processes. I also would like to thank Dr. Val Klump and Jessica Grow for their help with the ^{210}Pb dating. This work was funded by the National Science Foundation and Cooperative Institute for Great Lakes Research, and I am incredibly grateful for the conferences and research I was able to participate in thanks to these organizations.

Chapter 1: Introduction

Dreissena polymorpha (zebra mussels) and *Dreissena rostriformis bugensis* (quagga mussels) entered the Great Lakes in the late 1980s through ballast water. Zebra mussels rapidly colonized the littoral zones in Lake Michigan but were soon displaced by quagga mussels in southern Lake Michigan due to quagga mussels' ability to colonize soft substrates and live in cold temperatures (Dermott & Munawar 1993). In some areas, densities of quagga mussels reached over 10,000 mussels per square meter (Nalepa et al. 2010). The expansion of quagga mussels is considered one of the primary causes of the loss of the spring phytoplankton bloom due to their high grazing rates of phytoplankton during the isothermal period (Vanderploeg et al. 2010; Fahnenstiel et al. 2010). During the summer months, grazing is limited by stratification, which is why there is not a similar decrease in the surface mixed layer of chlorophyll *a* compared to the isothermal period (Fahnenstiel et al. 2010; Pothoven & Fahnenstiel 2013). Along with direct grazing effects, quagga mussels have altered the benthic environment in the Great Lakes through increasing light penetration and nutrient recycling. Increased light penetration and recycling of phosphorous by quagga mussels have led to the resurgence of nuisance benthic algal growth nearshore in Lake Michigan (Auer et al. 2010; Bootsma et al. 2004; Bootsma et al. 2015).

Quagga mussels also affect primary production and food web interactions by altering the flow of nutrients. Dreissenids are effective recyclers of nutrients because the majority of ingested materials are used for metabolic functions (Stoeckmann & Garton 1997). High capture rates of particulate phosphorus and high recycling in the form of dissolved phosphorus by dreissenid mussels had led to a decrease in particulate P to total phosphorus ratio in Lake Michigan (Pothoven & Fahnenstiel 2013; Mosley & Bootsma 2015). Nearshore (0-10m) by Milwaukee Harbor, mussels are able to excrete an amount of phosphorus that is equal loading by the

Milwaukee River, which helps support the growth of the nuisance benthic *Cladophora* (Bootsma et al. 2012; Bootsma & Liao 2014). In profundal regions, mussels still excrete relatively large amounts of phosphorus compared to the required portion for primary production. Using the mean summer area production rate of 473 mg C m^{-2} day^{-1} and a C:P ratio of phytoplankton of 2001:1 (Bockwoldt 2018), the required phosphorus for primary production in the summer is approximately 200 μmol P m^{-2} day^{-1}. Mosley and Bootsma (2015) estimated that mussel excretes approximately 129 μmol P m^{-2} day^{-1} at a 55 meter site offshore of Milwaukee in the summer, which is a 65% of the required phosphorus for phytoplankton growth. However, the excreted phosphorus remains in the hypolimnion during stratification, where light limitation reduces the ability for phytoplankton to utilize the nutrients. During the isothermal period, mussels grazing exceeds the phytoplankton growth rate, greatly reducing phytoplankton abundance (Vanderploeg et al. 2010). While primary producers may not be able to utilize the excreted phosphorus offshore, heterotopic bacteria may utilize mussel recycled products, increasing the importance of the microbial food web for energy transfer (Heath et al. 2003).

Mussels recycle a large portion of the phosphorus they capture in the form of biodeposits (Mosley & Bootsma 2015). There is a lot of uncertainty about the fate and environmental effects of the production of freshwater bivalve biodeposits (Strayer 2014). In marine environments, biodeposits increase the release of nutrients, bacteria growth, and alter surrounding invertebrate communities (Genz et al. 1990; Jansen et al. 2012; van Broekhoven et al. 2015; Giles and Pildith 2004, 2006; Hartstein & Rowden 2004). Models that look at the effect mussels have on phytoplankton growth either consider biodeposits a sink of phosphorus (Zhange et al. 2011) lump them together with other particulates (Rowe et al. 2017; Shen et al. 2018). The fate of this P has important implications for water column P concentrations. If this P is rapidly recycled, then as mussel populations stabilize, the supply of dissolved P to the water column may increase to levels similar to those before the establishment of dreissenids assuming shell and biomass P is also readily recycled. But if this P is refractory, then mussel grazing and biodeposit production will represent a net loss of P from the water column, with reduced availability to phytoplankton (Bootsma & Liao 2014).

Lake Michigan is currently meeting the target total phosphorus loading of 5600 MTA set by the Great Lake Water Quality Agreement. Still, mussel phosphorus recycling supports nuisance algal growth nearshore, while mussel grazing, along with reduced phosphorus loading, has depleted phosphorus and plankton offshore (Bootsma et al. 2012; Mida et al. 2010; Rowe et al. 2017; Shen et al. 2018). The total phosphorus concentrations during the spring have also declined due in part to decreases in phosphorus loading and mussel filtering of particulates from the water column (Mida et al. 2010). There is also a general trend of decreasing phosphorus concentrations in the summer; however, it is difficult to determine the relative importance of mussel mediated effects vs. reductions in nutrient loading (Mida et al. 2010; Pothoven & Fahnenstiel 2013; Rowe et al. 2017). The movement of nutrients nearshore to offshore represents another management challenge. Mussels may reduce offshore summer phosphorus concentrations through increased retention in the nearshore and mid-depth benthos (Hecky et al. 2004; Vanderploeg et al. 2010; Pothoven & Fahnenstiel 2013). This may be achieved in part through a reduction in sediment resuspension through the production of biodeposits which aggregate smaller particles (Hecky et al. 2004). Quagga mussels may also increase the effective settling rate of phosphorus by capturing light particles that would have remained suspended in the water column by mixing forces without mussels (Shen et al. 2018). This theory is supported by field observation by Mosley and Bootsma (2015) that mussels were capturing phosphorus at a rate that was 11 times greater than passive settling. Currently, the models used to set the targets for phosphorus loads in Lake Michigan did not take into account dreissenid mussels (Bootsma et al. 2012). Wise management decisions need to be supported by predictive models, and these models need to be guided by an understanding of how dreissenids have altered internal P dynamics.

The importance of mussel ecosystem effects is underscored by the adverse consequences for an economically important fishery. The expansion of dreissenid mussels has led pelagic fish to rely upon nearshore carbon sources (Turschak et al. 2014) and the overall biomass of fish to decrease in Lake Michigan (Bunnel et al. 2009). These changes have important economic effects because the Great Lakes sport fishery has an economic value between 4 and 7 billion US dollars (Breffle et al. 2013). There has not been a comprehensive study on the economic impact of invasive mussels on the economic value of the Great Lakes Fishery (Strayer 2009). However, a study of ship transported invasive species into the Great Lakes found that this group of invaders could account for a large reduction in economic and ecosystem service values for the Great Lakes fishery with an estimate of 138 to 800 million dollars in economic loss caused by invasive species (Rothlisberger et al. 2012).

The research presented in this thesis explores quagga mussel alterations to the phosphorus cycling in Lake Michigan. The focus of the chapters are quantifying mussel area capture rates of carbon, phosphorus, and nitrogen nearshore and in profundal regions (2), determining the fate of biodeposit (3), and developing a new conceptual framework phosphorus internal cycling in Lake Michigan (4). Each chapter is self-contained and includes relevant motivation, methods, and discussion for each topic. The overall summary is provided in chapter 5.

Chapter 2: Near to Offshore Capture rates of Nutrients by Quagga Mussels (Dreissena rotiformis bugensis) in Lake Michigan

Abstract

The effects of dreissenid mussels on nutrient cycling have been well documented in the littoral zone of some Great Lakes. However, mussel mediated effects moving near to offshore may be heterogeneous across Lake Michigan and requires more investigation. In this study, quagga mussel feeding and nutrient recycling rates at a 25 meter deep site (nearshore) and 55 meter deep site (mid-depth) near Milwaukee are compared. The capture rate of particulate phosphorus at the nearshore site (278 ± 388 μmol m^{-2}) was similar to that at the offshore site (324 ± 245 μmol m^{-2}). Based on carbon capture, the nearshore mussels would consume 34 ± 47%, and offshore would consume 72 ± 35% of phytoplankton production per day in the corresponding depth regions. Mussel also excreted a large portion of SRP at both sites, and excretion rates were similar to phosphorus cycling rates of Zooplankton. Combining the estimates of mussel excretion rates with past estimates <10m near Milwaukee harbor, mussels along 8 km of shoreline extending 8.25 km offshore excrete more phosphorus per day than is loaded into Lake Michigan via the Milwaukee River. Unlike the eastern side of Southern Lake Michigan, nearshore regions near Milwaukee contain a high amount of hard substrate that mussels are able to colonize. Due to the higher colonization of mussels nearshore, the highest capture rates by mussels occur in the 0-15 m depth range, but capture rates of nutrients remained high when moving into mid-depth regions. These results demonstrate that near Milwaukee Harbor, both the nearshore and mid-depth regions act as sinks for nutrients limiting the transfer offshore.

Introduction

In the late 1980s, the zebra (*Dreissena ploymorpha*) and quagga (*Dreissena rotiformis bugensis*) mussel entered the Great Lakes. Quagga mussel low metabolic rate (Stoeckmann 2003; Baldwin et al. 2002; Tyner et al. 2015), ability to colonize softer substrate (Dermott & Munawar 1993), and ability to reproduce in colder darker regions in Lake Michigan (Roe & MacIsaac 1997; Glyshaw et al. 2015) led to the expansion of quagga mussels and displacement of zebra mussels in southern Lake Michigan. Quagga mussels are effective filter feeders significantly reduce phytoplankton abundance during the isothermal period when they have access to the entire water column (Vanderploeg et al. 2010; Fahnenstiel et al. 2010). Along with reduced phytoplankton abundance, decreases in total phosphorus concentration offshore coincided with the expansion of quagga mussel into deeper regions of Lake Michigan. Although some of the decreases in spring phosphorus can be attributed to mussel grazing (Mida et al. 2010), it is difficult to determine the relative effects of mussel grazing vs. reduced external P loads (Rowe et al. 2017).

Phosphorus concentrations are directly affected by quagga mussels through the filtering of particulate phosphorus, excretion of dissolved inorganic and organic P, and egestion of biodeposits. In oligotrophic Lake Michigan, nearshore dreissenid excretion of SRP and increased water clarity have led to the resurgence of nuisance *Cladophora* (Auer et al. 2010; Bootsma et al. 2004; Bootsma et al. 2015). Nearshore mussels have access to the entire water column throughout the year (Rowe et al. 2017) and live in warmer more productive areas allowing them to have higher metabolic rates than those offshore (Tyner et al. 2015). However, a recent study on the eastern shore of Southern Lake Michigan found that mussel filtering had a limited impact on chlorophyll *a* and total phosphorus compared to tributary loading nearshore due in part to patchier mussel density (Pothoven & Vanderploeg 2020). On the eastern side of Southern Lake Michigan, the nearshore substrate is sandy and unstable under wave conditions leading to lower densities of dreissenid mussels (Nalepa et al. 2010). However, on the western side of southern Lake Michigan, the nearshore zone is characterized by hard substrate (Waples et al. 2005; Creque et al. 2010), allowing mussels to cover nearly 80% of the bottom in waters shallower than 10 meters (Bootsma & Liao 2014). The difference in the nearshore substrate between the western side and eastern side of Southern Lake Michigan may cause differences in mussel mediated effect on nearshore conditions, including the interception of nutrients as proposed in the nearshore shunt theory (Hecky et al. 2004). The nearshore shunt theory postulates that mussel nearshore reduces nearshore and offshore transfer of nutrients through nearshore mussels filtering nonpoint source phosphorus, typically in the form of smaller phosphorus bound particles, and packaging that material in larger aggregates through the production of biodeposits (Hecky et al. 2004).

Dreissenids’ access to particles is determined to a large degree by hydrodynamic processes (Zhang et al. 2011; Rowe et al. 2015; Rowe et al. 2017; Shen et al. 2018). Quagga mussel grazing reduces phytoplankton abundance during the isothermal period because the high rates of mixing allow mussels to access the entire water column (Rowe et al. 2017; Shen et al. 2018). Mussels’ ability to graze in the summer months is limited by stratification. Despite the limited availability of phytoplankton, Mosley and Bootsma (2015) did not observe any seasonal difference in particulate P capture rates between spring and fall in a 55 meter site offshore of Milwaukee. The lack of seasonal difference may be due to the relatively little change in the temperature of the benthos at this depth, but it is still unexpected considering that food supply to mussels is likely to be reduced during stratification relative to the isothermal period (Fahnenstiel et al. 2010). By contrast, temperature fluctuations in the nearshore zone appear to have a strong regulating effect on dreissenid metabolism (Tyner et al. 2015).

Egestion and excretion rates of mussels vary with seston stoichiometry (Bootsma & Liao 2014; Vanderploeg et al. 2017), hydrologic conditions (Rowe et al. 2015; Shen et al. 2018; Shen et al. 2020), food quality (Johengen et al. 2013; Bootsma & Liao 2014; Vanderploeg et al. 2017), and temperature (Johengen et al. 2013; Bootsma & Liao 2014). These factors make measuring rates of egestion and excretion in situ under a variety of conditions, including depth and season, important for understanding how mussels affect nutrient dynamics of large lake systems. There have been many studies examining the in situ effects of mussels in the littoral zone (Nalepa et al. 1991; Conroy et al. 2005; Turner 2010; Bootsma et al. 2012; Johengen et al. 2013). However, nutrient cycling by mussels in deeper regions of Lake Michigan have received less attention (Mosley & Bootsma 2015). In this study, respiration rates and phosphorus recycling rates were determined along with the capture of carbon, nitrogen, and phosphorus at an offshore (55m) and nearshore (25m) site under different hydrologic conditions. The results will better inform mussel mediated effects near and offshore during isothermal and mid-stratification periods.

Methods

Site Descriptions

Sampling was conducted at two different sites in Lake Michigan along a transect extending from Atwater Beach in Milwaukee, WI during the 2018-2019 field. The sites are AW25 and AW55 with depths of 25 and 55 meters respectively. The AW25 site was located approximately 2.75 km offshore (43° 5'41.88"N 87°50'19.80"W), and the AW55 site was located approximately 8.25 km offshore of Atwater Beach (43° 5'42.06"N 87°46'16.85"W). The substrate conditions at AW25 were heterogeneous with areas of dense clay, sandy substrate, and underwater mounds. The conditions at the AW55 site were more uniform, characterized by silty substrate.

Mussel Collection

Mussels from the AW25 and AW55 sites were collected using a Ponar grab sampler (22.5 x 22.5 cm sampling area). Multiple grabs were taken to determine length frequency, areal biomass of quagga mussels, and to collect mussels for use in incubations. Samples were taken in triplicate for length frequency and biomass analysis. Densities determined by the Ponar grab sampling were compared to densities determined using an underwater camera to ensure accurate density counts. The underwater camper was mounted to a 50 cm tall frame, and in the focal point of the camera was a grid used to measure the area. Image J image processing software was used to count mussels (Schneider et al. 2012). The areal counts of mussels with the Ponar were compared to the camera densities for each site using a simple t-test. The camera densities were not significantly different from the density determined using the Ponar, so only the Ponar densities are presented.

The mussels used for incubation experiments were immediately placed in a bucket filled with unfiltered lake water collected from below the thermocline. Temperature was maintained, and light exposure was limited by placing the buckets in coolers with ice. The mussels remained in buckets for less than an hour during transport to the lab. On some sampling days, incubation procedures began immediately after collection in the wet lab on the research vessel, *R/V Neeksay*. After transport, mussels were separated into bins containing unfiltered cool lake water. Only mussels that did not have visible shell damage were used in the incubations. The mussels were gently cleaned by placing them on mesh and allowing unfiltered water to slowly flow over them until no particulates were observed in the water. Two different mesh sizes, 0.4 cm and 0.75

cm, were used. Two mussel size classes were used for experiments: 5-14mm (small) and 15-25 mm (large). Each size class was run in triplicate. The number of mussels used in each chamber range from 25- 50 depending on how many mussels were available. Mussels used in the respiration/excretion incubations were gently scrubbed with a clean sponge in unfiltered lake water. These mussels were separated into three size classes 5-12mm (small), 12-19mm (medium), and 20-27 mm (large). The number of mussels used for each size class was 10, 4-5, and 4-5 for the small, medium, and large size classes respectively. All mussels were kept at near in situ temperature, cleaned, and placed in incubation chambers within two hours of collection, for the measured rates of excretion, respiration, and egestion to be as similar as possible to in situ rates.

Mussel Respiration and Excretion Rates

Temperatures for the AW55 experiments ranged from 3-6˚C, and temperatures for the AW25 experiments ranged from 3.5-8˚C depending on the temperature of near bottom water at the time of mussel collection. Respiration and phosphorus excretion rates were measured in acid-cleaned 250 ml syringes. After the mussels were cleaned, they were placed in a 250 ml syringe filled with filtered lake water collected within 5 meters of the bottom. The syringes had a valve attachment to ensure the water used in the incubation was closed off from the air. Mussels were left to stabilize for 15 minutes prior to making the initial measurements. After the stabilization period, 30 ml of water was withdrawn from the incubation syringe, filtered through a syringe filter (GF/F 0.7µm), and stored in a cooler for SRP and TDP analysis. SRP and TDP analyses were conducted within 24 hours according to the molybdate-antimony method, with TDP samples first being digested by the addition of H_2SO_4 and H_2O_2 followed by 2 hours of photo-oxidation (Stainton et al. 1974).

For a subset of experiments, a NeoFox sport micro-optical dissolved oxygen probe (Ocean Optics) was used to measure dissolved oxygen (DO) after SRP / TDP subsamples were removed from syringes. The probe was small enough to insert directly into the incubation syringe through the syringe valve. Following initial sampling, syringes were left in coolers for two hours. The two-hour incubation time was chosen so that changes in DO and phosphorus would be measurable while the decrease in DO concentration was small enough to avoid affecting mussel metabolism (Tyner et al. 2015). After the two-hour incubation, the final measurements of DO were taken prior to the final sample for SRP and TDP. Following incubations, mussel tissue was removed and lyophilized so that respiration and excretion rates could be normalized to dry tissue mass. Controls of filtered lake water were incubated along with the mussel syringes.

Egestion Rates

Mussels used for the egestion experiments were placed in 500 ml acid cleaned chambers. The control used for this experiment was filtered water in which mussels and mesh from one experimental chamber were placed and immediately removed, to account for any particulate material that may detach from mussel shells. The chamber temperature was maintained near in situ temperature as for the syringe experiments described above, and incubations were conducted for 2 hours. Following the 2-hour incubation, the mussels were removed from the chamber and frozen. The contents of the chamber were filtered onto pre-weighed ashed GF/F (0.7 µm) 47mm diameter filters. The chambers were rinsed with type 1 water to ensure all particulates were collected on the filters. Filters were dried at 70˚C for 12 hours and then weighed. The filter with the collected biodeposits was cored with a cleaned metal filter corer with a diameter of 18mm. Two of the cored subsection was used for particulate phosphorus, and two of the cored subsections were used for carbon and nitrogen analysis. The deviation between the core replicates was less than 5%. Particulate phosphorus was analyzed using the molybdate-antimony method (Stainton et al. 1974) after combustion at 550˚C and two-hour acid digestion with 2 ml of 1N HCl and 10 ml of type 1 water. An elemental analyzer (model: NA 1500 NCS from Carlo-Erba instruments) was used to determine carbon and nitrogen content using acetanilide standards ranging from 0.2 mg to 1.0 mg. Mussel soft tissue dry mass was measured following lyophilization, and all egestion rates were normalized to tissue mass.

Areal Respiration, Excretion, and Egestion Rates

Mussel length-weight relationships, areal density, and size-frequency were established for all sampling dates from 2018 to 2019. The counts of mussels and size-frequency per square meter were determined by using the three replicate Ponar grabs from each sampling date. All the mussels from each replicate were counted and measured to the nearest millimeter. Mussel tissue was removed from 25 mussels of known length from each replicate and lyophilized. The length to dry mass relationships were fitted to an allometric model $W= aL^b$ where W is the dry tissue mass (mg), and L is the length of the shell in mm (Nalepa et al. 1993). The size-frequency distribution was used along with the allometric model to determine dry mass as mg m^{-2}. This was then used with mass-normalized respiration, excretion, and egestion rates of different size classes to determine areal rates.

Ambient Water Condition

On each day that the egestion and excretion experiments were conducted, a water sample was taken one meter above the bottom for particulate phosphorus, carbon, nitrogen, and chlorophyll *a* analysis. Full water column sampling was completed for the majority of experiments. The sampling depths were 2 m, 10 m, 15 m, 20 m, 23 m, and 24 m at AW25, and 2 m, 10 m, 15 m, 20 m, 25 m, 30 m, 35 m, 40 m, 50 m, and 54 m at the AW55 site. The water was filtered onto GF/F filters with a diameter of 24 mm. Filters for particulate phosphorus, carbon, and nitrogen were analyzed as described above. Filters used for chlorophyll *a* were stored in a dark freezer until analysis, which was within two weeks of sample collection. Chlorophyll was extracted for 24 hours in a freezer using a methanol and acetone mixture following filter grinding, as described by Arar and Collins (1997). Fluorescence was measured using a Turner designs model 10 benchtop fluorometer after centrifuging the filter and extractant solution at 3000- 4000 rpms.

Clearance Rate

The mass-specific particulate phosphorus clearance rate (L mgDW^{-1} day^{-1}) was calculated as

$$C = \frac{CR}{[PP]B} \tag{1}$$

where CR is the capture rates of particulate phosphorus (µmol m^{-2} day^{-1}), [PP] is the concentration of particulate phosphorus near the bottom (µmol L^{-1}), and B is the areal biomass (mg m^{-2}). A conservative capture rate of phosphorus can be calculated by summing the areal phosphorus excretion and egestion rates and assuming that little phosphorus is proportioned to biomass (Stoeckmann & Garton 1997; Mosley & Bootsma 2015).

Carbon Capture rates

Areal carbon capture rates were calculated using three different methods: 1) That described in Tyner et al. (2015); 2) Adding the estimated CO_2 production to the carbon egestion rates (addition method); 3) Combining the clearance rate with near-bottom particulate carbon concentration. Methods 1 and 2 use respiration data collected with the optical dissolved oxygen probe. Tyner et al. (2015) determined 1mg of O_2 respiration equates to 0.42 mg of organic carbon captured using the assumptions that 1 mg O_2 equated to 3.38 calories (Crisp 1984), 88% of mussel energy is utilized in oxygen consumption (Stoeckmann & Garton 1997), quagga mussels have an 81% food assimilation efficiency (Baldwin et al. 2002), and there are 11.40 calories per mg of organic carbon (Platt & Irwin 1973). Method 2 used the egestion rates of carbon and a respiratory quotient of 0.75 μmol of CO_2 for 1 μmol of O_2 uptake (Martin et al. 2006; Martin et al. 2007; Ruginis et al. 2014). Method 3 used the conservative clearance rate derived from phosphorus excretion and egestion rates, as described above.

Statistics

Two-way ANOVA was used to compare excretion, respiration, and egestion rate by date and size class. One-way ANOVA was used for nitrogen egestion because the biodeposit samples collected from smaller size class mussels were often too small for accurate measurement of nitrogen content. One-way ANOVA analysis was also completed for the large mussel egestion rates of carbon and phosphorus because not all dates contained small mussel data. Prior to ANOVA, normality was confirmed using Q-Q plots and Levene's test for normality. ANCOVA was used to compare the log of mussel mass – length relationship by site and date. Prior to ANCOVA, the assumptions of linearity and homogeneity of regression slopes were checked. Normality of residuals was checked using a Shapiro test. The homogeneity of variances was confirmed with a Levene test. A simple t-test was used to compare SRP and TDP excretion rates, excretion rates by site, mussel density by site, and mussel biomass by site. All statistical analysis was performed with a significance level of 0.05.

Results

Mussel Biomass

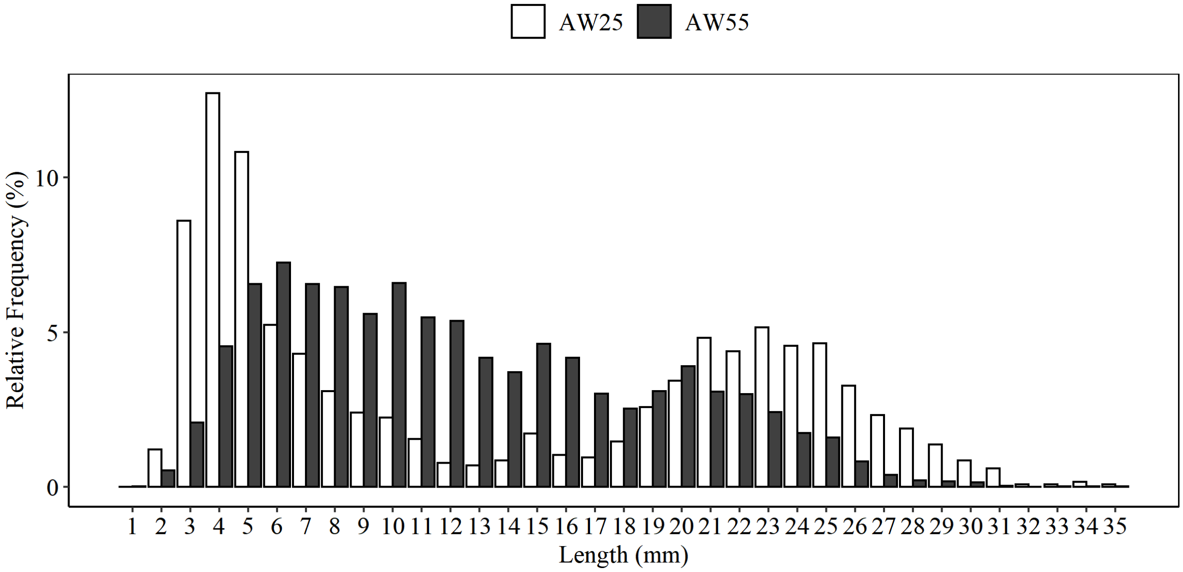

Figure 1: Histogram of the relative frequency of mussels of different lengths from AW25 and AW55.

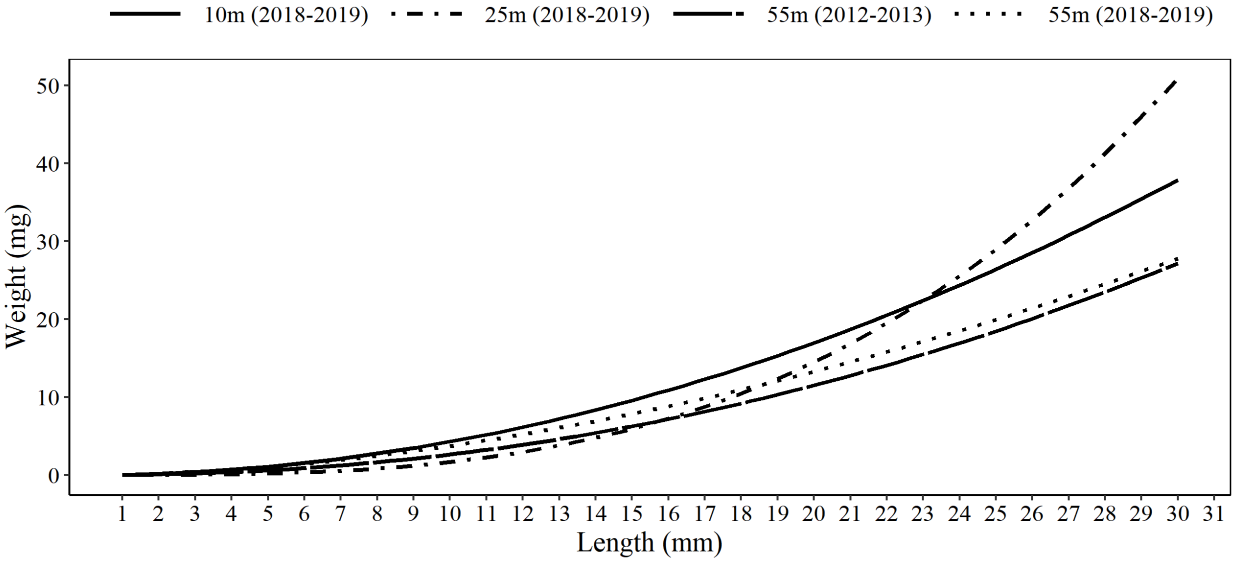

Figure 2: The length weight relationships for the 10m, 25m, and 55m sites along the Atwater Beach transect. The offshore 55 meter sites length weight relationships are included for the years 2012- 2013 and 2018- 2019. The number of mussels used to determine each relationship were 103, 195, 237, 276, 394 for 10m, 25m, 55m (2012-2013), and 55m (2018-2019) respectively.

The density of mussels at the AW25 site was significantly lower than at the AW55 site ($p = 0.006$.) The density of mussels at the AW25 and the AW55 were 2008 ± 1848 mussels m^{-2} and to 7136 ± 3105 mussels m^{-2} respectively. At both sites, there was a bimodal distribution, but the distinction between size classes was less pronounced at the AW55 site, and very small (<5 mm) mussels were relatively more abundant at the AW25 site (Fig. 1). ANCOVA indicated that the length-weight relationship was significantly different between the two sites ($p = 0.03$; Fig. 2). Larger Mussels at AW25 had a higher mass per unit length than those at AW55. The AW55 length-weight relationship was also compared to another 55 m site that was sampled in 2012/13 (Mosley & Bootsma 2015), as well as a 10 m site sampled in 2018/19. The length-weight relationship for mussel at a depth of 55 m did not significantly differ between 2012/13 and 2018/19 ($p = 0.73$). The 10 m site and 25 m site length to weight relationships were not statistically different ($p=0.16$). However, the length weight relationships between the 55 meter station and the 10 meter station were significantly different ($p = 0.002$).

Both sites had significant interactive effects of date and length on mussel weight based on the ANCOVA results ($p < 0.01$). The mass: length ratio for both sites decreased in the late fall of 2018 (Fig. 3), which may correspond to the end of spawning (Nalepa et al. 2010). However, the areal biomass did not vary significantly by date (one-way ANOVA: $p = 0.25$ for AW55; $p = 0.33$ for AW25) when calculated for each site and sample date based on the length-weight relationships, areal density, and length-frequency for that specific site and date. While there was a significant interaction between date and length on mussel weight, the one-way ANOVA results indicate that the mass per unit area did not change over time. The mean biomass per unit area for each site was used for all analyses presented in this paper. The mean biomass was 20900 ± 22900 mg m^{-2} at AW25 and 41500 ± 17255 mg m^{-2}.

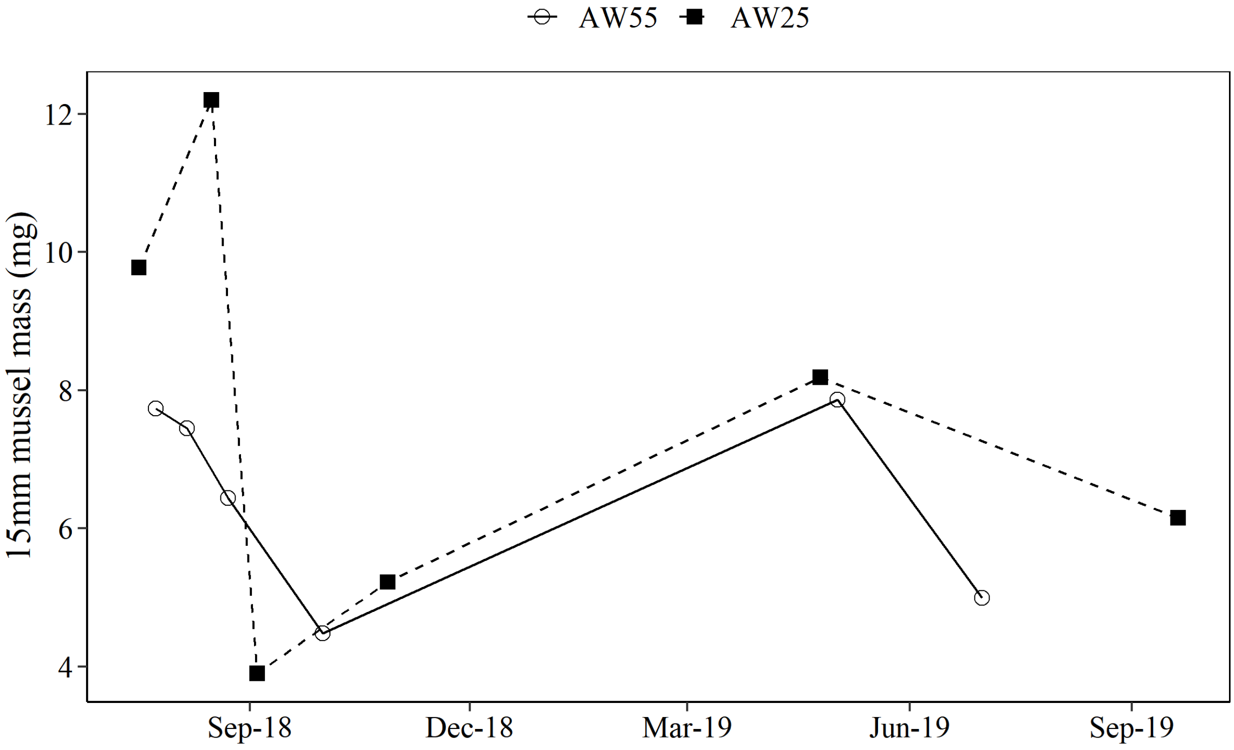

Figure 3: Graph of calculated 15mm mussels mass based on the length weight relationship by date for the AW55 and AW25 sites. Approximately 45 mussels were used to calculate the length weight relationship for each site on each date.

Excretion and Egestion Rates

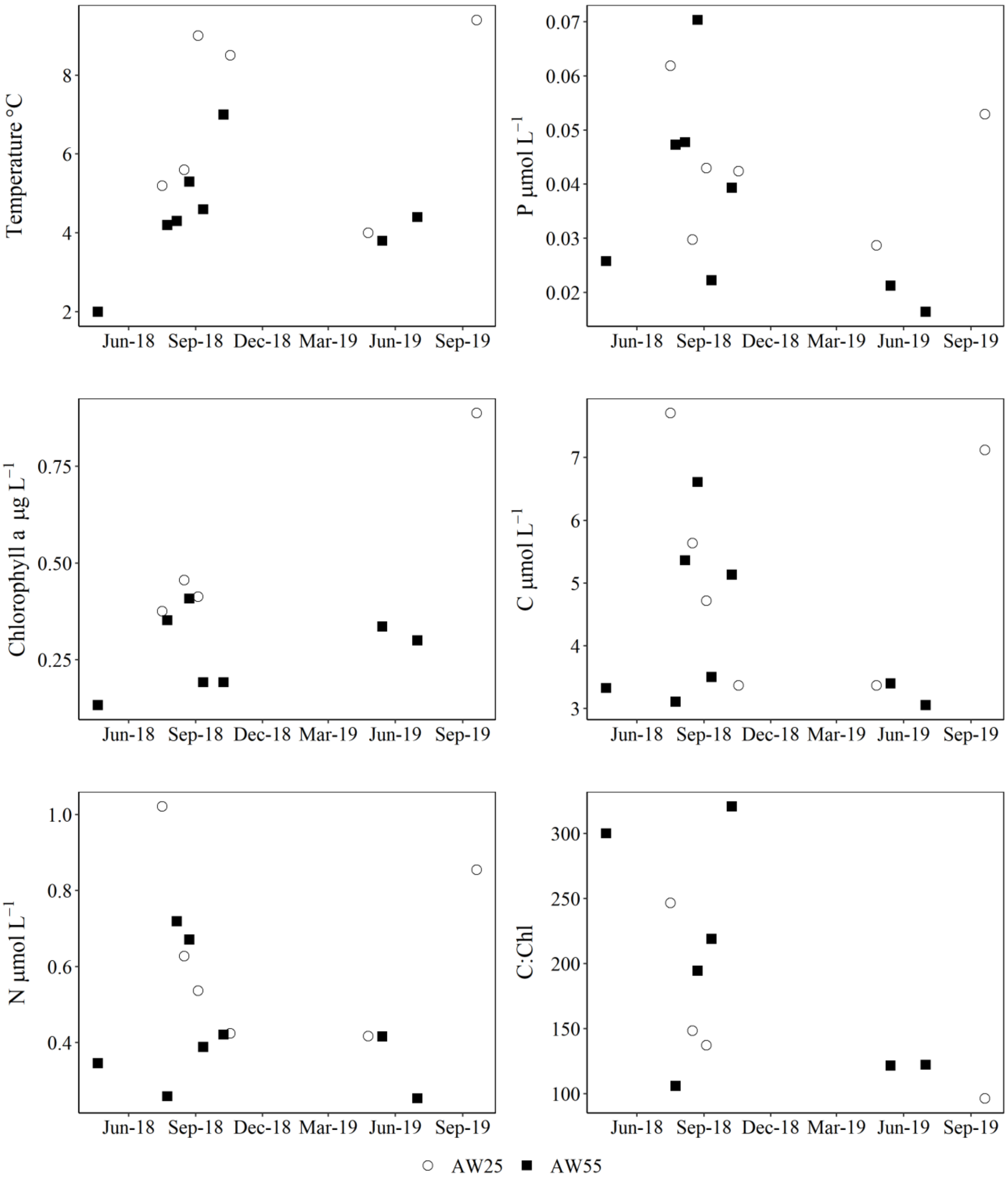

Figure 4: Near-bottom ambient water condition on each date that mussel experiments were conducted. The phosphorus, carbon, and nitrogen plots all refer to nutrients in the particulate form.

Table 1: Table summarizing results of the statistical analysis of egestion and excretion rate at each site.

Site	Comparison	Statistical Analysis	P value interaction	P value size	P value date
AW25 (6)	SRP excretion by size and date	two-way ANOVA	<0.01	<0.01	<0.01
AW55 (7)			0.32	0.16	0.06
AW25 (3)	Respiration by size and date	two-way ANOVA	<0.01	<0.01	<0.01
AW55 (5)			<0.01	<0.01	0.07
AW25 (4)	P egestion by size and date	two-way ANOVA	0.44	0.04	0.05
AW55 (6)			0.01	0.83	0.05
AW25 (4)	C egestion by size and date	two-way ANOVA	<0.01	<0.01	<0.01
AW55 (6)			0.16	0.87	0.11
AW25 (6)	Large mussels N egestion by date	one-way ANOVA	NA	NA	0.09
AW55 (8)			NA	NA	0.02
AW25 (6)	Large mussels P egestion by date	one-way ANOVA	NA	NA	0.02
AW55 (8)			NA	NA	0.21
AW25 (6)	Large mussels C egestion by date	one-way ANOVA	NA	NA	0.07
AW55 (8)			NA	NA	0.31

The change in dissolved phosphorus and dissolved oxygen of all size class (5-11mm, 12-19mm, and 20-27 mm) of mussels were statistically greater than the controls, and any change in the controls was factored out of the experimental data. The DOP excretion, calculated as the difference between the TDP and SRP excretion, was not significantly different from 0 for either site (AW25 p value= 0.08 and AW55 p value= 0.63), so the phosphorus excretion rates reported in this study are the SRP excretion rates. The mass normalized SRP excretion rates at the 25-meter site were significantly higher than at the 55-meter site (p = 0.02). The mass-normalized excretion rate of SRP at the AW55 site did not change size classes or date based on a two-way ANOVA. However, there was a significant interactive effect of date and size on SRP excretion rates at AW25 (Table 1). Rates were more variable overtime for the small mussel class than the larger size classes at AW25 (Fig. 5). On two dates, the smaller size class mass specific excretion rates were larger: September 2018 and October 2018. The temperatures of these experiments were higher (7.5 and 7˚C) because the temperature of the water near the mussel bed was higher on these dates (Fig. 4). This temperature response was not apparent in September 2019 (Fig. 5), but the egestion rate of nutrients was greater in September 2019 (Fig. 7). The temperatures at the AW55 site were never above 7˚C, which may explain why the SRP excretion did not change throughout the study period (Fig. 4 and Fig. 5).

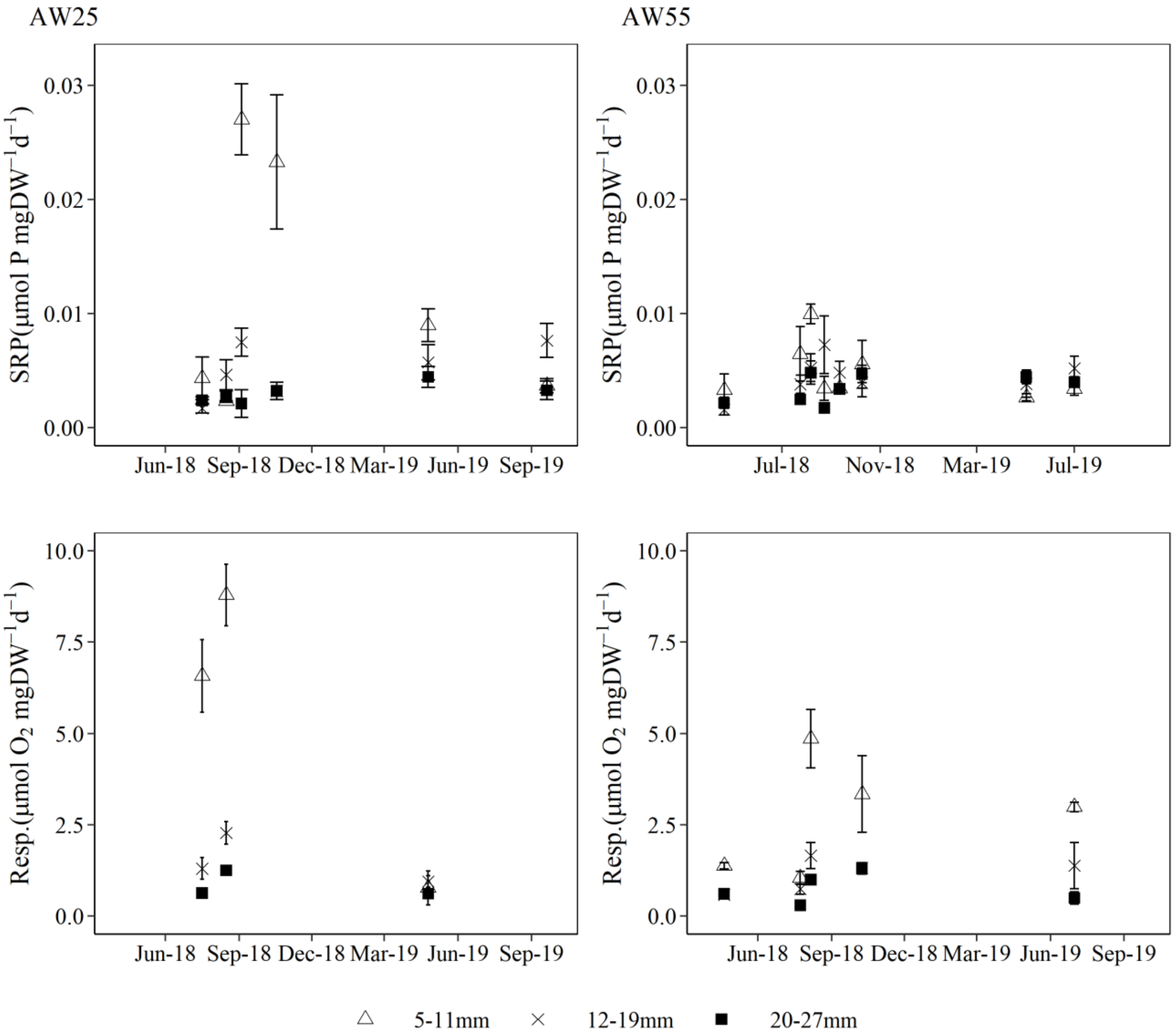

Figure 5: Size specific excretion and respiration rate by date normalized to dry, shell-free mass. The left panels are the excretion and respiration rates from AW25 and the right panels are from AW55. The error bars represent standard error.

There was a significant interactive effect of size class and date on mass specific respiration rate at each site (Table 1). Mass-normalized respiration rate was greater for small mussels than for the larger size classes (Fig. 7), and was more variable over time (Fig. 5). There was no significant difference between the depths with regard to respiration rate for all size classes ($p = 0.08$).

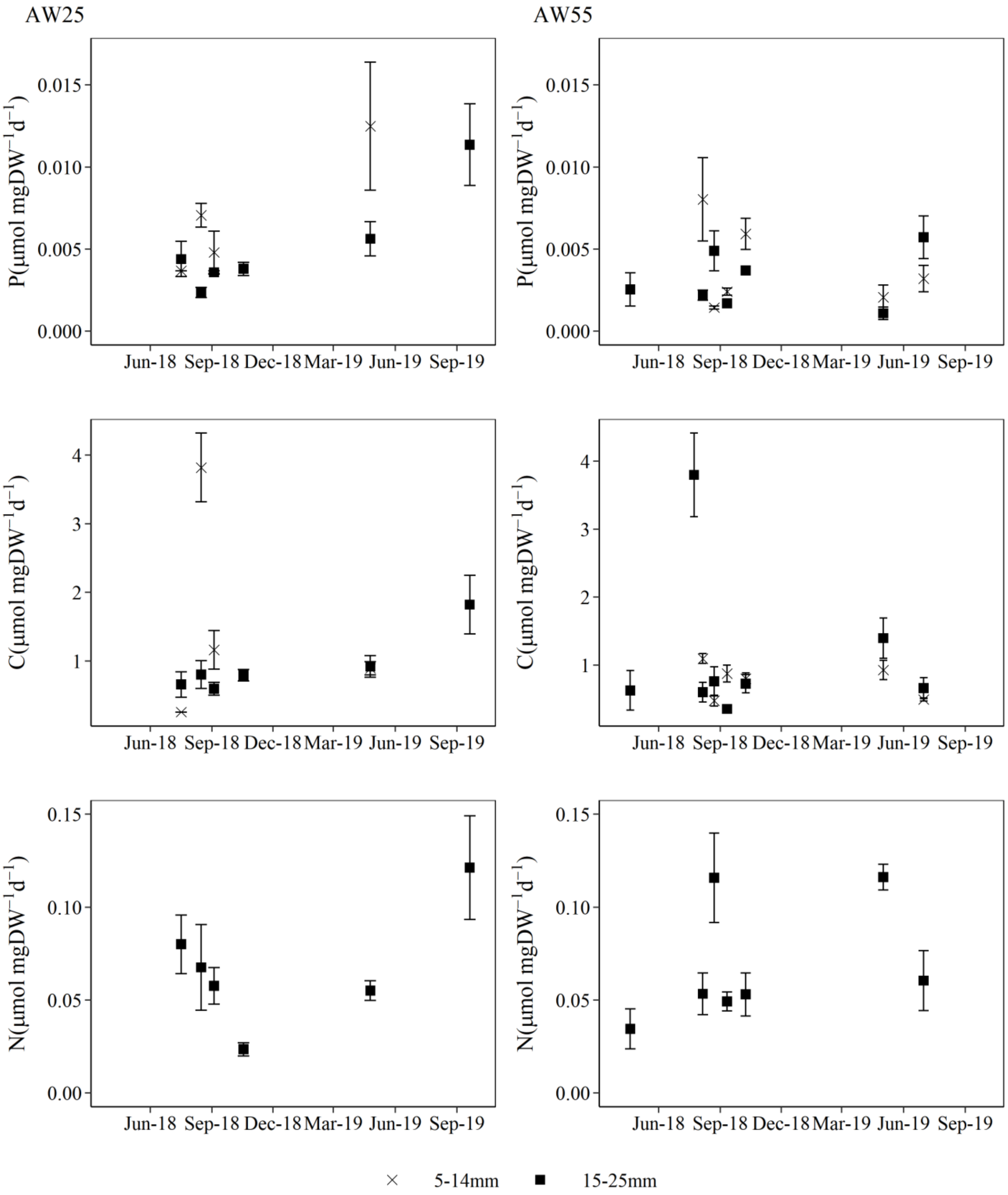

Figure 6: Size specific egestion rates of P, C, and N by date normalized to dry mass. The left panels are egestion rates from AW25, and the right panels are egestion rates from AW55. The error bars represent standard error.

The mass normalized phosphorus egestion rates at the AW25 site were significantly higher than at the AW55 site (p = 0.009), but no spatial difference was apparent for carbon and nitrogen egestion. For the three dates on which small and large mussel egestion rates were measured at AW25, the smaller size class had a significantly higher mass normalized phosphorus egestion rate than the larger size class (p= 0.04), and there was no interaction between date and mussel size. The larger size classes phosphorous egestion rates were compared using a one-way ANOVA by date for the AW25 site, and based on subsequent Tukey HSD testing, the experiment conducted in September 2019 had a significantly higher phosphorus egestion rate. There was an interactive effect of size and date for P egestion at the AW55 site (Table 1). The large mussel size class was compared with a one-way ANOVA at the AW55 site because there was one date without small mussel data, and the large mussels P egestion rates did not vary with the date.

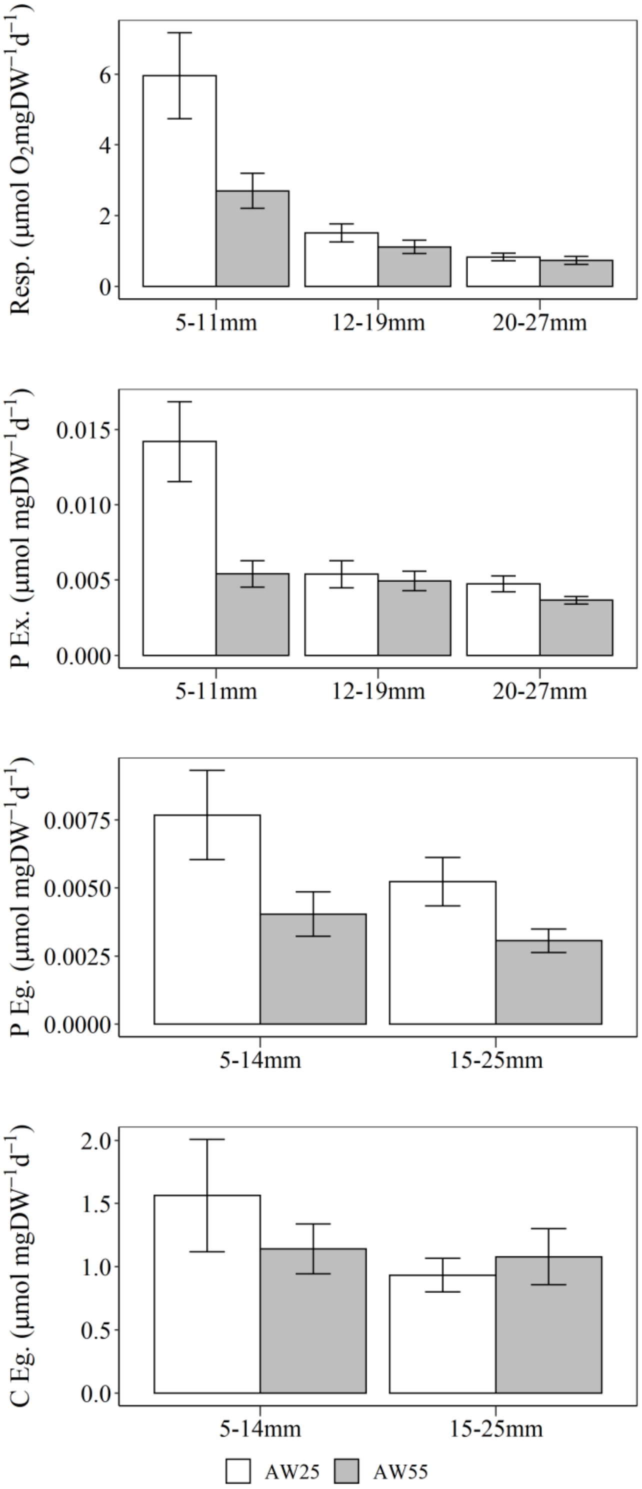

Figure 7: Size specific mass normalized excretion, respiration and egestion rates for both sites. The error bars represent standard error.

The carbon egestion rates at the AW55 site did not vary by size or date (Table 1). However, the nitrogen egestion rates did vary by date. Based on subsequent Tukey HSD, the April 2018 experiment had a significantly lower nitrogen egestion rate than two of the other sampling dates at AW55. There was a significant interaction between date and size as predictors of mass normalized carbon egestion rates for AW25. The large mussels' nitrogen and carbon mass normalized egestion rates were not significantly different by date at AW25. The mean carbon egestion rates were 1.14 ± 0.78 and 0.77 ± 0.30 μmol mgDW^{-1} day^{-1}, and the mean nitrogen egestion rates were 0.067 ± 0.035 and 0.066 ± 0.04 μmol mgDW^{-1} day^{-1} for AW25 and AW55 respectively.

Areal Clearance and Capture Rates

The data presented above were used with areal biomass estimates to calculate areal excretion, egestion, and respiration rates for each date. The mean areal excretion, egestion, and respiration rates are summarized in table 2. The area excretion and egestion rates varied more at the AW25 site due to the greater variation of biomass. The areal excretion and egestion rates of phosphorus were then used with near bottom particulate phosphorus to calculate a conservative clearance rate for each sampling date (Fig. 8). The mean clearance rate was 0.32 ± 0.47 L mgDW^{-1} day^{-1}, at AW 25 and 0.26 ± 0.18 L mgDW^{-1}day^{-1} at AW55.

Table 2: Areal excretion, egestion, and respiration (± standard deviation) rates based on mean mass normalized excretion, egestion, and respiration rates and areal biomass with units of μmol m^{-2} day^{-1}.

Site	P excr.	P eg.	C eg.	N eg.	O_2 resp.	CO_2 resp.
AW25	144 ± 220	128 ± 169	24000 ± 30900	1400 ± 1720	23200 ± 27000	17400 ± 20300
AW55	178 ± 140	145 ± 110	32000 ± 1640	2740 ± 182	50000 ± 11850	37500 ± 8890

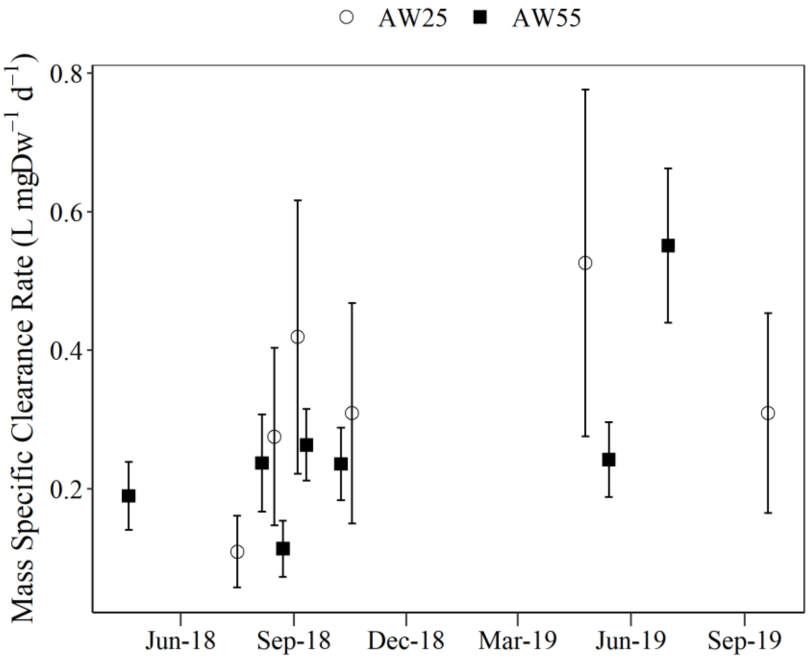

Figure 8: The mass specific clearance rate by date calculated using the mussel area egestion rate of P, area excretion of P, biomass per m^2, and near bottom concentration of particulate phosphorus. The error bars represent the standard error.

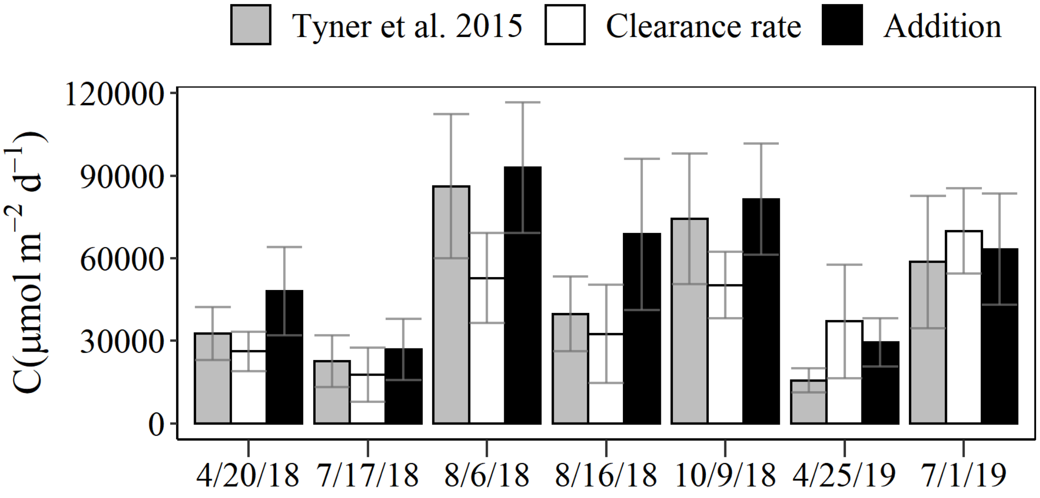

Figure 9: The area capture rates calculated using the methods described in Tyner et al. (2015), clearance rate and near bottom seston C, and by adding the CO_2 production and the C egestion rate. The error bars represent the standard error.

The capture rate of carbon was calculated using three different methods, as described above. The calculated carbon capture per area was not significantly different between the methods based on a one-way ANOVA ($p = 0.40$; (Fig. 9). The area capture rates of C and N were calculated based on the clearance rates and near bottom seston nutrient content because the capture rates could be calculated for more dates using this method, and it allowed for an estimate of nitrogen capture (Fig. 10). The AW25 and AW55 sites were similar in P, C, and N capture rates.

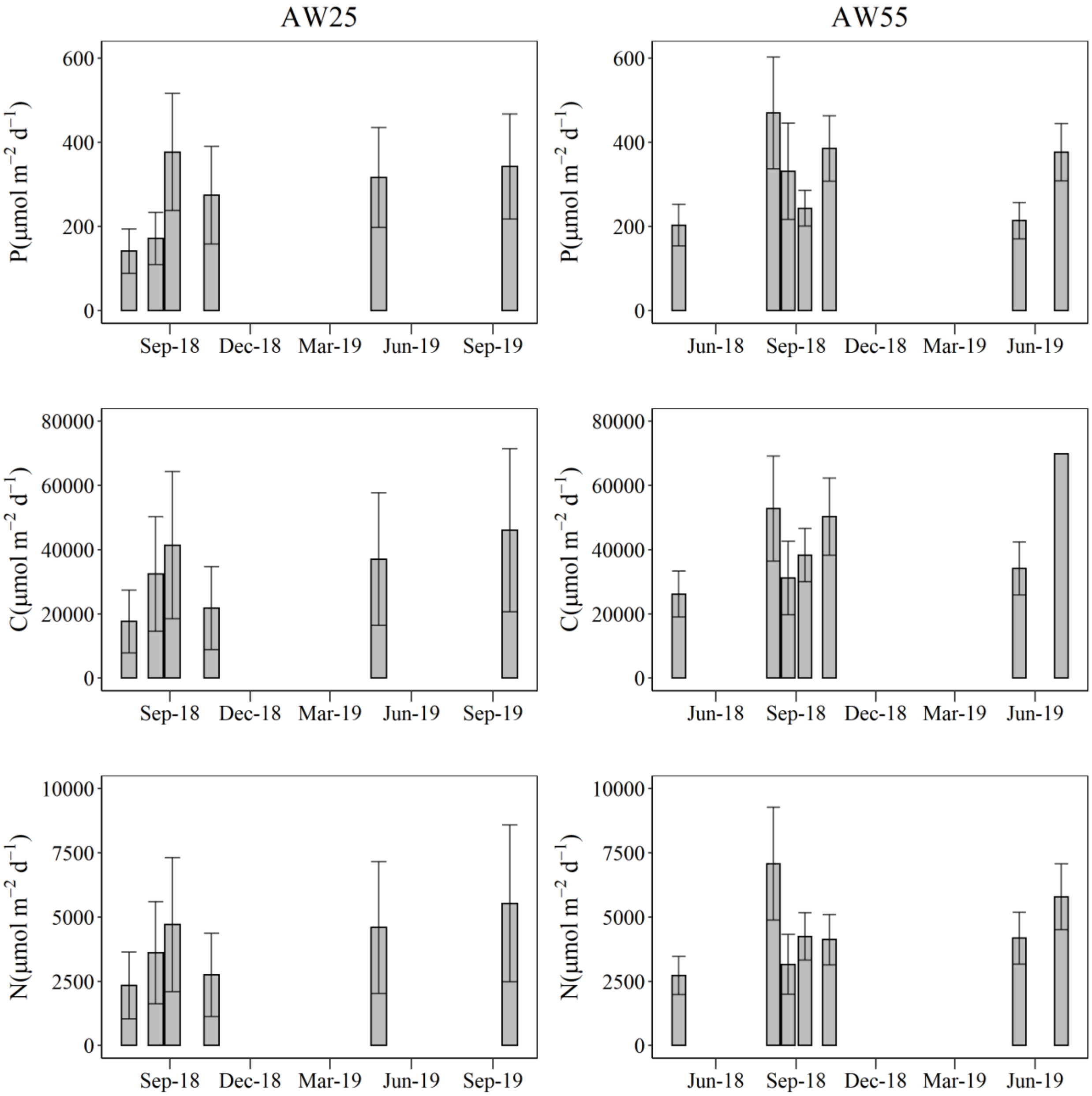

Figure 10: Areal capture rates of C, P and N for AW55 and AW25. P capture rates were calculated using the excreted P and egestion P. The capture rates of C and N were calculated using the clearance rates and the near bottom seston C and P. The error bars represent standard error.

Stoichiometry

Table 3: C:P, N:P, and C:N of biodeposits, excreted material, and seston from AW25 and AW55 ± the standard deviation. Biodeposit and excreted values that are significantly different from seston values are indicated with * (based on a t test, $\alpha = 0.05$). The seston nutrient ratios are the nutrient ratios from below the thermocline on each sampling date.

Site	Size class ex.	Exc. C:P	Size class eg.	Bio. C:P	Bio N:P	Bio. C:N	Seston C:P	Seston N:P	Seston C:N
AW25	S (5-11mm)	820± 860	S	NA	NA	NA	114 ± 26	15 ± 5	9.5 ± 1.8
	M (12-19mm)	215 ± 144							
	L (20-27 mm)	283 ± 148 *	L	240 ± 190 *	11 ± 5	17 ± 9 *			
AW55	S (5-11 mm)	434 ± 278 *	S	220 ± 120*	NA	NA	133 ± 40	14 ± 4	9.3 ± 1.7
	M (12-19 mm)	160 ± 140							
	L (20-27 mm)	183 ± 155	L	183 ± 71 *	19 ± 5	11 ± 5			

The seston C:P values during the 2018-2019 field season are similar to those reported in Mosley and Bootsma (2015). In the Mosley and Bootsma (2015) study, seston C:P values ranged from 124 to 288 in the hypolimnion, and C:P ranged from 112 to 301 in the epilimnion during stratification at a 55 meter site in 2013. In the current study, hypolimnetic seston C:P range from 61 to 250 with a mean of 136 ± 42 at AW55. The epilimnion C:P ranged from 111 to 311 with a mean of 174 ± 55. The biodeposits' C:P were statistically higher than the surrounding seston for both sites and size classes. The biodeposit N:P was not different than seston values at either site. However, biodeposit C:N was significantly higher than seston C:N at AW25 for the large size class. Excreted C:P was statistically higher for the large size class at AW25 and the small size class at AW55 (Table 3). At both sites, the small mussels had the largest C:P values, but the small mussel size class C:P ratios varied by a large amount at the AW25 site. The variation in C:P for excretion is consistent with the SRP excretion and respiration results for the smaller size class at the AW25 site. The comparison of near bottom seston C:P and areal calculations for mussel C:P products for each experimental date are presented in figure 11.

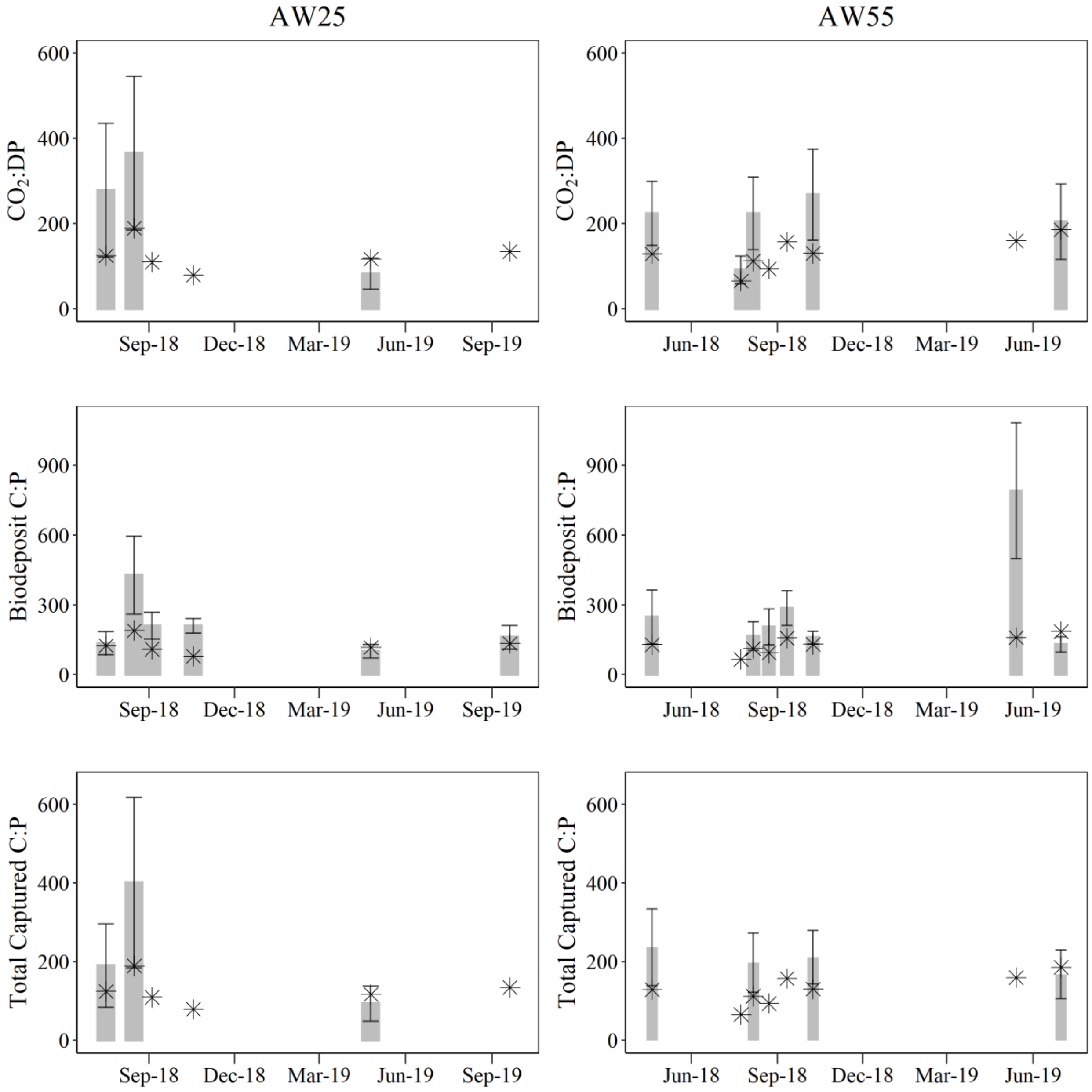

Figure 11: C:P ratios of the dissolved products, egested products, and total capture C:P at the AW25 and AW55 sites (assuming low C and P assimilation into biomass). The error bars represent standard error. The star symbol indicates the C:P ratio of the near bottom seston. CO_2 production was calculated using the areal oxygen consumption rates and a respiratory quotient of 0.75 (Bruce 1926; Martin et al. 2006; Martin 2007; Ruginis et al. 2014).

Discussion

Mussel Community Structure

The bimodal distribution of mussels nearshore and offshore may be explained by round goby feeding because the decrease of mussels in the size range of 6 to 18 mm corresponds to preferential feeding by round gobies (Ray & Corkum 1997; Barton et al. 2005). Smaller gobies tend to rely less upon mussels when other food sources are available, which could explain why smaller mussels in the nearshore zone are more abundant than offshores (Ray & Corkum 1997). While gobies have been found at depths exceeding 55 m, they are more abundant nearshore due to rockier substrate and greater food availability (Corkum et al. 2004). Gobies' diet may also change with depth. Some studies have shown an increase in the consumption of native invertebrate, including *Mysis relicta*, with increasing depth (Schaeffer et al. 2005; Walsh et al. 2007). Both the increased abundance and potential change in food preference make predation pressure of round gobies on dreissenids higher at AW25 compared to AW55, which may explain why the bimodal distribution is more pronounced at the nearshore site.

The AW25 site consistently had a higher mass per mussel length than the AW55 site, most likely due to greater access phytoplankton at the AW25 site due to greater transport of phytoplankton to the benthic boundary layer and higher phytoplankton production (Rowe et al. 2017; Bockoldt 2018). However, the temporal trends of the mass:length ratio was similar at both sites (Fig. 3). The mass of the 15mm mussel can be used as an indication of the nutritional status of the mussel population (Nalepa et al. 2010). The mass of the 15mm mussel during the fall is used to compare mussel nutritional status because generally, this is after spawning occurs (Nalepa et al. 2010). However, Glyshaw et al. (2015) demonstrated that spawning at a 25 meter depth may occur later and that the 15mm mussel mass and reproductive status may not be well correlated. The 2018 September 15mm mussel masses were 6.2 and 3.9 for the AW25 and AW55 sites respectively indicating higher nutritional content for the nearshore mussels.

The mussel density at the AW55 site is lower than the mussel densities determined in 2012-2013 by Mosley & Bootsma (2015). Despite lower mussel counts, the areal biomass in this study at a 55 meter station offshore Milwaukee was higher than the values reported by Mosley and Bootsma (2015). The difference between the two studies can be explained by a decrease in the relative frequency of smaller mussels <8 mm and an increase in the relative frequency of larger mussels (Mosley & Bootsma 2015). The increase in larger mussels compared to smaller mussels may indicate the mussel populations are continuing to stabilize at mid-depth regions (Nalepa et al. 2010) or could be caused by spatial differences between the two sites.

Excretion, Egestion, and Respiration Rates

Mussel respiration, excretion, and egestion are known to change with mussel size, temperature, and food quality (Summers et al. 1996; Arnott & Vanni 1996; Tyner et al. 2015; Conroy et al. 2005; Mosley & Bootsma 2015). In this study, the smaller mussels seemed to be most sensitive to seasonal changes. These results are consistent with Tyner et al. (2015), who showed that smaller mussel respiration rates differed more at ambient water conditions than the larger mussels. The lack of difference between the mussel size classes and excretion rate at AW55 is also consistent with results from Mosley & Bootsma (2015), who noticed little difference between mussels' size excretion at a profundal site in Lake Michigan. At the AW55 temperature inhibits metabolic rates of the mussel, and Tyner et al. (2015) demonstrated that size class difference in respiration rate decreased at lower temperatures. Mussel excretion and egestion are also a function of the food consumed by the mussels (Vanderploeg et al. 2010;

Vanderploeg et al. 2017), and mussel excretion seems to be sensitive to season and temperature differences (Ozersky et al. 2015). When food supplies are low, mussel pumping rate and respiration decrease to basal metabolism (Tyner et al. 2015). As food quality and quantity increase, the respiration increases (Tyner et al. 2015). Although there were limited experiments with respiration data, the dates with the highest respiration rate for both sites corresponded to the dates with the highest chlorophyll *a* concentration and high temperature (Fig. 4 and Fig. 5).

A similar study examined the phosphorus excretion and egestion rates offshore of Milwaukee at a 55 meter site from 2012 and 2013 (Mosley & Bootsma 2015). The Mosley and Bootsma (2015) study estimated a mean phosphorus capture rate of 215 μmol m^{-2} day^{-1}, which is in range of the mean phosphorus capture rate estimated in this study, 324 ± 245 μmol m^{-2} day^{-1}. The former study also noted a high DOP excretion ranging from 10% to 80% of excreted phosphorus, while the DOP excretion measured in this study was not statistically different from 0. Most studies measure either measure SRP or TDP excretion, and not both (Arnott & Vanni 1996; Conroy et al. 2005; Johengen et al. 2013; Ozersky et al. 2015; Vanderploeg et al. 2017), so it is unclear what environmental factors may promote DOP excretion. Despite the differences in excretion, the clearance rates calculated in both this study and that of Mosley and Bootsma (2015) were similar with a mean value of 0.28 L $mgDW^{-1}$ day^{-1} in the Mosley and Bootsma (2015) study and 0.26 ± 0.18 L $mgDW^{-}$ day^{-} calculated here. The mass normalized capture rates were also similar in both studies with an estimate of 0.007 μmol P mg^{-1} d^{-1} in Mosley and Bootsma (2015) and 0.008 ± 0.005 μmol P mg^{-1} d^{-1}.

In Mollusca, egestion rates of phosphorus tend to be more variable than excretion rates (Halvorson & Atkinson 2019). Biodeposits represent both feces and pseudofeces, and pseudofeces are membrane bound particles that do not pass through the gut of a mussel.

Biodeposit production is related to seston quality and abundance with greater nonalgal seston leading to higher rates of pseudofeces production (Bootsma & Liao 2014; Vaughn & Hoellein 2018). Marine studies of biodeposits have shown that pseudofeces and feces vary in C:N:P masses (van Broekhoven et al. 2015; Jansen et al. 2012; Navarro & Thompson 1997). In the Great Lakes, the seston level is typically too low for significant pseudofeces production (Bootmsa & Liao 2014). However, there were two experiment runs where pseudofeces production was visually distinguishable: 8/23/2018 (AW25) and 5/2/2019 (AW55). The biodeposits on these dates contained higher C:P ratios than the other experiments (Fig. 11). This result is consistent with previous studies examining biodeposit composition in marine systems, where pseudofeces contained higher amounts of carbon, but similar amounts of phosphorus (Navarro & Thompson 1997; van Broekhoven et al. 2015). The higher carbon content in pseudofeces may be due to selective feeding processes by the mussels, which may allow the mussel to ingest particles with relatively higher P and N while rejecting particles that contain pure carbon (Newell & Jordan 1983). The long term fate of biodeposit bound nutrients have important implication for Lake Michigan and are discussed in further detail in chapter 3.

Vanderploeg et al. (2002) proposed that quagga mussels follow the rules of homeostatic maintenance of constant nutrient content, which means that mussels may selectively retain nutrients that are in low abundance in the seston relative to their requirements. The seston N:P ratios for both sites were close to the Redfield ratio of 16:1, but the seston C:P and C:N were both higher than the Redfield ratios of 106:1 and 6.6:1 (Table 3). However, N:P ratios in mussel tissue can be much higher than the Redfield ratio, and this can cause a shift to nitrogen limitation because mussels selectively retain more nitrogen in biomass than phosphorus (Arnott & Vanni 1996; Bootsma & Liao 2014). The N:P ratios of the biodeposits were not statistically different than the seston values; however, this does not indicate if mussels are selectively retaining nitrogen because nitrogen excretion was not measured in this study. It does appear that mussels are selectively retaining phosphorus compared to carbon because both the egested and certain size classes' excreted material contained higher C:P than hypolimnion seston (Table 3).

Implications for Lake Michigan

The capture rates of nutrients nearshore have important implications for nutrient dynamics in the Great Lakes because greater retention of nutrients nearshore can lead to further nutrient limitation offshore (Heck et al. 2004). The nearshore zone also represents an important link between tributaries and the offshore regions of Lake Michigan. On the eastern side of Lake Michigan, quagga mussel density is limited by unstable sandy substrate (Nalepa et al. 2010; Pothoven & Vanderploeg 2020). Due to the low density of mussels, the filtering effects of mussels on spring primary production are dampened by the tributary loading nearshore (Pothoven & Vanderploeg 2020). The western side of Lake Michigan is different, with hard substrate covering approximately 80% of the nearshore zone near Milwaukee (Bootsma & Liao 2014). This rocky substrate was not sampled in this study, but nearshore in situ phosphorus excretion studies have been conducted in this area before (Bootsma 2009), and monitoring of the mussel community is completed fairly often at the AW10 site. AW10 was sampled six times between the 2018 and 2019 field seasons by divers from the Bootsma Lab at the University of Wisconsin Milwaukee. During sampling, divers scrape a 20 cm by 20 cm plot collecting mussels located on the harder substrate, and these samples were counted and measured as described for the AW25 and AW55 site. Using these estimates, the areal density at the 10 meter station is 2930 ± 600 mussel m^{-2}. Using the length to weight analysis for AW10 (Fig. 2), the areal dry mass at this site is 51000 ± 9900 mg DW m^{-2}. Assuming that the AW10 site is similar to AW25 and

AW55 with 40% of recycled phosphorus being in the form of biodeposits, the estimates of dry mass normalized in situ excretion rates of phosphorus presented in Bootsma and Liao (2014) can be used to estimate a phosphorus capture rate nearshore. The in situ excretion rates ranged from 0.0048 to 0.016 μmol P mgDW^{-1} day^{-1}, which equates to a capture rate of 460 to 1530 μmol P m^{-2} day^{-1} at the 10 meter site. This estimation of P capture rate is comparable to estimates in Bootsma et al. (2012) when adding egestion and excretion rates of phosphorus, with p capture rates ranging from 499 to 1257 μmol P m^{-2} day^{-1}. Unlike the eastern side of Lake Michigan, where the highest capture rates occur at mid-depth regions (Vanderploeg et al. 2010), the highest capture of nutrients occurs nearshore near Milwaukee, meaning that mussel filtering activity could have larger effects relative to tributary loading in the area.

Mussel also captured a large portion of carbon along this transect. In order to put the capture rate of carbon in the perspective of lake process, these values can be compared to late summer to early fall areal phytoplankton production values determined along a transect from Atwater beach in 2017. During this period, the phytoplankton carbon uptake ranged from 176 to 1215 mg C m^{-2} day^{-1} at a15 meter site and 283 to 895 mg C m^{-2} day^{-1} at a 45 meter site (Bockwoldt 2018). Assuming the primary production values were similar in 2018, the mussels at AW25 would consume 34 ± 47%, and the mussel at AW55 would consume 72 ± 35% of production per day. The estimate at AW55 is slightly higher than those presented by Tyner et al. (2015), which estimated mussels consumed 54% of primary production annually in Lake Michigan. However, the consumption rate of primary production at the AW25 site was similar to that predicted by Tyner et al. (2015). In the nearshore area, Tyner et al. (2015) estimated that mussels consume 267 mg C m^{-2} day^{-1} equaling roughly 31 % of primary production nearshore during late summer into Fall (Bockwoldt 2018). Future work should examine the effects of the

Milwaukee River loading and nearshore mussels on primary production throughout the year to determine nearshore retention of energy by dreissenid mussels during different seasons.

While mussels capture large amounts of phosphorus, mussels also excrete a large portion of phosphorus in the form of SRP. In some nearshore zones (0 to 10m), the combination of high excretion rates by mussels and increased water clarity has led to the resurgence of nuisance benthic algae *Cladophora* (Bootsma et al. 2004; Auer et al. 2010; Bootsma et al. 2015). One of the key strategies in controlling *Cladophora* growth is reducing phosphorus loading. However, this method may not be effective due to the high excretion rates of mussels (Bootsma et al. 2015). At the same time, increase external phosphorus loading may help promote phytoplankton growth offshore (Rowe et al. 2017). Bootsma and Liao (2014) demonstrated that mussel living within an 8 km stretch in the 0-10 m depth zone near Milwaukee excreted amounts of dissolved phosphorus that was similar to phosphorus loading into Lake Michigan by the Milwaukee River. The work presented here demonstrates that high capture rates and recycling rates of phosphorus continue from nearshore to mid-depth regions offshore of Milwaukee. Within an 8 km stretch of shoreline and extending to the 8.25 km offshore, mussels excrete 12700- 30200 moles P day^{-1} with 50-65% of excretion occurring in areas 0-15 meters in depth based on the phosphorus excretion estimates in this study and bathymetry of Southern Lake Michigan (National Geophysical Data Center 1996). This amount far exceeds the 8000 moles P day^{-1} estimate of the Milwaukee River loading into Lake Michigan (Bootsma & Liao 2014), demonstrating the difficulty in managing low phosphorus concentration in nearshore benthic regions.

While this excreted phosphorus may promote phytoplankton growth, phytoplankton have limited ability to utilize this resource in deeper regions that experience stratification and light limitation (Zhang et al. 2011; Shen et al. 2018). Historically, large amounts of phosphorus were recycled by Zooplankton in the euphotic zone. Current estimates of Zooplankton recycling can be calculated using estimated clearance rates of zooplankton (Scavia & Fahnenstiel 1987), the zooplankton biomass after the mussel invasion (Vanderploeg et al. 2012), and the concentration of particulate phosphorus. The estimate of current zooplankton recycling rates of phosphorus would be between 20-190 μmol P m^{-2} day^{-1} at AW55 and 30-230 μmol P m^{-2} day^{-1} at AW25, which are similar to the measured mussel excretion in this study. Based on this, a large portion of SRP, equal to the amount recycled in the water column, is excreted in the benthos, where phytoplankton cannot take advantage of it. However, benthic bacteria may utilize a large portion of the excreted phosphorus, which could have important implications for benthic nutrient cycling (See Chapter 3). More work is needed to determine the fate of nutrients in the benthos and the potential uptake of nutrients by benthic bacteria.

Summary

Profundal mussels have relatively constant capture rates of nutrients compared to the nearshore mussels, partly due to persistent cold temperatures in the benthos. The capture and recycling rates of nutrients for near-shore mussels vary more seasonally due to the larger fluctuations in temperature. Nearshore mussels also have higher excretion, respiration, and egestion rates per unit dry mass than the mid-depth region mussels. However, mussels live in much higher densities at the 55 meter site compared to the 25 meter site. The high density of mussels at AW55 site led to similar capture rates of nutrients at this site compared to the 25 meter site.

In the nearshore zone close to Milwaukee harbor, mussels are able to colonize roughly 80% of the substrate (Bootsma & Liao 2014), and past studies have demonstrated how mussels excretion in this area can promote the growth of *Cladophora* (Bootsma et al. 2012). This study demonstrates that the highest capture rates by mussels are nearshore, but remain relatively high into the mid-depth regions when compared to primary production. The results of this study indicate that both the nearshore and mid-depth regions near Milwaukee Harbor may act as sinks for nutrients furthering offshore limitation.

CHAPTER 3: Quagga mussel (*Dreissena rostriformis bugensis*) biodeposit effects on benthic nutrient cycling in Lake Michigan

Abstract

Dissolved nutrient production by *dreissenid* mussels is well understood, but the fate of biodeposits and their effect on nutrient cycles is not well understood. In Lake Michigan, biodeposits represent a significant fraction of the phosphorus ingested by dreissenids, and so their fate may have important implications for P cycling. In this study, a series of experiments were conducted to determine the fate of biodeposits and their effect on dissolved nutrients over time scales of 2-3 weeks. Biodeposits promoted bacteria growth, which in turn led to an uptake of dissolved forms of C, N, and P. The bacteria depleted dissolved phosphorus concentration to below detection limit, 0.016 μmol/L, within ten days of incubation. After 12-15 days, dissolved P concentration increased to levels higher than the starting conditions, indicating that biodeposits were a net source of dissolve P over longer time scales.

Introduction

Dreissena polymorpha (zebra mussels) and *Dreissena rostriformis bugensis* (quagga mussels) invaded the Great Lakes in the late 1980s, altering critical ecosystem processes including nutrient cycling and primary production. In Lake Michigan, zebra mussels spread quickly, colonizing the shallow nearshore. However, quagga mussels soon displaced zebra mussels reaching densities over 10,000 mussels per square meters in some areas of the southern basin of Lake Michigan due to the ability of quagga mussels to colonize soft sediments in the deeper, colder, less productive waters (Nalepa et al. 2010). Quagga mussels' high grazing rates have caused significant declines in spring phytoplankton productivity (Fahnenstiel et al. 2010; Vanderploeg et al. 2010). At the same time, increased nutrient recycling and water clarity in the nearshore zone have promoted the growth of nuisance *Cladophora* (Bootsma et al. 2004; Auer et al. 2010; Bootsma et al. 2015). In order to better understand the ecosystem response to these changes, several studies have examined how quagga mussels have modified the Great Lakes' nutrient cycles (Hecky et al. 2004; Zhang et al. 2011; Mosley & Bootsma 2015; Rowe et al. 2017; Shen et al. 2018). Most of these studies have focused on the direct effects of mussel grazing and the excretion of dissolved nutrients. Although much of the material ingested by dreissenids is egested as biodeposits (feces and pseudofeces) (Lauringson et al. 2007; Mosley & Bootsma 2015), there have been virtually no measurements of the fate of this pool of carbon and nutrients (Bootsma & Liao 2014).

The ability of dreissenids to filter particulates and recycle nutrients is determined to a large degree by particle delivery rate, so hydrodynamic processes modulate their effects on plankton and nutrient dynamics (Zhang et al. 2011; Row et al. 2015; Row et al. 2017; Shen et al. 2018). In Lake Michigan, dreissenid grazing significantly reduces phytoplankton abundance during the isothermal period because the high rates of mixing allow mussels to access the entire water column (Rowe et al. 2017; Shen et al. 2018). While mussels in the nearshore zone continue to have access to phytoplankton in the euphotic zone throughout the year, grazing of phytoplankton by profundal mussels is limited to the hypolimnion with the lower 10 meters experiencing the most considerable phytoplankton reduction (Shen et al. 2018).

Mussel mediated alteration of phosphorus dynamics in Lake Michigan and other Great Lakes has created a dilemma for managers. Currently, Lake Michigan is meeting the target total phosphorus loading of 5600 MTA set by the Great Lake Water Quality Agreement, and in-lake total P concentrations are below the target of 7 μg/L (Mida et al. 2010). These low loads, along with mussel grazing, have depleted pelagic phytoplankton (Fahnenstiel et al. 2010; Bootsma et al. 2012; Rowe et al. 2017; Shen et al. 2018) with negative effects on higher trophic levels (Vanderploeg et al. 2002; Turschak et al. 2014). At the same time, mussel phosphorus recycling, along with increased water clarity, supports nuisance algal growth in the nearshore zone (Auer et al. 2010; Bootsma et al. 2015). Dreissenid mussels may decrease offshore pelagic phosphorus concentrations through retention in both the nearshore zone (Hecky et al. 2004) and the profundal benthos (Chapra & Dolan 2012; Mosley & Bootsma 2015; Rowe et al. 2017). This may be achieved in part through a reduction in sediment resuspension through the production of biodeposits, which aggregate smaller particles (Hecky et al. 2004).

Biodeposits represent up to 40% of the P released by mussels at mid-depth regions in Lake Michigan, equating to 86 μmol P m^{-2} day^{-}(Mosley & Boostma 2015). To put biodeposit production in context, phytoplankton require roughly 104 μmol P m^{-2} day^{-} for primary production, based annual areal phytoplankton production rates at mid-depth regions reported by Fahnenstiel et al. (2016), and a seston C:P ratio of 200:1 (Bockwoldt 2018). The biodeposit production rate is also six times higher than the passive settling rate of phosphorus (Mosley & Bootsma 2015), reflecting the mussels' ability to scavenge P from the water column (Shen et al. 2020). The fate of this P has important implications for water column P concentrations. If this P is rapidly recycled, then as mussel populations reach a steady state (in that there is no net loss of P to mussel biomass), the supply of dissolved P to the water column may increase to levels similar to those prior to the establishment of dreissenids. However, if this P is refractory, then mussel grazing and biodeposit production will represent a net loss of P from the water column, with reduced availability to phytoplankton (Bootsma & Liao 2014).

Freshwater bivalves typically egest more nitrogen and phosphorus than they excrete (Halvorso & Atkinson 2019), but the fate of freshwater biodeposits and bound nutrients are not well understood (reviewed by Strayer 2014). In marine environments, studies of bivalve biodeposits in mussel farming regions have demonstrated that decomposition is associated with increased bacterial growth (Grenz et al. 1990; Jansen et al. 2012; van Broekhoven et al. 2015). Giles and Pildith (2004; 2006) demonstrated that bacterial decomposition of biodeposits in a marine system increased oxygen consumption, altered P and N dynamics, and occurred at a rate faster than phytoplankton decomposition. In freshwater systems, dreissenid mussels are associated with an increased abundance of heterotrophic bacteria in the benthos (Roditi et al. 1997; Lohner et al. 2007; Vaughn & Hoellein 2018). Biodeposits, or the bacteria growing on them, may serve as a food source for benthic invertebrates (Lohner et al. 2007). Hence, the carbon and phosphorus in biodeposits may be returned to the pelagic food web through a mechanism similar to the microbial loop (sensu Pomeroy 1974), with bacteria, protozoans, and benthic invertebrates serving as vectors, as has been observed in some marine systems (Genz et al. 1990; Giles and Pildith 2006; Jansen et al. 2012; van Broekhoven et al. 2015). The purpose of this study was to determine the short-term (days-weeks) fate of quagga mussel biodeposit phosphorus, carbon, and nitrogen in Lake Michigan, and these nutrient pools may affect whole-lake nutrient and carbon dynamics.

Methods

Biodeposit Collection

Mussels used for biodeposit production were collected with a Ponar grab sampler from two different sites in Lake Michigan offshore of Milwaukee. Mussels used for batch experiments were gathered from a 25 meter deep site (AW25), and mussels used for flow-through experiments were collected from 55 meter deep site (AW55). Around 150 mussels were used to collect biodeposits in the first experiment. After the first experiment, 400 mussels were used to collect a greater amount of biodeposits so that the measured response would be more detectable. Mussel ranging from 8 to 25 mm were used for biodeposit collection.

Mussels were cleaned immediately after collection by placing them on 0.75 cm mesh and gently rinsing with unfiltered lake water until no particulates were observed detaching from the mussels. After the mussels were cleaned, the mesh containing the mussels was placed in a 5.7 liter chamber filled with unfiltered lake water collected from below the thermocline. The mussels were left in the chamber for 48 hours in a cooler at 4˚C to produce biodeposits. The upper half of the water in the chambers was decanted and replaced with unfiltered cold hypolimnetic water every 6 hours to provide food and prevent hypoxia. Phytoplankton within the chamber represents an insignificant contribution to the deposited material because, assuming an average concentration of chlorophyll *a* of 0.7μg/L, phytoplankton account for 67 μmol of carbon, calculated using a 16.7:1 of carbon to chlorophyll *a* (Fahnenstiel and Scavia 1987). If all phytoplankton settled to the bottom, it would represent less than 2% of the particulate carbon within the biodeposit mixture at the end of the collection period.

After the 48-hour biodeposit production period, biodeposits were condensed into a 200 ml slurry using a gravimetric separation funnel. Biodeposits include both feces and pseudofeces. Pseudofeces are membrane bound particles that do not pass through the gut of the mussel and are easily distinguished from feces. No pseudofeces were present in the biodeposit slurry based on visual inspection. The slurry was gently homogenized, and acid-washed plastic syringes were used to take 10 mL subsamples. The subsamples were used as biodeposit additions, and to determine the biodeposit mass and composition prior to incubation.

Biodeposit Chemical Analysis

A subset of the biodeposit subsamples was filtered on pre-weighed Whatman GF/F filters (0.7 µm nominal pore size) and dried at 70˚C for 12 hours. The remaining subsamples were frozen and stored at -20˚C to later determine bacterial abundance. Freezing at this temperature is a common practice for fecal samples and has shown limited effects on bacteria abundance counts (Vlčková et al. 2012; Mathay et al. 2015). The filters were weighed and analyzed for particulate phosphorus, nitrogen, and carbon. Phosphorus was analyzed using the molybdate-antimony method (Stainton et al. 1974) after combustion at 550˚C and two-hour acid digestion with 2 mL of 1N HCl and 10 mL of type 1 water. An elemental analyzer (model: NA 1500 NCS from Carlo-Erba instruments) was used to determine carbon and nitrogen content with acetanilide standards ranging from 0.2 to 1.0 mg.

Microbial cell counts

Bacterial abundance was analyzed using the DAPI staining technique (Porter & Feig 1980). The frozen biodeposit samples were thawed at 4°C overnight, diluted 10-times in phosphate buffer saline (PBS), fixed by mixing a 1 mL sample with 111 µl of 21% formaldehyde, and stored at 4°C until ready for staining. Six-µl 4′,6-diamidino-2-phenylindole (DAPI) fluorescent dye was added to fixed 1 mL samples, inverted to mix, and incubated at room temperature in the dark for 15 minutes. Stained samples were filtered onto a 0.22-µm, 17-mm polycarbonate filter and mounted to glass slides with one drop of immersion oil and coverslips. Slides were stored at -20°C until ready for microscopy.

Bacteria samples were photographed at 630x magnification with a Zeiss Axio Imager upright confocal fluorescence microscope. The area of the filter each image covered was 0.05 mm^2, so each image represented 0.02% of the total filter area. Ten images were taken of each slide, and each image represented 0.0002 mL of the original sample. The bacteria count per milliliter of the sample was calculated for each image, and this was used to determine the total amount of bacteria within the subsample, which was then converted into cell/mg using the known mass of the biodeposit in the subsample.

Batch Experiment

Table 4: Conditions for each of the three batch experiments. The experiments were terminated when a noticeable biofilm was observed in the FW+ treatment. The biodeposit mass was increased after the first experiment in order to make the response of biodeposits easier to detect.

Batch Experiment Conditions				
Experiment	Duration (days)	Volume (L)	Biodeposit Starting Mass (mg)	Temperature (˚C)
1	14	0.5	1.95 +/- 0.85	4
2	17	0.5	13 +/- 0.4	4
3	22	3	10.3 +/-0.95	4

The batch experiments were performed in glass chambers filled with filtered (0.7μm GF/F) lake water collected 1 meter above the lake bottom. The batch experiments were conducted on three occasions. Each experiment consisted of two treatments carried out in triplicate: filtered water with the addition of biodeposit slurry (B), and filtered water with added biodeposit slurry plus 1 μmol/L potassium phosphate (B+P). In addition, triplicate controls of filtered lake water with added 1 μmol/L potassium phosphate were set up (FW+). Experimental conditions are summarized in Table 4. The purpose of the phosphorus addition was to determine the potential P demand of bacteria growing on biodeposits. All chambers were gently aerated to ensure the water remained oxygenated and mixed without resuspending the biodeposits. The chambers were loosely covered with aluminum foil to prevent particulate contamination while allowing air to escape. Incubations were conducted in a dark walk-in cooler maintained at 4˚C.

Water samples for soluble reactive phosphorus (SRP) and total dissolved phosphorus (TDP) analysis were taken 1, 12, and 24 hours after the slurry addition. After the 24-hour sample time, samples were taken every other day for a total experiment time of 14 to 22 days. All water samples were filtered through Whatman GF/F filters prior to analysis. SRP and TDP analyses were conducted according to the molybdate-antimony method, with TDP samples first being digested by the addition of H_2SO_4 and H_2O_2, followed by 2 hours of photo-oxidation (Stainton et al. 1974). The dissolved organic phosphorus concentration (DOP) was calculated as the difference between the TDP and SRP. At the end experiments 1 and 2, all of the biodeposits were condensed using a gravimetric separation funnel. The slurry was gently homogenized and subsampled in equal volumes for bacteria counts, mass, phosphorus, carbon, and nitrogen. The bacteria count samples are not dried and weighed prior to analysis, so the mass of these samples was accounted for by assuming that the subsample used for bacteria counts had the same mass as the other subsamples. In experiment 3, the ending volume within the chamber was too large to condense the entire portion of biodeposits. The chambers were gently homogenized, and approximately 1 liter of the ending volume was condensed and subsamples as described for experiments 1 and 2. The remainder of the biodeposits were filtered onto two GF/F filters to account for the total mass.

Biofilm Sampling

A noticeable biofilm started to grow on the walls of all chambers around day 13. The biofilm was sampled in experiment 3 and in the flow-through experiment (described below) to allow for the calculation of C, N, and P mass balances. In order to sample the biofilm, the water and biodeposits in each chamber were first siphoned into an acid cleaned container, after which Type 1 water was added to the chamber. The walls of the chamber were scraped with a clean brush to suspend the biofilm. The biofilm slurry was gently homogenized. The slurry volume divided in half and filtered onto two GF/F filters for phosphorus, carbon, and nitrogen analysis.

Mussel Flow-Through Experiment

A flow-through experiment was designed to better mimic in-lake conditions. Two different treatments were used in this experiment: filtered water with biodeposits (B), and filtered water with biodeposits and antibiotics (B+A). Antibiotics were added to test the hypothesis that bacterial growth was responsible for the uptake of dissolved P. In addition, three control chambers (C) were run conjunction with the biodeposit treatments with filtered lake water. In all treatments and the control, potassium phosphate was added to produce a concentration of 0.065 µmol/L, which is similar to concentrations measured immediately above the lake bottom. The antibiotic ciprofloxacin was added at a concentration of 5 µg/L in the antibiotic treatment. Chamber design is shown in Fig. 12. The same reservoir was used for all triplicate chambers of the same treatment. The outflow of each chamber flowed back into the reservoir to minimize the volume of filtered water needed to conduct the experiment. While this resulted in a slow increase in the concentration of dissolved P in the reservoir, it did not affect measurements of recycling

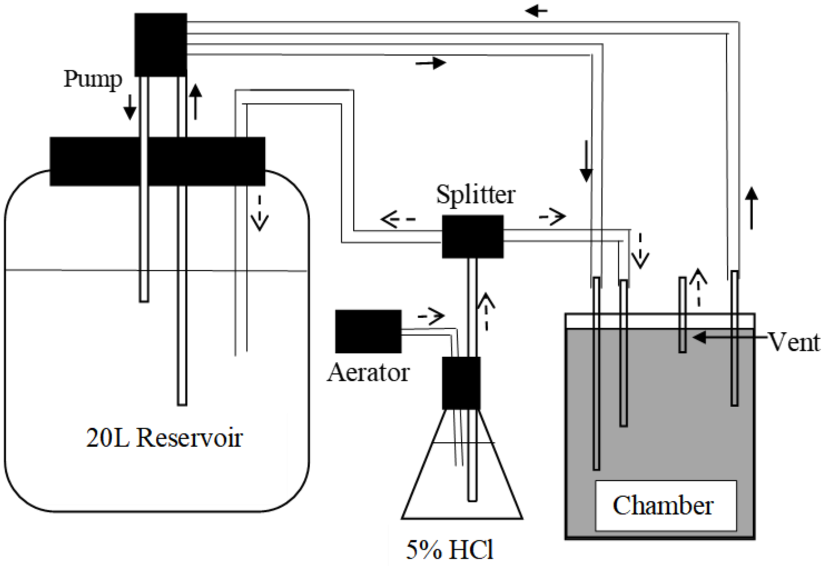

Figure 12: Diagram of the flow through experiment set up. Solid arrows show the water flow direction. Dashed arrows show the air flow direction. Air is allowed to escape the reservoir through the loosely secured top.

rates, which are determined based on the difference between chamber inflow and outflow dissolved P concentrations. A peristaltic pump was used to maintain a continuous flow rate of 1 ml/minute in and out of the 1 L chamber. The residence time of water within the chambers was 16.7 hours. An aerator was pumped through a 5% HCl solution before entering the chamber to minimize bacterial contamination. Both the chambers and the reservoirs were aerated to ensure the water remained well mixed and oxygenated. Reservoirs were changed every three days, and on those days, all tubing was rinsed with 5% HCl followed by type 1 water to minimize biofilm growth. The incubation was conducted in a dark walk-in cooler similar to the batch experiments.

Water samples were collected daily from the reservoir and outflow tubes. All water samples were filtered through 0.2 μm membrane filters prior to analysis. Water samples were analyzed for SRP, TDP, dissolved organic carbon (DOC), and total dissolved nitrogen (TDN). SRP and TDP were analyzed using the methods described above. DOC and TN were analyzed on a total organic carbon analyzer (model: TOC-L CPH/CPN from Shimadzu). Incubations lasted 12 days, after which the biodeposits and biofilm were sampled and analyzed as described above.

The uptake/production rate of nutrients in the flow-through experiments was calculated as

$$R = \frac{(C_i \times V - C_o \times V)}{T_r} \qquad (2)$$

where R is the uptake rate in μg/hr, C_i is the inflow concentration of the previous day (to account for chamber residence time), V is the volume of the container, C_o is the outflow concentration, and T_r is the residence time of water in the chambers.

Water Column Sampling

Bi-weekly water column sampling was conducted at AW55 from April 2018 through October 2018. Water samples were taken with a 5 L Niskin bottle at depths of 2 m, 10 m, 15 m, 20 m, 25 m, 30 m, 35 m, 40 m, 50 m, and 54 m for particulate phosphorus, total dissolved phosphorus, and soluble reactive phosphorus measurements. The measurements of phosphorus were used in a model to determine the effects of biodeposits on water column phosphorus concentrations. Known volumes of water were filtered onto GF/F filters, and the filtrate was collected. The filters were used to analyze particulate phosphorus, and the filtrate was analyzed for TDP and SRP, as described above.

Statistical analysis

The final biodeposit composition was compared to the initial subsamples using a t-test with a significance level of 0.05. Variance among treatments was determined using a one-way ANOVA, followed by a Tukey HSD test for multiple comparisons with a significance level of 0.05. Prior to analysis, normality was confirmed using Q-Q plots and Levene's test for normality.

Biodeposit Model

Table 5: List of assumptions for the biodeposit model.

Mussel Biomass (B)	41,000 mg m^{-2} (Ponar densities from 2018 unpublished data)
Mussel Clearance rate (C)	0.28 L mgDW^{-}d^{-} (Mosley & Bootsma 2015)
Starting [SRP]	0.017 µmol L^{-}
P Excretion (µmol m^{-2} day^{-1})	0.60*CR
P Egestion (µmol m^{-2} day^{-1})	0.40*CR
Starting [PP]	0.072 µmol L^{-}
Portion of PP lost to sedimentation (S)	0.007 (MacLellan-Hurd & Bootsma unpublished)
Phytoplankton C:P	200: 1 (Bockwoldt 2018)
Mean Phytoplankton Uptake of P	104 µmol m^{-2} day^{-1} (Fahenstiel et al. 2016)
External input of P	3.44 µmol m^{-2} (Dolan & Chapra 2012)

The potential effects of mussel biodeposit production on water column P concentration were explored with a simple model that simulated mussels grazing, egestion, and excretion for a 55 meter deep site under mixing conditions. The model assumptions are provided in Table 5. The total concentration of phosphorus was calculated as the sum of particulate phosphorus and total dissolved phosphorus. DOP concentrations remained constant in the simulation, so any changes to the dissolved P were accounted for in the SRP pool. The concentration of particulate P (µmol m^{-2}) was calculated using the following equation

$$[PP]_x = [PP]_{x-1} - CR - S + PG \tag{3}$$

where x is days, CR is the capture rate of phosphorus by mussels, S is the loss to sedimentation, and PG is phytoplankton growth. The capture of phosphorus by mussels was calculated as

$$CR_x = [PP]_{x-1} * B * C \tag{4}$$

where B is the biomass of mussels in mg m^{-2}, and C is the clearance rate of mussels in mg DW^{-} day^{-}. Phytoplankton growth in terms of P was set to the mean phytoplankton uptake of phosphorus unless SRP concentrations fell below this value. If SRP concentrations were below the mean phytoplankton uptake of phosphorus, then the phytoplankton growth in terms of P was set equal to the input of SRP on that day (i.e., mussel excretion and external inputs). The concentration of SRP (µmol m^{-2}) in the model was calculated with the following equation.

$$SRP_x = SRP_{x-1} - PG + Mussel\ Excretion \tag{5}$$

The simulations with the recycling of biodeposits added a portion of the egested P from the previous day into the SRP pool. The model results are presented in the discussion section.

Results

Batch Experiments

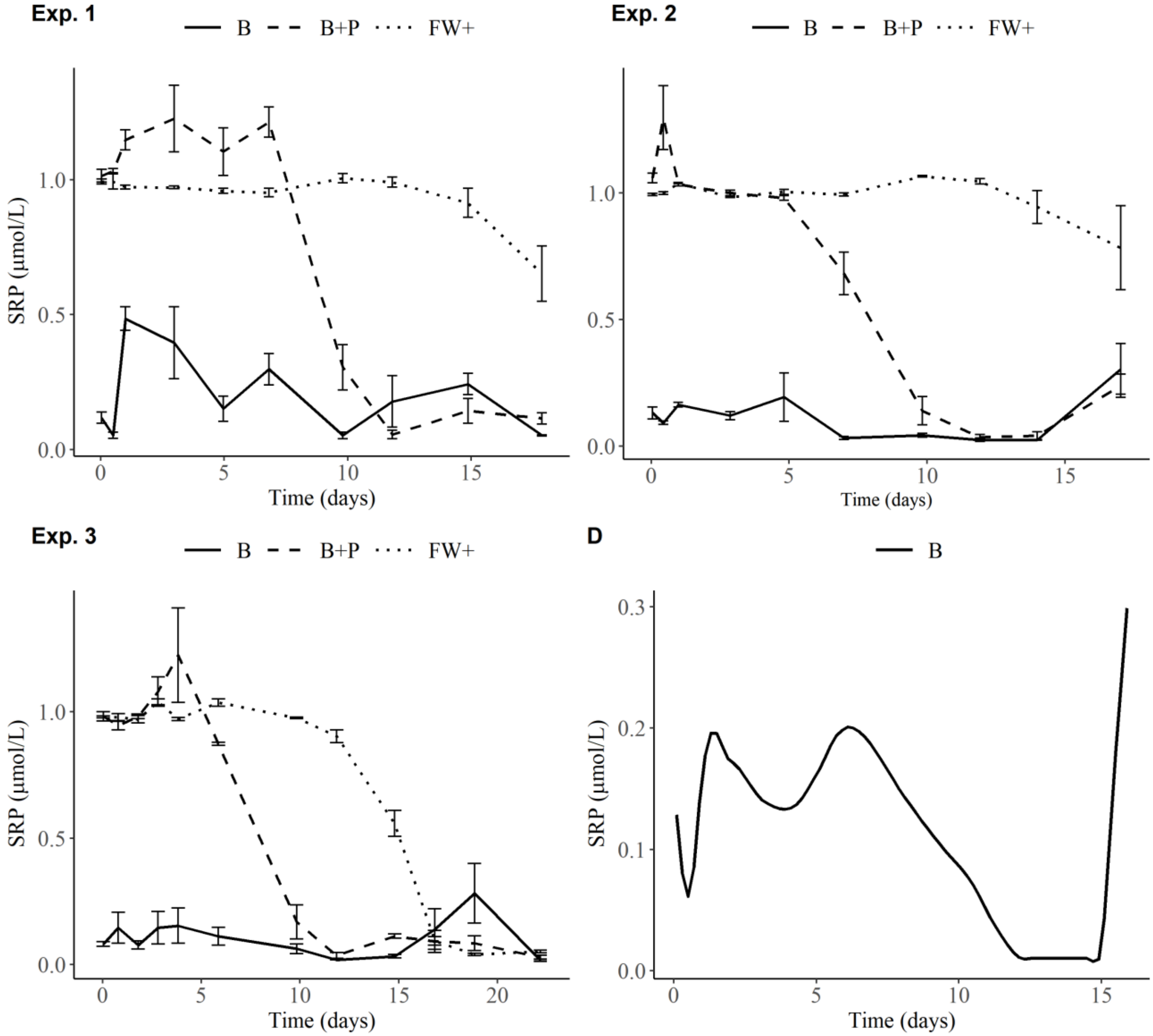

Figure 13: Changes in SRP concentrations in the batch experiment chambers over time. The starting biodeposit mass for experiment 1, 2, and 3 are 1.95 +/- 0.85 mg, 13+/- 0.4 mg, and 10.3 +/- 0.95 respectively. Vertical bars represent the standard error among replicates. Plot D: Conceptual pattern of SRP concentration of the biodeposit treatments over time. The time scale is not the same for all plots and varies based on the duration of the experiment.

SRP decreased in all the chambers in the batch experiments (Fig. 13). The loss of SRP in the control (FW+) was caused by biofilm growth on the sides of the chamber. It is assumed that both biodeposit treatments started to experience biofilm growth at the same point as the FW+

treatment, which was supported by visual inspection of the chamber walls. The SRP concentration in both biodeposit treatments in all trials declined below the detection limit (0.016 μmol/L) around day 10, prior to the start of biofilm effects. In all three experiments, the SRP concentrations in treatments with biodeposits alone (no added phosphate) showed similar temporal trends, albeit with different magnitudes and slightly different timing: a gradual decrease in SRP up to day 10-15, followed by a several-day increase in SRP. In experiments A and C, this was followed by another decrease in SRP (Fig. 13).

The DOP concentration increased in all the chambers with the exception of the B treatment in experiment 2, but DOP concentrations were lower than SRP concentrations, with the exception of FW+ control in experiment 3 (Fig. 14). The DOP concentration in the B+P treatment was consistently higher than in the B treatment. The B+P concentrations of DOP were constantly higher around day 7 to day 12 than the FW+ treatment in each experiment, which may be due to increased bacterial activity on the biodeposits. The FW+ treatment DOP concentration increased after day 10-15 depending on the experiment run, likely due to the biofilm biological activity converting SRP into DOP.

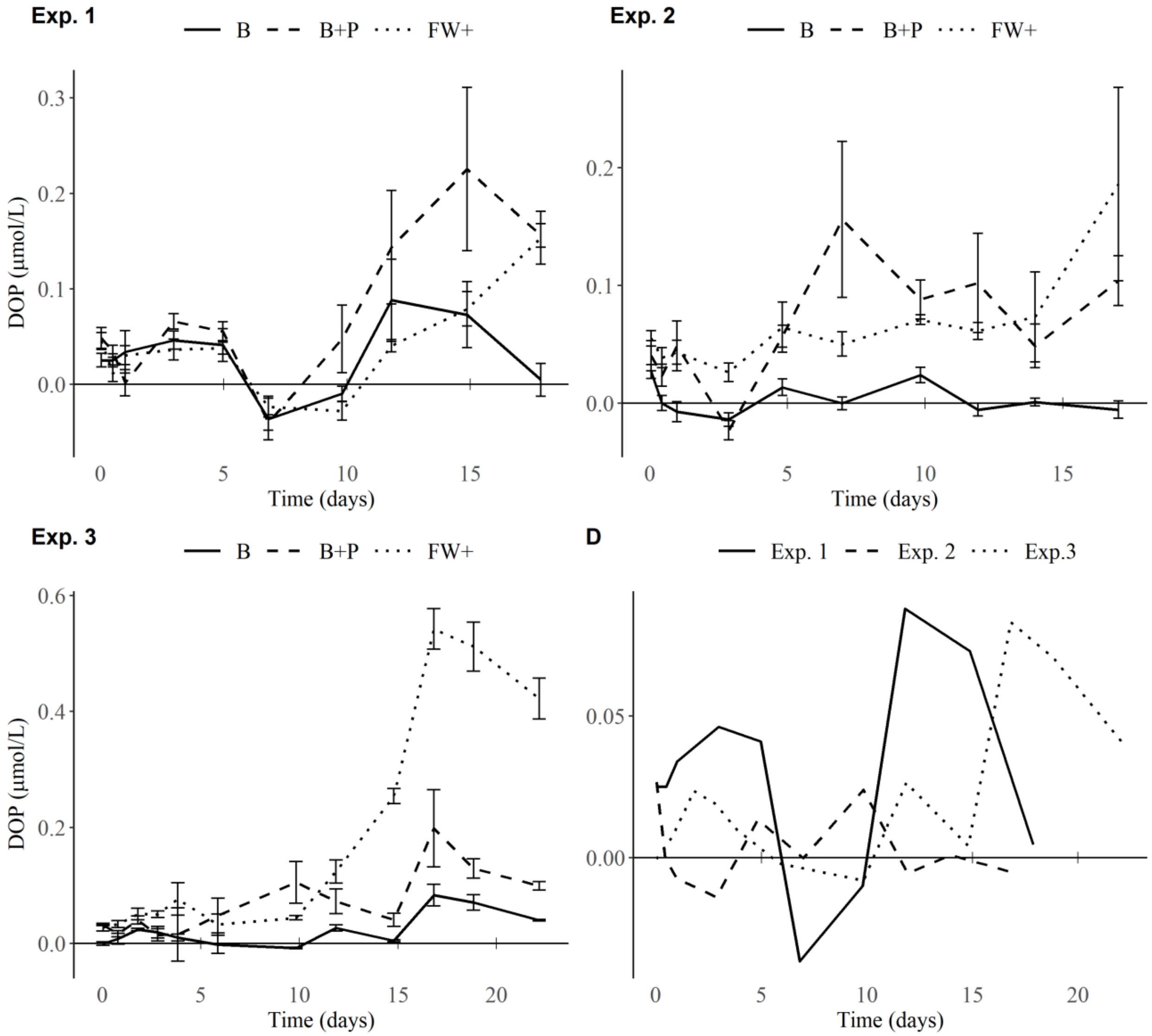

Figure 14: Graphs showing the changes in DOP concentrations in the chambers over time for experiments 1, 2, and 3. The starting biodeposit mass for plots A, B, and C are 1.95 +/- 0.85 mg, 13+/- 0.4 mg, and 10.3 +/- 0.95 respectively. The error bars represent the standard error among the replicates. Plot D: DOP concentration of the biodeposit treatments for all three experiments.

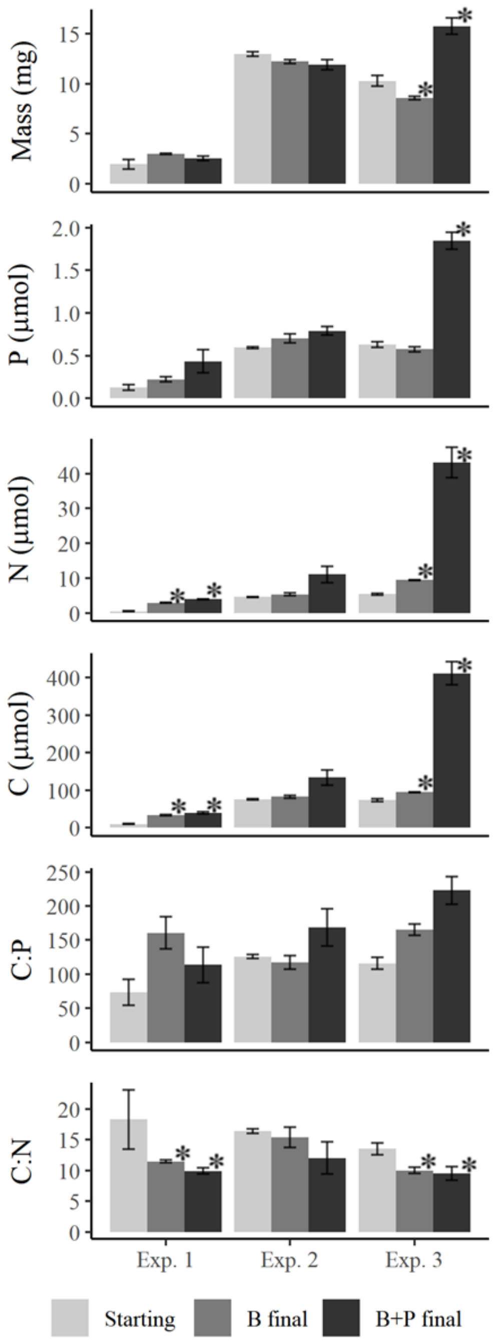

Figure 15: Biodeposit composition in batch experiments 1, 2 and 3 with durations of 14, 17, and 22 days respectively. B represents biodeposits from the filtered water treatment, and B+P represents biodeposits from the filtered water with added phosphorus treatment. Vertical lines represent the standard error among replicates. * symbol represents significant difference between the initial and final composition based on t-test (p< 0.05).

In batch experiment 3 (the longest experiment), the addition of biodeposits + phosphate resulted in a significant increase in the biodeposit mass, along with the total mass of particulate C, N, and P (Fig. 15). A similar increase was observed in batch experiment 1 for C and N. The starting biodeposit mass in experiment 2 was much larger than the starting mass in experiment 1, which may account for the differences in the results of those two experiments. The average concentration of DOC at AW25, the site water was collected for these experiments, was 2.0 ppm with a standard deviation of 0.2 ppm. In experiments 1 and 2, that would equate to about 80 µmol DOC, and in experiment 3, this would equate to about 570 µmol DOC at the start of the experiment. The mass of carbon in the DOC is sufficient to account for the increase in biodeposit carbon for all experiments.

Experiment 3 was exposed to the largest amount of phosphate (3 µmol compared to 0.5 µmol SRP) due to the larger volume of water used in this experiment, and experiment 3 was allowed to continue for the longest period of time making biodeposit composition differences easier to detect in this experiment. The final mass of the biodeposit in the B treatment (no P added) in experiment 3 was significantly lower than the starting mass, indicating that the biodeposits were being decomposed. Similar results are not noted in the other trials most likely due to the shorter durations, although experiment 2 did show that biodeposits were releasing dissolved P near the end of the experiment. Also, Experiment 2 did not result in any significant differences in biodeposit composition, but the biodeposit P mass in the B+P treatment increased (p = 0.08), consistent with the experiment 3 results.

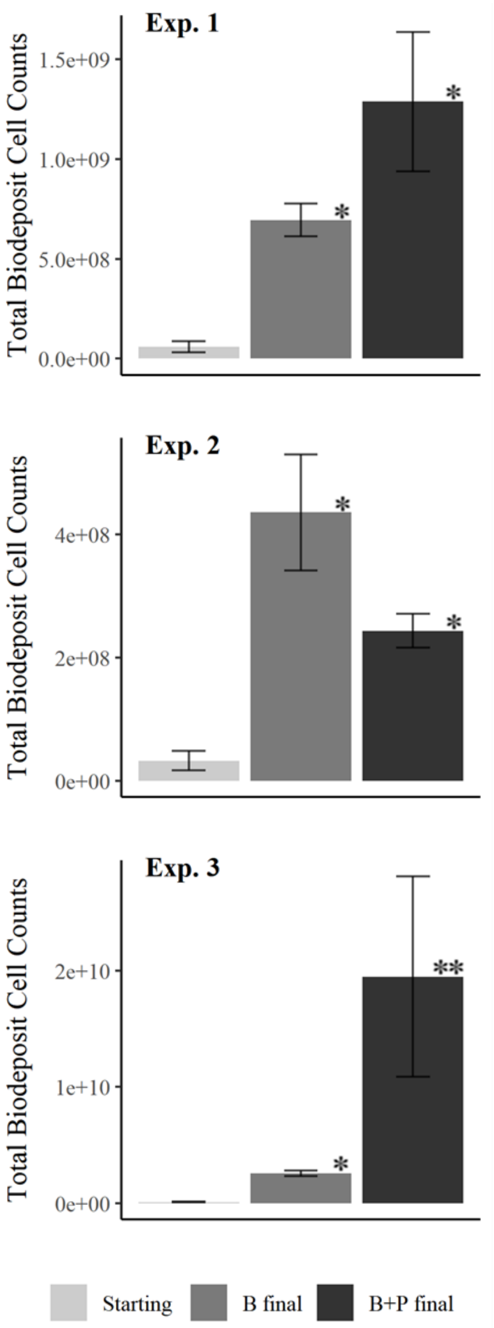

Figure 16: Total bacterial cell numbers on the biodeposits for experiment 1, 2 and 3. * symbol represents statistical difference between the starting cell counts and the ending cell counts for the two treatments based on a t test with a 0.05 significance level. ** symbol represent statistical difference between the B and B+P treatments based on a t test with a 0.05 significance level. The error bars represent standard error.

Bacteria grew on the biodeposits in both treatments in all three experimental runs (Fig. 16). All bacterial cell counts for the biodeposits treatments were significantly higher than the starting biodeposits based on a student's t-test. The bacteria counts were significantly higher in the B treatment for experiment 3, even though the biodeposit mass significantly decreased in this treatment (Fig. 15). This suggests that the change of mass is due to the microbial breakdown of the biodeposit and not by bacteria mortality. The final bacteria counts were not significantly different between the two biodeposit treatments for runs 1 and 2 with p values of 0.12 and 0.06 when compared with a t-test based on a 0.05 significance level. The biodeposit with added phosphorus had a higher bacterial abundance than the biodeposit treatment in experiment 3 with a p-value <0.01.

Biofilm samples were collected in Experiment 3. In this experiment, more phosphorus was assimilated by bacteria growing on the biodeposits than the bacteria going in the biofilm (Table 6). The biofilm in the FW+ control contained a much higher phosphorus mass than the biofilm in either of the biodeposit treatments (Fig. 17), suggesting that much of the phosphorus in the treatments were utilized by bacteria on the biodeposit prior to biofilm growth occurred. The C:P ratio in the biofilms of the B+P treatments was higher than that in the B treatment, indicating that phosphorus was limiting. Accounting for the biofilm in experiment 3 allowed for a phosphorus mass balance for each of the chambers. The total P measured in most of the chambers was slightly less at the end of the incubation compared to the starting amount, but in most cases, the difference was less than 13%. Three biodeposit treatments exceeded this: biodeposit treatment replicate B, and biodeposit treatment with added phosphorus replicates A and C. The biodeposit treatment discrepancies in phosphorus mass balance may be due to leaching of P from the biodeposit immediately following the initial addition (Carlsson 2010). This would have resulted in this P being accounted for twice because the leached P would have been included in the initial dissolved P pool and particulate pool because initial dissolved P measurements were taken 1 hour after the biodeposit addition. The B treatment replicate A is not included in the budget because the glass chamber broke prior to when the biodeposits could be sampled.

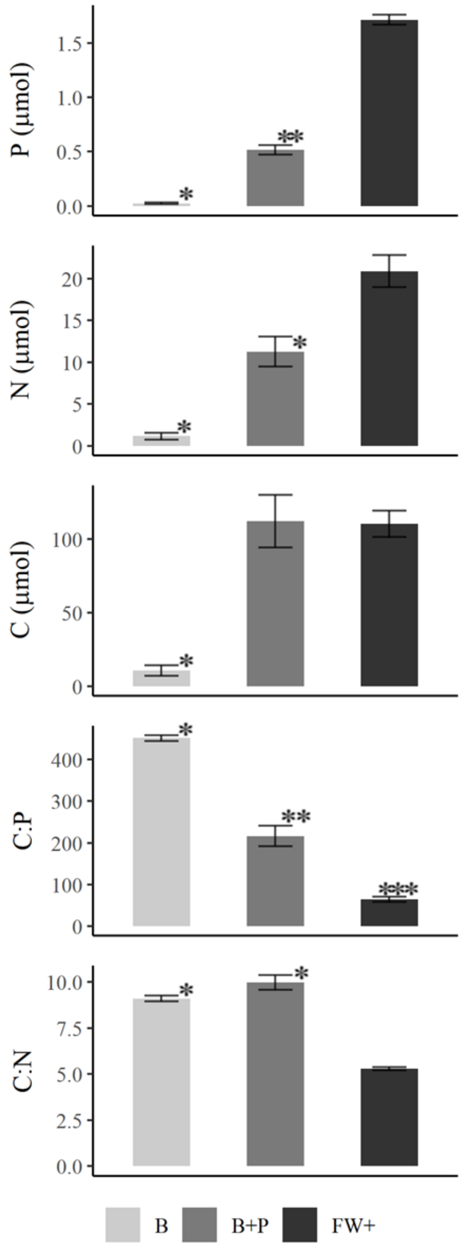

Figure 17: Bar plot showing the differences in the biofilm composition within the three treatments of experiment 3. Error bars represent standard error among replicates. * symbol represents statistical difference based on one-way ANOVA results to the 0.05 significance level. Columns that contain the same number of * symbols are not significantly different from one another.

Table 6: Phosphorus mass balance for experiment 3 for the filtered water with added phosphorus (FW+), biodeposits treatment (B), and biodeposit treatment with added phosphorus (B+) chambers. All P values are in μmol. The final column represents the difference between the starting total P and ending P.

	Rep.	Starting DP	Starting P Biodeposits	Starting Total P	Final P Biodeposits	Final Biofilm P	Final DP	DP removed for analysis	Ending Total P	Starting and ending difference
FW+	A	3.09	NA	3.09	NA	1.74	1.08	0.36	3.17	-0.08 (7%)
	B	3.01	NA	3.01	NA	1.61	1.51	0.32	3.44	-0.43 (13%)
	C	2.97	NA	2.97	NA	1.80	1.16	0.31	3.27	-0.30 (9%)
B	B	0.29	0.63 ± 0.06	0.90	0.53	0.04	0.13	0.06	0.76	0.16 (22%)
	C	0.23	0.63 ± 0.06	0.83	0.62	0.01	0.15	0.05	0.83	0.02 (3%)
B+	A	3.16	0.63 ± 0.06	3.77	1.62	0.57	0.35	0.27	2.82	0.97 (35%)
	B	2.97	0.63 ± 0.06	3.58	2.04	0.56	0.39	0.26	3.26	0.34 (10%)
	C	2.99	0.63 ± 0.06	3.60	1.87	0.41	0.27	0.20	2.75	0.87 (32%)

Flow Through Experiment

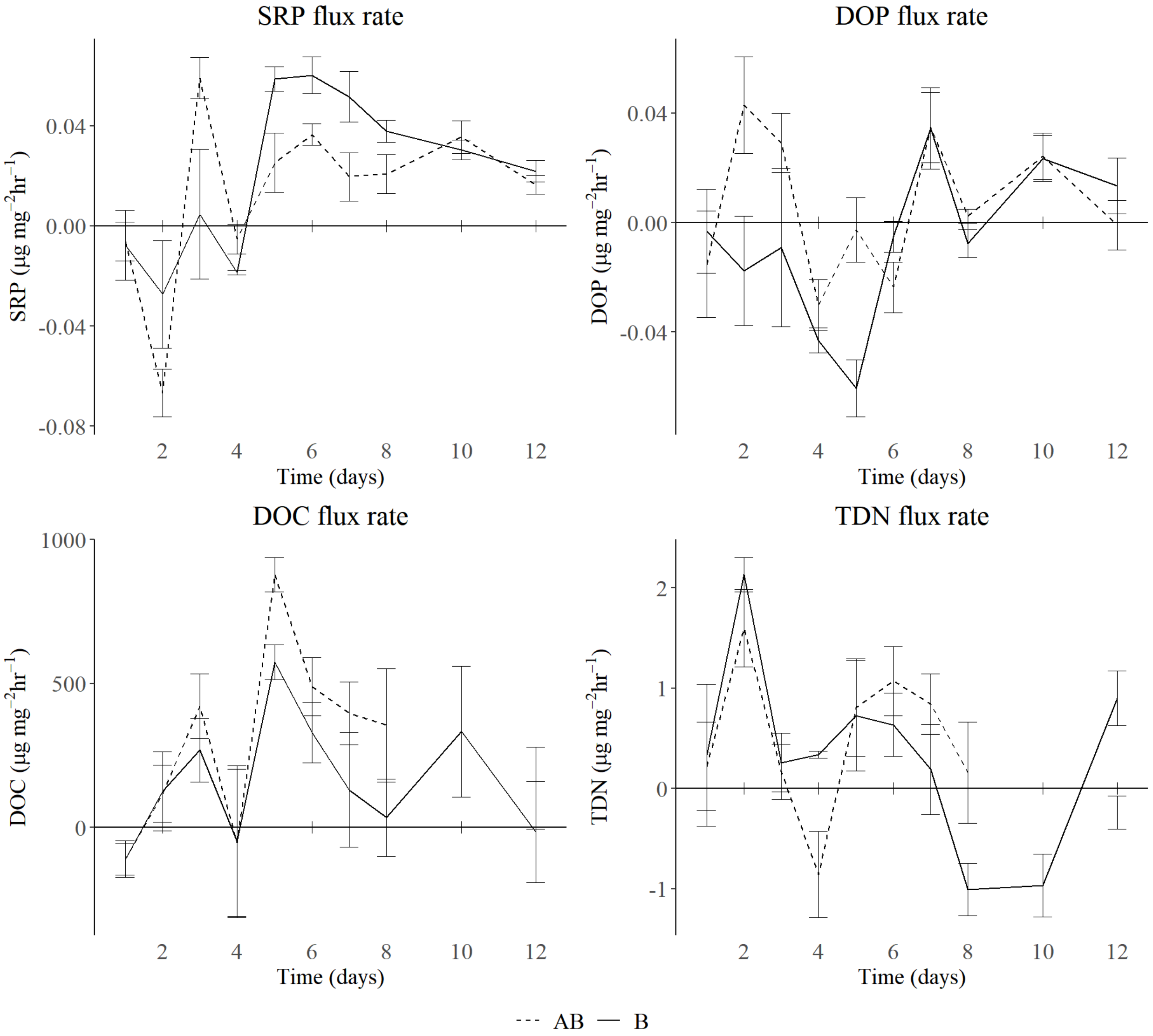

Figure 18: Flux rates of SRP, DOP, DOC, and TDN in flow-through chambers with biodeposit alone (B) and biodeposit + antibiotic (AB) normalized to the control and starting biodeposit mass. Vertical lines represent the standard error among replicates. Positive values indicate nutrient capture, and negative values indicate nutrient release by the biodeposit.

Growth of biofilm in the AB treatment chambers indicated there was growth of antibiotic resistant bacteria. As a result, the uptake rates of SRP, TDP, DN, and DOC in the AB treatment were similar to those in the treatment with biodeposit only (Fig. 18), although there were some notable differences. The AB treatment released a high amount of SRP on the second day of the incubation, possibly due to the death of bacteria caused by the antibiotic. Subsequently, SRP uptake increased on day three, suggesting antibiotic resistant community began to grow at that time. After day three, the carbon and nutrient fluxes were similar in the two treatments. The AB treatment assimilated a large portion of DOP on day 2 and 3, while the B treatment was continuously losing DOP until day 6. The initial uptake in DOP in the antibiotic treatment (AB) may be due to the mode of action of ciprofloxacin, which inhibits DNA replication through disrupting DNA topoisomerase and DNA-gyrase. The inhibition of DNA replication may have caused the antibiotic resistant bacteria to use some DOP to meet their cellular requirements (Sisma-Ventura & Rahav 2019). On day 6, the DOP fluxes of the two treatments were nearly identical. Between days 5 and 12, the flux of SRP decreased in both the B and AB experiments, possibly due to the stabilization of the bacterial community.

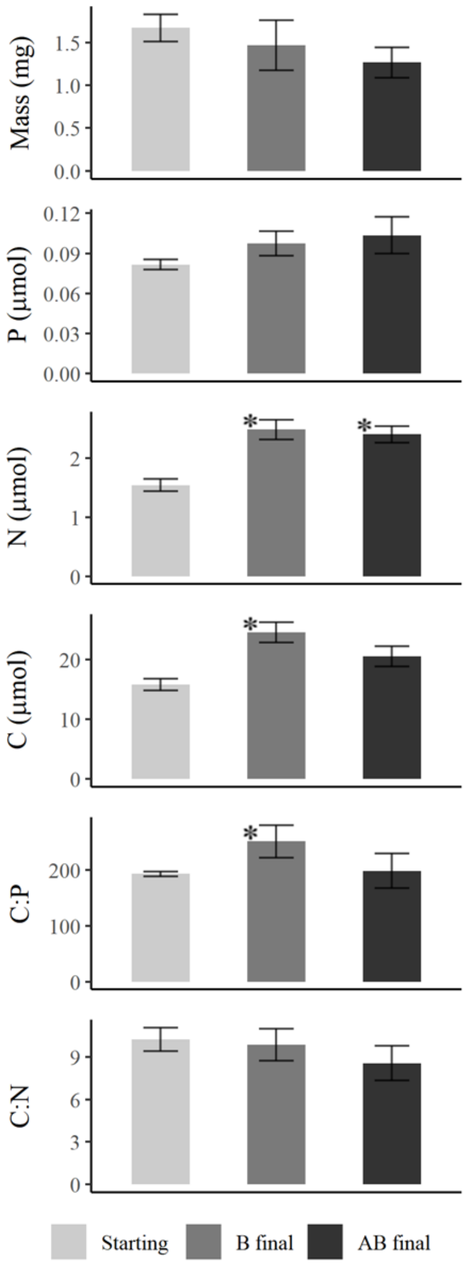

Figure 19: Changes in biodeposit mass and composition during the flow through experiment in chambers with biodeposits only (B) and biodeposits + 5 µg/L ciprofloxacin (AB). Flow-through experiment contained a dissolved phosphate concentration of 0.065 µmol/L, and was conducted for 12 days. Vertical lines represent the standard error among replicates. * represents statistical difference between the treatment and the starting biodeposit using a t test with a 0.05 significance level.

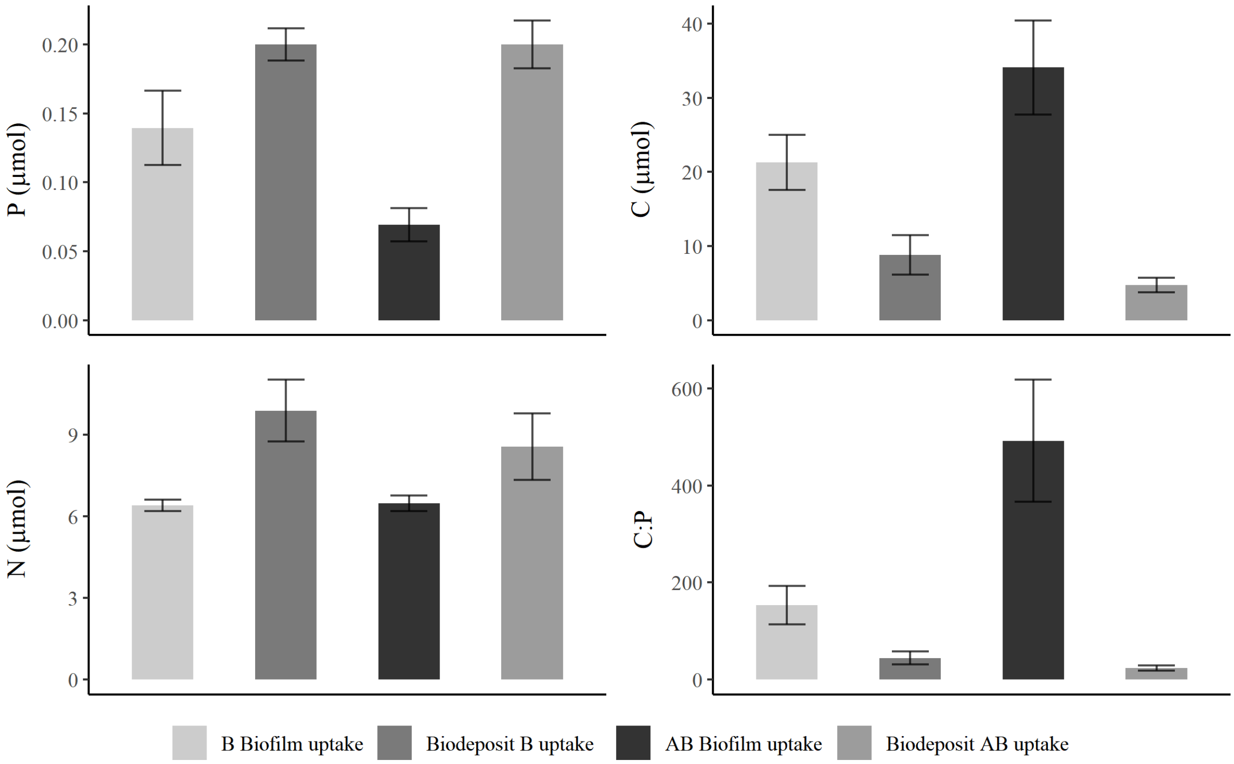

Figure 20: Uptake P, C, N, and C:P ratio of the captured nutrients by the biofilm and biodeposits in the flow-through experiment. Vertical lines represent the standard error among replicates. Flow-through experiments was conducted for 12 days.

In both treatments, the biodeposit N mass increased significantly over time. Significant increases of biodeposit C and C:P only occurred in the B treatment (Fig. 19), suggesting that bacterial growth was at least partially inhibited in the AB treatment. The final mass of the AB biodeposits was lower than the starting mass (p = 0.06), which may be caused by initial changes caused by the antibiotic treatment. The bacteria assimilated more phosphorus and nitrogen on the biodeposit than the bacteria in the biofilm. However, more carbon was assimilated by biofilm bacteria (Fig. 20). DOC uptake may have been driven more by bacteria growing on the chamber walls than bacteria growing on the biodeposits. Still, the biodeposit increased in C mass for the biodeposit-only treatment demonstrating that DOC was also taken up by biodeposit bacteria.

Discussion

Nutrient uptake by bacteria

Bacteria growing on the biodeposits are using dissolved forms of phosphorus, carbon, and nitrogen to meet growth requirements. Carbon and nutrient uptake was demonstrated by the decrease in phosphorus in the batch experiments and nutrient flux rates in the flow-through experiment. Nutrient ratios dictate bacteria uptake in nutrients from biodeposits. Heterotrophic bacteria tend to maintain internal nutrient ratios through the process of homeostatic maintenance, as has been demonstrated for Escherichia coli (Makino et al., 2003). However, there is evidence that bacteria are more flexible with C:P ratios than C:N ratios (Cotner et al., 2010). The flexibility in C:P ratios is most likely due to the ability to substitute sulfolipids for phospholipids in membranes (Geiger et al., 1999; López-Lara et al., 2003; Cotner et al., 2010). In order to maintain nutrient ratios, bacteria utilize dissolved nutrients to supplement those available in the biodeposits. The mean starting C:N:P of the biodeposits in this study was 112:7:1 for the batch experiments and 193:19:1 for the flow-through experiments, with the difference due to the different mussel collection depths. Based on these ratios, a large decrease in the C:P ratio for the flow-through experiments was expected, but the C:P increased. The DOC to DP ratio in the inflow water was 1500:1, so the increase in C:P ratio in the biodeposits in the flow-through experiment may be caused by the relatively low amount of dissolved phosphorus available in the incubation. However, the C:N ratio of the biodeposits did not change in the flow-through experiment and decreased in the batch experiments. These results are consistent with observations by Cotner et al. (2010) that bacteria maintain C:N ratios and are more variable with C:P ratios.

This study demonstrates bacterial colonization of biodeposits but does not explore the grazing of bacteria that might lead to the subsequent release of nutrients. In pelagic systems, bacteria utilize large portions of phosphate competing with phytoplankton for this resource (Cotner and Wetzel, 1992), but bacteria do not represent long-term storage of nutrients due to high grazing by protozoa (Scavia and Laird, 1987; Carrick et al., 1992; Kirchmann, 1994). The results from this study demonstrate that bacterial growth on the biodeposits acts as a sink for dissolved P for two to three weeks, after which the biodeposits become a net P source. However, the experiments were conducted in filtered water to observe the effects of bacteria growth. Unfiltered lake water would likely have a more significant release of biodeposit nutrients due to a higher protozoan to bacteria ratio than was present in these experiments (van Broekhoven et al., 2015). The only way protozoans could enter the chambers was through the biodeposit slurry. Marine studies have also demonstrated that biodeposit decomposition rate over sediment is higher than in experiments with water alone (van Broekhoven et al., 2015; Giles and Pildith, 2006; Jansen et al., 2012), most likely due to mature bacteria and protozoan communities in the sediment. A study of zebra mussels' effects on nutrient regeneration at the sediment-water interface showed that the presence of zebra mussels altered the community composition of protozoans in the sediment with an increased relative abundance of Uronema sp. (Lavrentyev et al., 2000). Smaller protozoans, like Uronema sp., rely on bacteria as a food source and have higher growth rates than larger protozoa, making them effective controls of bacteria abundance (Finlay and Esteban, 1998). While the experiments presented in this study demonstrate the effects of biodeposits on bacteria growth, more work is needed to understand the role of sediment protozoa because bacteria-protozoa interactions may have important implications for nutrient cycles.

Role of Benthic Invertebrates

Dreissenid mussels may promote other invertebrate communities by providing food in the form of biodeposits and by enhancing habitat structure (Bially et al., 2000). Lohner et al. (2007) observed increases in benthic invertebrate numbers under dreissenid clusters and an increase in the ability to utilize different carbon sources. In the Lake Michigan profundal benthos, the densities of non-dreissenid benthic invertebrates, especially Diporeia and Sphaeriidae, have declined (Burlakova et al., 2018). However, offshore oligochaete populations have increased since the expansion of dreissenid mussels and may be benefiting from dreissenid mussels (Burlakova et al., 2018; Mehler et al., 2020). In nearshore zones, an increased abundance of amphipods, isopods, oligochaetes, and chironomids have been associated with the expansion of dreissenid mussels (Stewart et al., 1998; Kuhns and Berg, 1999; Jimenez et al., 2011). There have been many studies examining the effects of benthic invertebrate community changes on Lake Michigan food webs (Pothoven and Madenjian, 2008; Bunnell et al., 2009; Turschak et al., 2014; Madenjian et al., 2015). However, relatively little work has examined how these changes may alter organic matter cycling in the benthos in Lake Michigan, which has important implications for nutrient cycles (Mermillod-Blondin and Rosenberg, 2006). Future work should examine the connection dreissenid mussels, other invertebrate communities, and the brown food web in the Great Lakes.

Implications for Lake Michigan Nutrient Cycles

The results from our batch experiments indicate that bacterial growth on biodeposits may depend on ambient dissolved phosphorus concentrations. The excretion of dissolved P by profundal quagga mussels in Lake Michigan (Mosley and Bootsma, 2015) may result in concentrations of dissolved P in the near-bottom layer that are much greater than those in the water column. In the profundal region, near-bottom turbulence is relatively low much of the time, which may allow for the accumulation of dissolved P in the near-bottom boundary layer. In a separate study, measurements of SRP concentration 3 cm above the mussel bed at the AW55 site were measured and were four times greater than that one meter from the bottom with a concentration of 2 µg/L (Jin, 2019). This concentration was used in the flow-through experiment in order to simulate in situ conditions. Our results suggest that a portion of dissolved P excreted by mussels may be assimilated by bacteria growing on biodeposits. However, there remains uncertainty about the long-term fate of biodeposit-bound nutrients in Lake Michigan. It appears that at least some of this P is eventually recycled, as demonstrated by the long-term increase in dissolved P concentration in some of the batch experiments. However, the mass of biodeposit phosphorus either did not change or increased over the duration of the experiments. The total mass of the biodeposits in our batch experiments decreased by only 17% after 22 days in filtered lake water and actually increased over the same period when exposed to a dissolved phosphate concentration of 1 mmol/L, indicating that biodeposit decomposition is affected by ambient nutrient concentrations.

The importance of biodeposit recycling was explore through a 1-d model of phosphorus dynamics at a 55 meter site similar to AW55. The results indicate that a portion of freshly produced biodeposit bound phosphorus (between 25-50%) must be recycled within 1 day to maintain water column concentrations of phosphorus (Fig. 21). Water column total phosphorus concentrations measured over the course of 2018 were relatively constant with a mean of 0.09 µmol/L. If no biodeposits are recycled, then water column phosphorus concentrations would drop until stabilizing at low concentrations after 80 days. The model does not take into account bacteria uptake of nutrients, which would further deplete the water column of phosphorus. The model clearly demonstrates biodeposits do not represent a sink of nutrients, and regeneration of biodeposit needs to be accounted for in future Lake Michigan nutrient models.

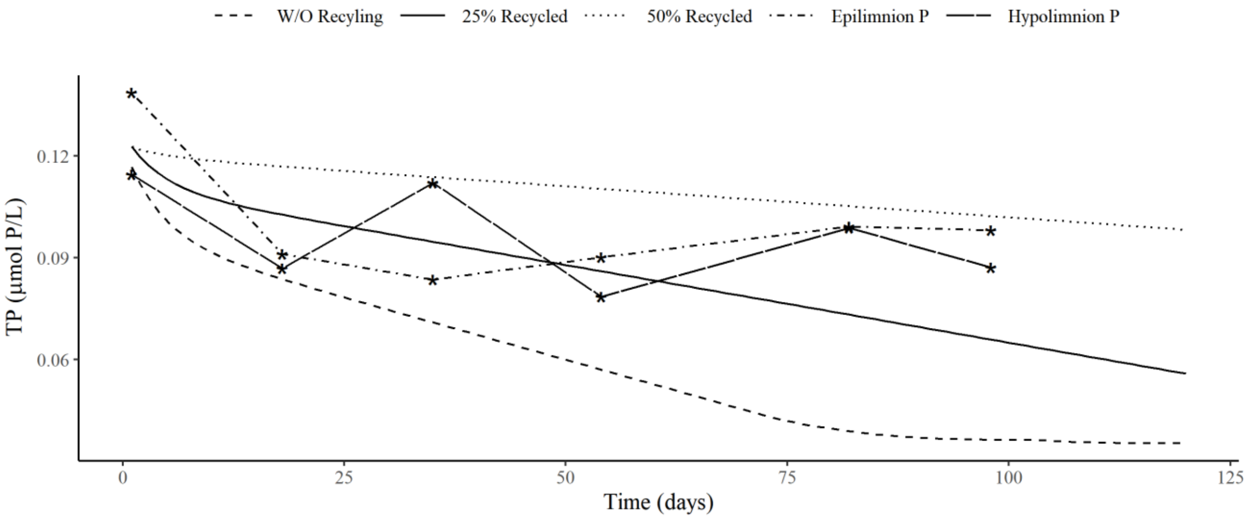

Figure 21: Model showing the simulated water column depletion of phosphorus due to biodeposit production under mixing conditions. Starting TP values were those measured in July 2018 because TP measurements were highest on this date for the year 2018. The epilimnion P and hypolimnion P are measurements from the AW55 site during the 2018 field season.

Summary

The long-term fate of dreissenid biodeposits has important implications for the Lake Michigan phosphorus cycle because they represent a significant fraction of the P removed from the water column due to mussel grazing. The results of the study demonstrated that biodeposits promote the growth of bacteria, which causes biodeposits to be a short term sink in dissolved phosphorus. However, a simple model simulation indicates that total pelagic P concentrations would be much lower than observed if biodeposit P were not recycled. Hence a significant fraction of biodeposit P must be recycled over the long term to maintain observed TP concentrations. While bacteria growing on biodeposits appear to act as a P sink, we suggest that grazing of bacteria by protozoans promotes P recycling. Future work should focus on bacteria -

protozoan - macroinvertebrate relationships in the benthos, and their implications for nutrient recycling and energy transfer.

CHAPTER 4: Internal loading of phosphorus in Lake Michigan post dreissenid mussel invasion

Abstract

Since the expansion of dreissenid mussels in Lake Michigan, there has been limited investigation of changes to internal loading of phosphorus despite known differences in physical and chemical processes, including the absence of calcite whiting events, decreased nepheloid layer, and increase retention of nutrients in the benthos. This study examines internal phosphorus loading at two sites: one from the depth region with the highest mussel density, and a deeper site that experiences high deposition. Despite lower water column concentrations of total phosphorus, the current sediment burial rate of phosphorus is similar to rates measured in the 1980s, reflecting a decrease in water column phosphorus residence time. Approximately 60% of recently deposited phosphorus at the sediment-water interface is recycled back into the water column. Organic phosphorus and non-apatite inorganic phosphorus were the most readily recycled forms of phosphorus within the sediment. However, apatite bound phosphorus represented a further sink of dissolved phosphorus at the shallower site and a source of phosphorus at the deeper site less impacted by mussels. Measurements of sediment fluxes including sedimentation, accumulation, and permanent burial rate were combined with mussel fluxes to create a new conceptual model of internal P cycling in Lake Michigan. Before the mussel invasion, zooplankton within the water column were responsible for the bulk of phosphorus recycling. In the new model, the majority of phosphorus cycling occurs in the benthos with heterotrophic bacteria playing a larger role.

Introduction

Dreissenid mussels entered the Great Lakes in the 1980s. The early invasion was characterized by the rapid expansion of zebra mussels in the littoral zone. However, they were eventually displaced in Lake Michigan by quagga mussels due to their ability to colonize soft substrate (Dermott & Munawar 1993), lower metabolic rates (Stoeckmann 2003; Baldwin et al. 2002; Tyner et al. 2015), and ability to reproduce in colder profundal regions (Roe & MacIsaac 1997; Glyshaw et al. 2015). As quagga mussels expanded into deeper areas, spring primary production and total phosphorus concentration decreased due to the strong grazing effects of mussels (Fahnenstiel et al. 2010; Rowe et al. 2017; Bockwoldt 2018). Before the mussel invasion, the majority of phosphorus cycling occurred in the water column by zooplankton, but zooplankton abundances have decreased with the mussel invasion (Vanderploeg et al. 2012). Currently, a large amount of phosphorus is cycled in the benthos because quagga mussels are effective nutrient recyclers, and increased benthic cycling has led to the resurgence of the nuisance benthic algae, *Cladophora* (Auer et al. 2010; Bootsma et al. 2015). However, there is a limited understanding of the indirect effects of mussels on phosphorus cycling, including the exchange of nutrients at the sediment-water interface.

Phosphorus speciation analysis on sediments is rarely conducted in oligotrophic systems saturated with oxygen throughout the year due in part to the paradigm that phosphorus release from sediment is controlled by fluctuations in dissolved oxygen (Hupfer & Lewandowski 2008). However, in the 1980-1990s there was a series of studies that examined internal loading in Lake Michigan in response to efforts to reduce phosphorus loading and to understand phosphorus sources for the spring phytoplankton bloom (Eadie et al. 1984; Conley et al. 1988; Nürnberg 1991; Shafer & Armstrong 1994; Brooks & Edgington 1994). During this period in Lake

Michigan, the internal loading of phosphorus from sediment was controlled by apatite dissolution (Brooks and Edgington 1994), microbial decomposition of organic matter, and resuspension events (Eadie et al. 1984; Shafer & Armstrong 1994). Before the mussel invasion, less than 40% of phosphorus that reached the sediment surface was permanently buried, and the low burial efficiency resulted in a residence time of 5 years for phosphorus within the water column (Shafer & Armstrong 1994). However, the phosphorus residence time in the water column may be affected by quagga mussels. High excretion rates of dissolved phosphorus (Mosley & Bootsma 2015) at the sediment-water interface may interfere with apatite dissolution, which is driven by a decrease in dissolved phosphorus concentrations above the sediment causing a shift in the equilibrium of dissolved and apatite bound phosphorus (Brooks and Edgington 1994). Apatite bound phosphorus can be formed through precipitation, adsorption, and biological mediated processes (Dittrich 2000; Goldhammer et al. 2010; Sø et al. 2011). Adsorption vs. precipitation is partially mediated by the surrounding dissolved phosphorus concentration (Sø et al. 2011). Higher excretion rates may also increase pore water concentrations of dissolved phosphorus, leading to increased precipitation (Dittrich 2000). Along with excretion of dissolved phosphorus, mussel grazing during the isothermal period has led to the loss of the spring phytoplankton bloom (Vanderploeg et al. 2010). Historically, the high demand for phosphorus during the bloom would decrease phosphorus concentrations at the sediment-water interface, causing apatite dissolution (Brooks & Edgington 1994).

Besides effects on apatite bound phosphorus, dreissenid mussels may decrease offshore pelagic phosphorus concentrations through retention in both the nearshore zone (Hecky et al. 2004) and profundal benthos (Chapra & Dolan 2012; Mosley & Bootsma 2015; Rowe et al. 2017). Since the establishment of mussels, the nepheloid layer has disappeared due to the filtering activities of the mussels (Watkins et al. 2007). Prior to the mussel invasion, the presence of the nepheloid boundary layer during stratification increased soluble reactive phosphorus within the benthic region (Eadie et al. 1984), indicating that the nepheloid boundary may have enhanced sediment cycling of phosphorus. Mussels may also reduce resuspension by aggregating particles in biodeposits (Hecky et al. 2004). Along with changes in sediment suspension, some studies have suggested that mussels increase the apparent settling velocity particles within the water column by decreasing the residency time of small particles in the water column (Chapra and Dolan 2012; Shen et al. 2018). At the same time, mussels increase the amount of organic material at the sediment-water interface, which can increase microbial activity leading to more rapid cycling of the freshly deposited material (Giles & Pilditch 2004, 2006). Microbial activity and bioturbation by mussels can also alter dissolved oxygen penetration within the sediment, causing potential changes to redox-sensitive forms of phosphorus (Vaughn & Hakenkampt 2001; Newell 2004; Giles & Pilditch 2004; Turner 2010).

Along with the expansion of dreissenid mussels, phosphorus loading decreased in Lake Michigan (Dolan & Chapra 2012), and the combined effects of reductions in loading and mussel grazing have resulted in lower water column total phosphorus concentrations (Mida et al. 2010; Rowe et al. 2017). Even though lake Michigan has a long hydrological residence time, the lake should respond to internal and external changes to phosphorus loading within 5-15 years (Shafer & Armstrong 1994; Katsev 2017). Despite the indirect effects of mussels on nutrient cycling and decreased phosphorus loading, there has been limited effort to determine changes to the internal loading of phosphorus in Lake Michigan since the 1990s. The research presented here examined the internal fluxes of phosphorus from sediment in two regions – one mid-depth region where mussel densities are high, and a deeper region where mussel densities are lower but deposition rates are higher. The measurements of internal cycling are combined with other measures of mussel-mediated phosphorus fluxes to create a conceptual model of internal phosphorus dynamics within Lake Michigan.

Methods

Sediment collection

Sediment was collected from offshore Lake Michigan from two different sites during the 2018-2019 field seasons. Cores were collected from a 55 meter deep station offshore from Milwaukee in July 2018 with coordinates 43˚ 04.498'N 87˚45.581'W, and cores were collected from a 100 meter deep station offshore from Muskegon in July 2019 with coordinates 43˚ 11. 182'N 86˚ 30.544'W. The mussel densities are 7136 ± 3105 and 2,747 ± 858 mussels m^{-2} at the 55 and 100 meter site respectively (Chapter 2; Nalepa et al. 2020). The historical sediment accumulation rate at the 55 depth offshore of Milwaukee ranges from -0.010 to 0.008 g cm^{-2} yr^{-1}, and the historical accumulation rate near the 100 meter site ranges from 0.099 to 0.2 g cm^{-1} yr^{-1} (Eadie et al. 2008).

Cores were collected in polycarbonate tubes using a gravity corer and were immediately placed in a cooler in the upright position in the dark. Six cores were collected from each site. After transport to the laboratory, a dissolved oxygen profile was measured with a subset of cores using a Neo Fox optical dissolved oxygen probe that was secured to a stand using a three-prong clamp. The probe was inserted vertically into the sediment in 0.2 cm intervals by adjusting the position of the clamp by hand. Sediment was then extracted using a hydraulic extruder. Sediment was subdivided into 0.2-0.5 cm sections for the first 3 cm, and 0.5 cm sections below 3 cm. After the wet mass was determined for each section, the sediment was air dried.

Sediment Pore Water SRP

Pore water samples were collected at the 100 meter site. Pore water was collected using Rhizon samplers with a diameter of 2.5 mm and a pore size of 0.15 μm. The samplers were inserted into predrilled holes in the polycarbonate tube that were sealed using silicone tape. The rhizon sampler tubing was connected via a sterile needle to an acid washed vial that was under vacuum pressure, allowing the pore water to flow through the filter of the sampler and into the collection tube. The collected water was analyzed for soluble reactive phosphorus (SRP) content using the molybdate-antimony method (Stainton et al. 1974).

The pore water concentration profile of SRP was used to determine sediment SRP flux based on Fick's first law of diffusion:

$$F = \rho \times D_s \times \frac{\Delta c}{\Delta z} \tag{6}$$

where F is the flux (μmol cm^{-2} s^{-1}), ρ is the porosity as a proportion of pore volume to total volume, D_s is the diffusion coefficient in cm^2 s^{-1}, c is the concentration of SRP (μmol cm^{-3}), and z is the depth of sediment (cm). D_s can be calculated using the Stokes-Einstein relationship:

$$\frac{DV}{t} = \frac{D_s V_s}{t_s} \tag{7}$$

where D is the diffusion of phosphate ions in water at 18˚C (Li & Gregory 1974), V is the kinematic viscosity of freshwater at 18˚C, and t is 18˚C. V_s is the viscosity of water at ambient temperature (ITTC 2011), and t_s is the ambient temperature for the core.

Porosity and Dry Bulk Density

Porosity (φ)is calculated as:

$$\rho = \frac{f_w}{(f_w + (1 - f_w)\rho_w/\rho_s} \tag{8}$$

Where ρ is porosity, f_w is the fraction of water in the wet sediment, ρ_w is the density of pore water (1 g cm^{-3}), and ρ_s is the density of dry solids, set at 2.5 g cm^{-3} (Baskaran et al. 2014). The fraction of water in wet sediment is determined from the loss of mass following drying.

Bulk density is calculated as:

$$Dry\ bulk\ density\ (g/cm3) = \frac{weight, Dry\ sample\ (Wd)}{Total\ sample\ volume\ (Vt)} \tag{9}$$

Burial Rate

The radionuclide ^{210}Po was measured in each sediment subsection in two cores from each site as a proxy for ^{210}Pb (Robbins & Edgington 1975; Waples 2020). ^{209}Po was added to approximately 0.5g of homogenized dried sediment in order to determine the efficiency of the extraction recovery, which is used to calculate the activity of the sample. Following the addition, the spiked sediment was digested with 50ml of 6N HCl and 30% hydrogen peroxide for four hours. The filtrate was removed by filtering through Whatman number 42 filter paper. The filtrate was boiled down to 5ml, and then the volume was increased to 50ml with 0.1 M HCl. The pH of the solution was adjusted to 0.5-1.0 with 6 M HCl, and 0.1g of L-ascorbic acid (powder) was added to complex out any dissolved iron in the sample. The Po isotopes were plated onto polished 2.2 cm diameter copper discs at 90˚C for 24 hours (Mackenzie & Scott 1979). Duplicates were run within each grouping of samples, and duplicates were run for each sample at the 55 meter site. The duplicates differed by less than 10%.

The sedimentation rate for each site was determined using the rapid steady-state mixing model, as described in Robbins and Edgington (1975). Activity of ^{210}Pb was first plotted against cumulative mass to correct for compaction. The sedimentation rate (g cm^{-2} yr^{-1}) was then calculated as:

$$S = \frac{\lambda(m_2 - m_1)}{ln(\frac{A_1}{A_2})} \tag{10}$$

where λ is the radioactive decay constant for ^{210}Pb, A is the unsupported active decay rate (decays min^{-1} g^{-1}), and m is the cumulative mass at each depth (g cm^{-2}). The unsupported active decay is calculated by subtracting the supported decay from the total measured decay. The supported decay is the decay rate at depths where the activity is constant over depth. The supported decay was 0.38 pCi g^{-} at the 55 meter site, and 0.29 pCi g^{-} at the 100 meter site. The sedimentation rates were then used to calculated sediment age (years) as:

$$A = \frac{C}{S} \tag{11}$$

where C is the cumulative mass of dry sediment in g cm^{-2}. The sediment core aging was truncated when the uncertainty in age was greater than the difference in ages between two subsections.

Phosphorus fractionation

The particulate phosphorus fractions within the sediment, including inorganic (IP), organic (OP), total (TP), non-apatite inorganic (NAIP), and apatite bound (AP) phosphorus, were measured using a sequential extraction procedure (Ruban et al. 1999). This method was chosen for its reproducibility, although this method may overestimate bioavailable inorganic phosphorus, and loss of organic phosphorus is possible during calcification, which is common with methods that use burning to isolate organic phosphorus (Pardo et al. 2003). All sediment extractions were conducted on a shaker table overnight, with the exception of the second night of the NaOH extraction (Ruban et al. 1999). At least 200 mg of dried sediment were used for each extraction. A NaOH extraction was used to determine NAIP with a subsequent HCl extraction to determine AP. IP was determined using 1N HCL extraction. The sediment remaining after IP analysis was calcinated at 450˚C for 3 hours, followed by 1N HCl extraction to determine OP. TP was determined by calcinating the samples at 450˚C for 3 hours with a subsequent HCl extraction. All extraction solutions were diluted with type 1 water and were analyzed for dissolved phosphorus using the molybdate blue method as described by Stainton et al. (1974). Samples were diluted to ensure color development because HCl can inhibit the molybdate blue reaction (Nagul et al. 2015). Blanks of the extractants were run from start to finish for each sediment sequential excretion.

Carbon and nitrogen analysis

Total carbon and nitrogen were determined for both the 55 meter site and 100 meter site using an elemental analyzer (Carlo-Erba model: NA 1500 NCS) with acetanilide standards ranging from 0.2 to 1.0 mg. Organic carbon was determined using the elemental analyzer after acidification for the 100 meter site cores. Before analysis, 100 mg of dried sediment was weighed into a glass centrifuge tube, and 250 μL of 1M HCl was added to the sediment. Sediment was placed in an ultrasonic bath for 30 seconds, and then vial was left loosely covered in a fume hood for one hour. After the one hour period, 100 μL of 1M HCl was added following the process used for the first addition until effervescence ceased (Brodie et al. 2011; Komada et al. 2008). The sediment was washed with type 1 water after digestion and dried in a desiccator at room temperature prior to weighing for organic carbon content analysis. Inorganic carbon was calculated as the difference between total carbon and organic carbon.

Sediment traps

Sediment traps were deployed at the AW55 site from April 5th until October 10th during the 2018 field season. The traps were 15.25 cm in diameter and were deployed in triplicate at depths of18, 35, and 53 m. Chloroform (5ml) was added to each trap to preserve settled particulate matter. Trap material was collected monthly. The collected trap material was air dried and weighed to the nearest mg, after which it was analyzed for particulate carbon, nitrogen, and phosphorus as described above.

Water Column Sampling

Water column sampling was conducted biweekly at the 55 meter site, and water was collected from 2, 10, 15, 20, 25, 30, 35, 40, 50, and 54 meters using a 5 L Niskin bottle. Water samples were filtered through GF/F filters. Filters were used for particulate phosphorus and chlorophyll *a* analysis. The filtrate was saved for total dissolved phosphorus analysis. Particulate phosphorus was analyzed using the molybdate-antimony method (Stainton et al. 1974) after combustion at 550˚C and two-hour acid digestion with 2 ml of 1N HCl and 10 ml of type 1 water. Total dissolved phosphorus was determined according to the molybdate-antimony method with samples after digesting with H_2SO_4 and H_2O_2 followed by 2 hours of photo-oxidation (Stainton et al. 1974). Filters used for chlorophyll *a* were stored in a dark freezer until analysis, which was within two weeks of sample collection. Chlorophyll was extracted for 24 hours in a freezer using a methanol and acetone mixture following filter grinding, as described by Arar and Collins (1997). Fluorescence was measured using a Turner designs model 10 benchtop fluorometer after centrifuging the filter and extractant solution at 3000- 4000 rpms.

Results

Porewater Flux

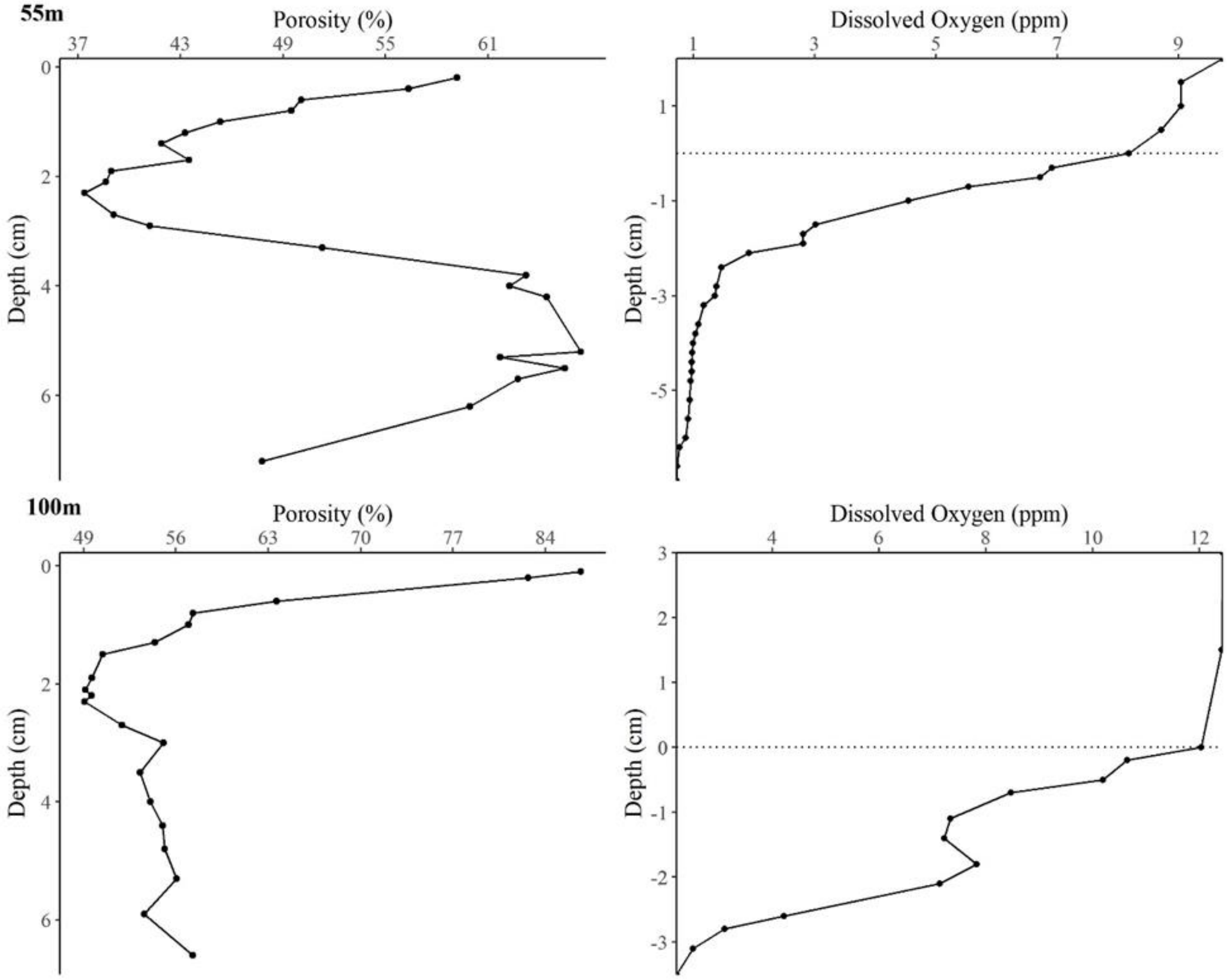

Figure 22: Porosity and dissolved oxygen by depth for both the 55 meter and 100 meter sites. The dotted line represents the sediment-water interface.

The composition of the material in the cores was move variable at the 55 meter deep site than at the 100 meter site. The 55 meter core contained a dense clay layer starting around the 4 cm depth and is evident in the porosity profile by an increase in porosity (Fig. 22). The composition of the material at the 100 meter site was visually uniform. 100 meter site cores had similar dissolved oxygen profiles with a decrease in dissolved oxygen between the sediment surface and 2 cm depth, a slight increase in dissolved oxygen at ~2 cm, followed by another decline in dissolved oxygen and anoxia at 3.5 cm. The depth of the oxic-anoxic transition varied at the 55 meter site with the depth of anoxia ranging from the 2-8 cm depending on the core. The variability of dissolved oxygen profiles at the 55 meter site may be due to bioturbation activities by the mussels, which can increase oxygen penetration (Vaughn & Hakenkamp 2001; Roley & Tank 2016), or resuspension.

The SRP pore water profile indicates a flux of soluble reactive phosphorus from the sediment into the overlying water (Fig. 23). The decrease in SRP concentration in the pore water below the 1.5-2 cm depth may be due to a decrease in labile phosphorus at the deeper depths (Fig. 23 and 25) (Chen et al. 2016), and the SRP being converted into some other form below 2 cm. Over dissolved compounds, such as Fe (II), were not measured in this study, so it makes it difficult to determine what happens to the SRP below 2 cm. The sediment-water SRP flux at the 100 meter site calculated using eq. 6 was between 1.2 and 1.4 μmol P m^{-2} day^{-1} which is in range of values reported by Conley et al. (1988) at a similar site in July of 1984 (1.1 ± .2 μmol P m^{-2} day^{-1}).

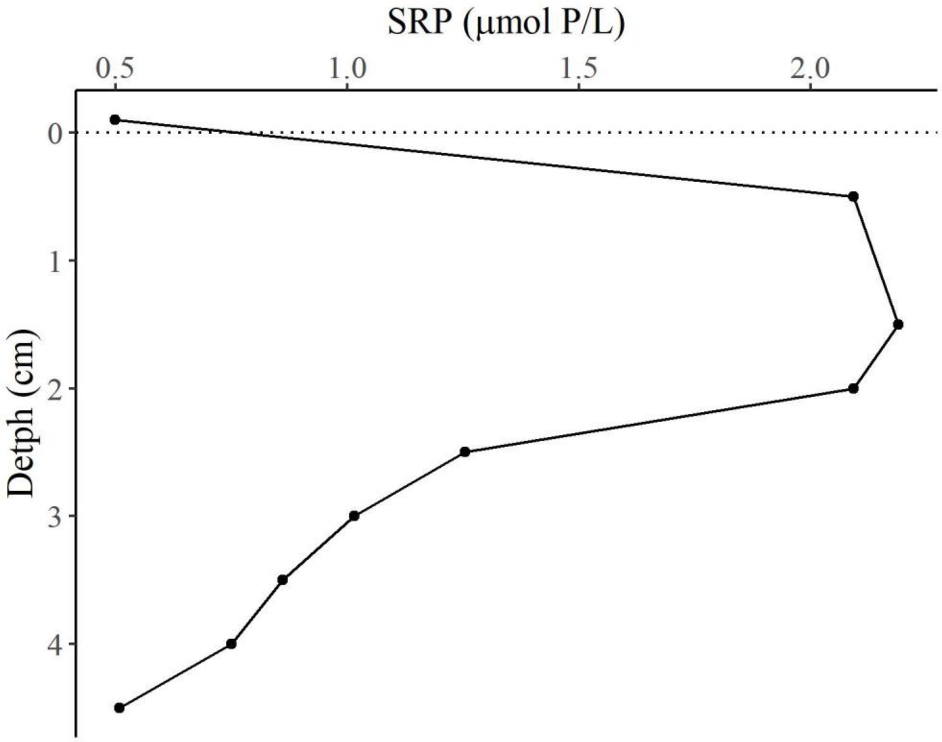

Figure 23:Pore water profile from the 100 meter site. The dotted line represents the sediment surface.

Sedimentation Rate

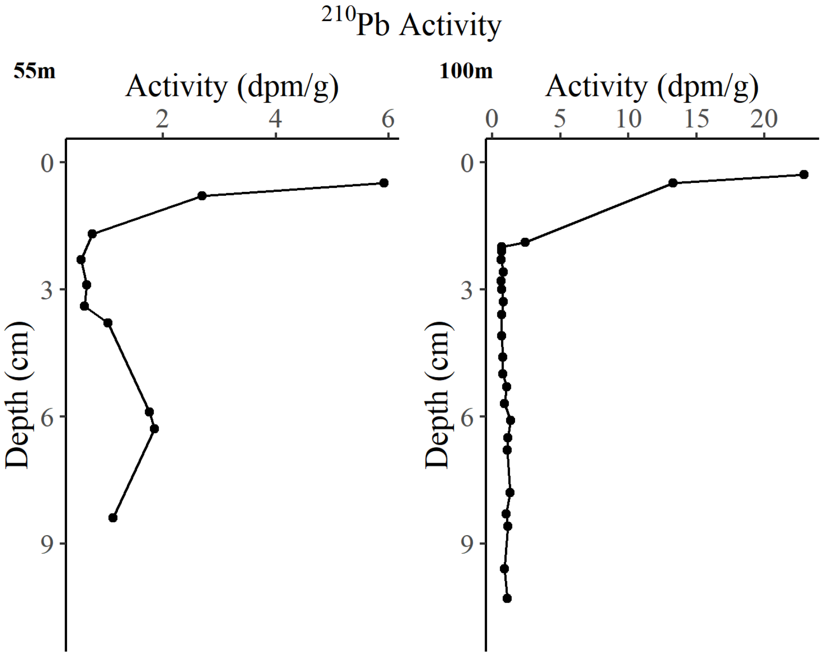

Figure 24: ^{210}Pb activity profiles for both the 55 and 100 meter sites.

The surface sedimentation rate at the 55 meter site was 0.027 ± 0.004 g cm^{-2} yr^{-1}, which equates to 0.024 ± 0.004 cm yr^{-1}. The surface sedimentation rate at the 100 meter site was 0.022 ± 0.001 g cm^{-2} yr^{-1} for one core and 0.014 ± 0.006 g cm^{-2} yr^{-1} for the other core which equated to 0.047 ± 0.001 cm yr^{-1} and 0.039 ± 0.016 cm yr^{-1}. No core profiles are represented by age because the age of the sediment was uncertain below the depth that unsupported activity was undetectable.

Sediment Phosphorus composition

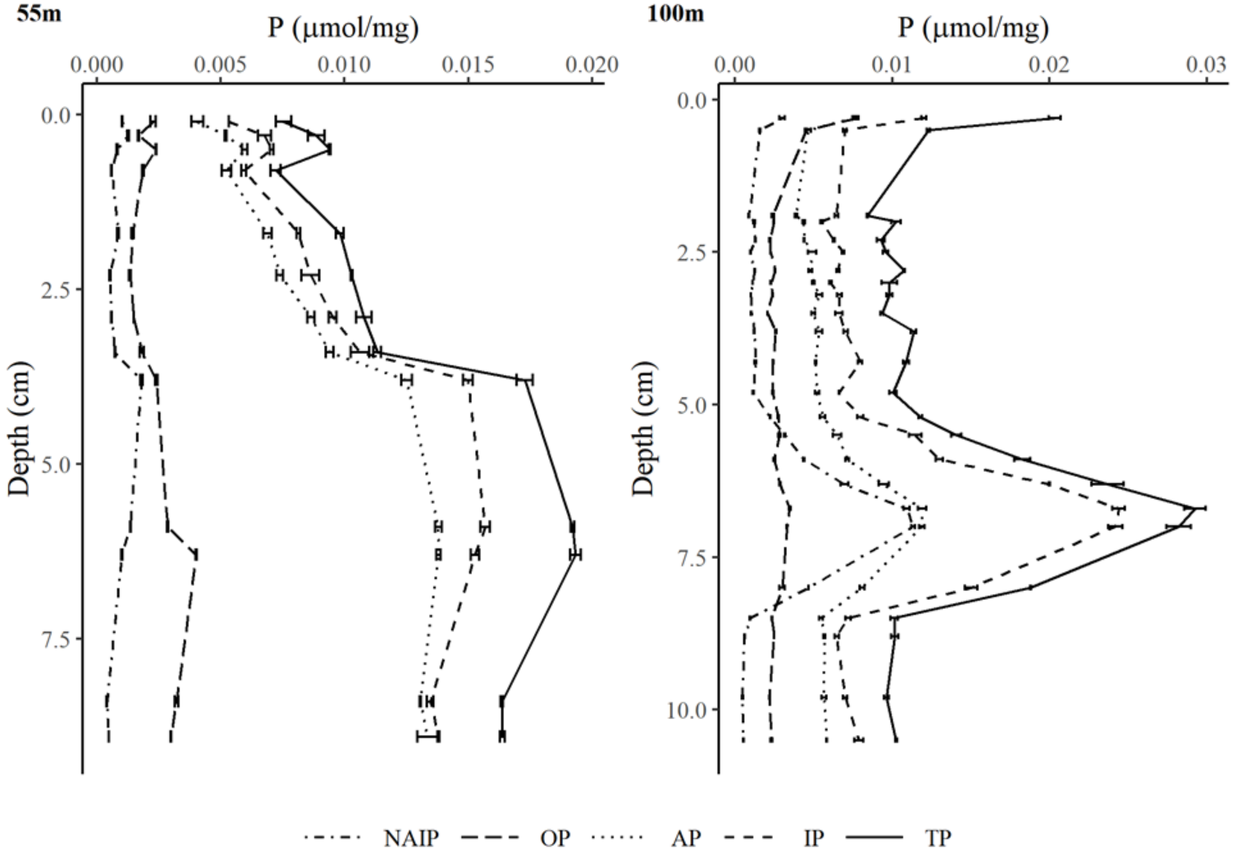

Figure 25: Particulate phosphorus fractions by depth for both the 55 (left) and 100 (right) meter site. The error bars represent standard error of triplicate subsamples from each core slice. NAIP, OP, AP, IP, and TP represent non-apatite inorganic, organic, apatite, inorganic, and total bound phosphorus respectively. The concentrations are absolute concentrations, and the y scale is different between the two plots.

The dominant sediment phosphorus pool in Lake Michigan is AP (Fig. 25). The peak of NAIP, AP, and IP in the 100 meter core between the depths of 5.0 and 8 cm may be associated with a period of eutrophication. During eutrophication, the higher concentration of SRP in the water column may inhibit the dissolution of calcium associated P, leading to higher concentrations of AP accumulating in the sediment (Gonsiorczyk et al. 1998). If there were higher SRP concentrations during this period, then that could lead to higher precipitation of apatite bound phosphorus (Dittrich 2000). However, the proportionally higher increase in NAIP at this depth could indicate the increase in AP is due to changes in external loading compared to internal processes. The higher abundance of NAIP at the surface is due to the higher availability of oxygen. In the anoxic zones of the 100 meter core, oxidized forms of Fe are reduced, releasing bound phosphorus (Mortimer 1942; Hupfer and Lewandowski 2008; Wu et al. 2014).

In the 55 meter core, NAIP and OP made up a relatively small fraction of total P throughout the core, most likely due to resuspension that would promote less accretion of temporary pools of phosphorus (Fig. 25). The increase in AP with depth at the 55 meter site coincides with an increase in porosity (Fig. 22 and 25). The increase in porosity indicates smaller grain size and a larger surface area for adsorption reactions to occur, potentially leading to more dissolved phosphorus to bind with apatite. The near-surface sediment accumulation rate for the two sites is summarized in table 7.

Table 7: Surface burial of phosphorus calculated using the sedimentation rate determined with ^{210}Pb dating and the phosphorus binding fractions at the top most layer of the core. Phosphorus burial rate units are μmol m^{-2} yr^{-1}.

Core	NAIP	AP	IP	OP	TP
55 m	280 ± 46	1400 ± 230	1700 ± 270	590 ± 100	2300 ± 360
100 m A	660 ± 50	1700 ± 80	2600 ± 130	1700 ± 80	4500 ± 230
100 m B	350 ± 140	770 ± 320	1200 ± 500	840 ± 350	2500 ± 1000

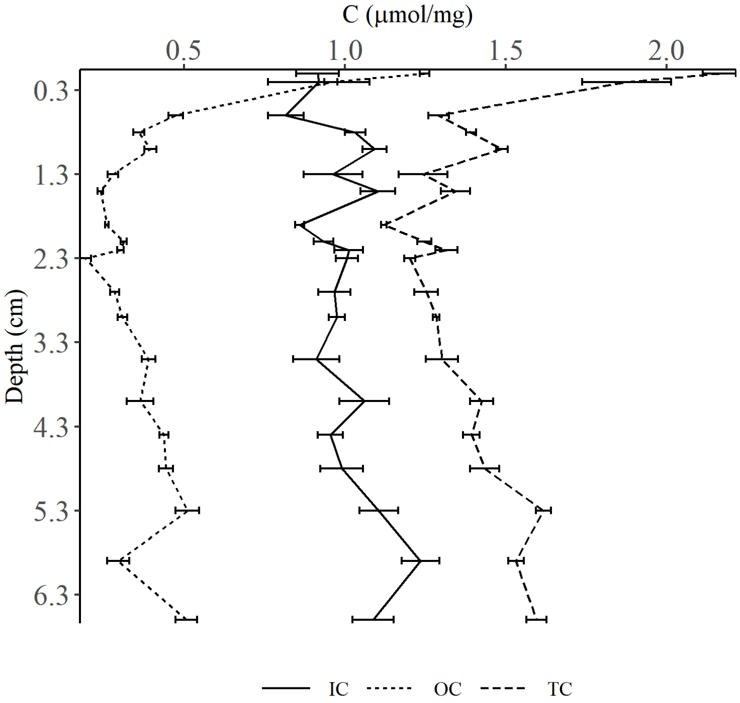

Figure 26: Carbon profile from the 100 meter station. IC, OC, and TC represent inorganic carbon, organic carbon, and total carbon respectively. Error bars represent standard error among triplicate replicates from each core slice.

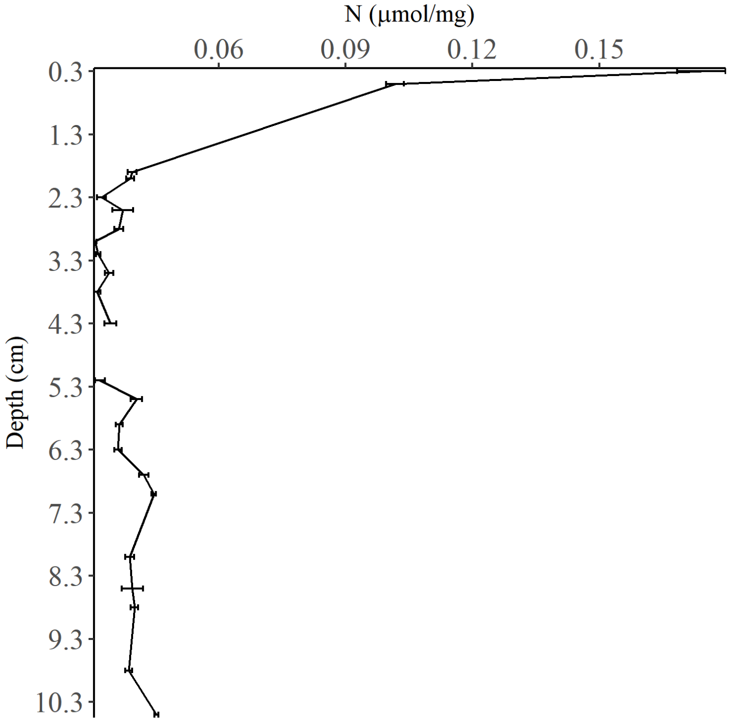

Figure 27: Sediment total nitrogen profile at the 100 meter site. Error bars represent standard error among triplicate replicates from each core slice.

The carbon in the 100 meter cores decreased in concentration within the first centimeter. The decrease may be due to the breakdown of carbon within the oxic layer (Fig. 26 and Fig. 22). The concentration of inorganic carbon remained constant with depth. Nitrogen at the 100 meter site is mineralized primarily in the oxic zone, most likely due to nitrification/denitrification and decomposition of organic material. Nitrogen regeneration within the oxic layer was much greater than phosphorus and carbon regeneration at both sites, as indicated by the decrease of N:P and the increase in C:N with depth (Fig. 28). In the 100 meter core, the C:P and N:P ratios dropped between 5 and 8 cm, reflecting the large increase in phosphorus that was not accompanied by an increase in C or N at those depths (Fig. 26 and Fig. 27). The ratio of N:P in the sediment traps is much higher than the surface of the sediment at the 55 meter station, indicating that much of the nitrogen is regenerated quickly (Table 8). The TC:TP at the surface of the sediment was 183 ±

11, but just below the surface, the TC:TP increased to 322 ± 11 in the 55 meter core. A similar trend in TC:TP is noted in the 100 meter core, which suggests that carbon regeneration is a rapid process that occurs soon after deposition while phosphorus regeneration is slower and less complete, occurring over the timescale of years.

Table 8: Table of deposition rates measured from sediment traps deployed from April 2018 to October 2018 and surface sediment burial at the 55 meter and 100 meter stations. The rates are presented in units of µmol m^{-2} yr^{-1} ± the standard error. The * symbol indicates that total carbon values were used instead of organic carbon because organic carbon data was unavailable.

	OC	N	P	C:P	N:P	C:N
18m	750000 ± 120000	60000 ± 6200	3400 ± 470	220 ± 50	18 ± 3	12 ± 2
35m	1200000 ± 130000	93000 ± 11000	5600 ± 670	220 ± 40	17 ± 3	13 ± 2
53m	1400000 ± 150000	110000 ± 20000	5900 ± 520	240 ± 33	18 ± 4	13 ± 3
55m Burial	*600000 ± 110000	9200 ± 1500	2300 ± 360	*183 ± 11	4 ± 0.2	*50 ± 3
100m Burial	420000 ± 20000	40000 ± 2200	4500 ± 230	94 ± 6.6	8.6 ± 0.7	11 ± 0.8

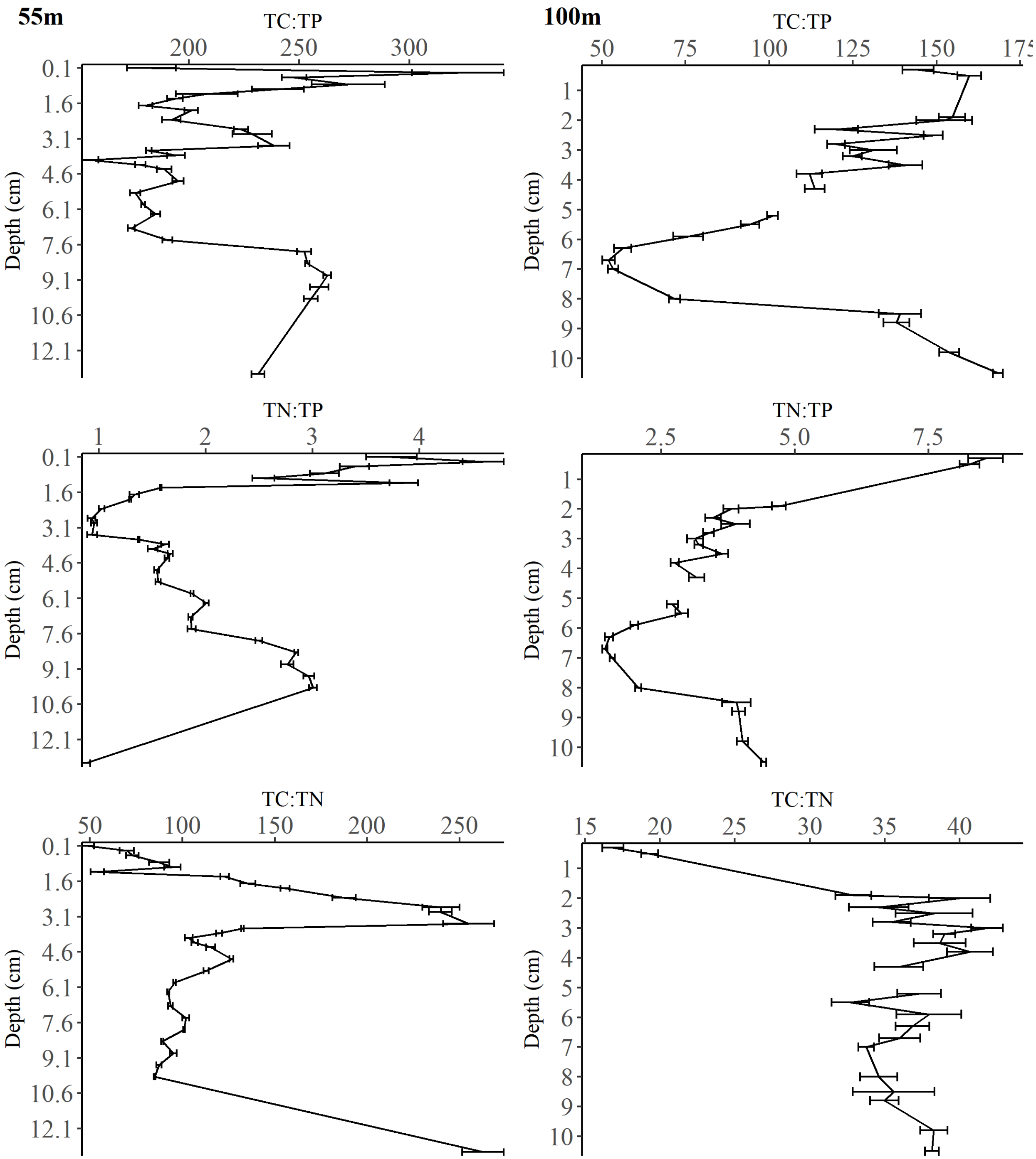

Figure 28: TC to TP, TN to TP, and TC to TN by depth for the 55 meter cores (left) and the 100 meter cores (right). Error bars represent standard error among triplicate replicates from each core slice

Deposition

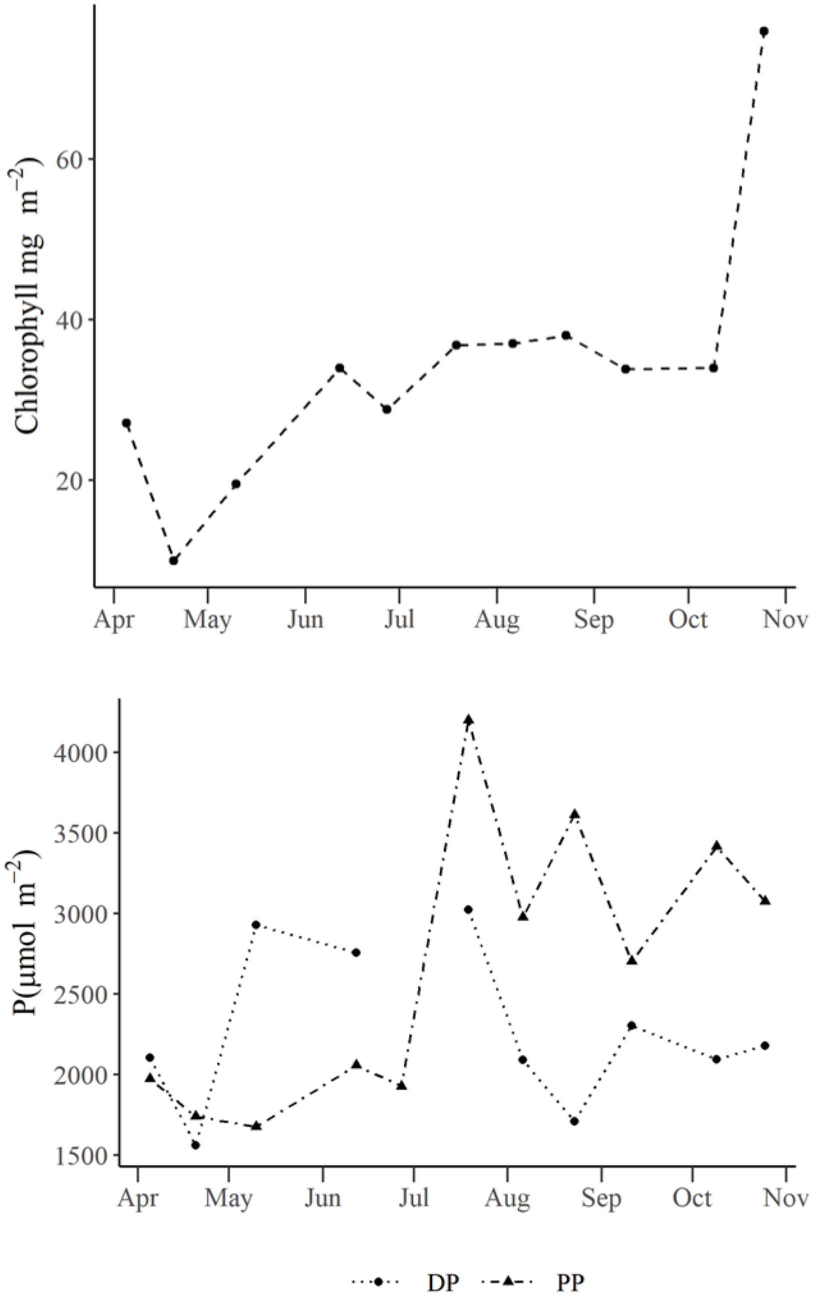

Figure 29: Integrated water column chlorophyll and phosphorus at the 55 meter station. DP represents total dissolved phosphorus and PP represents particulate phosphorus

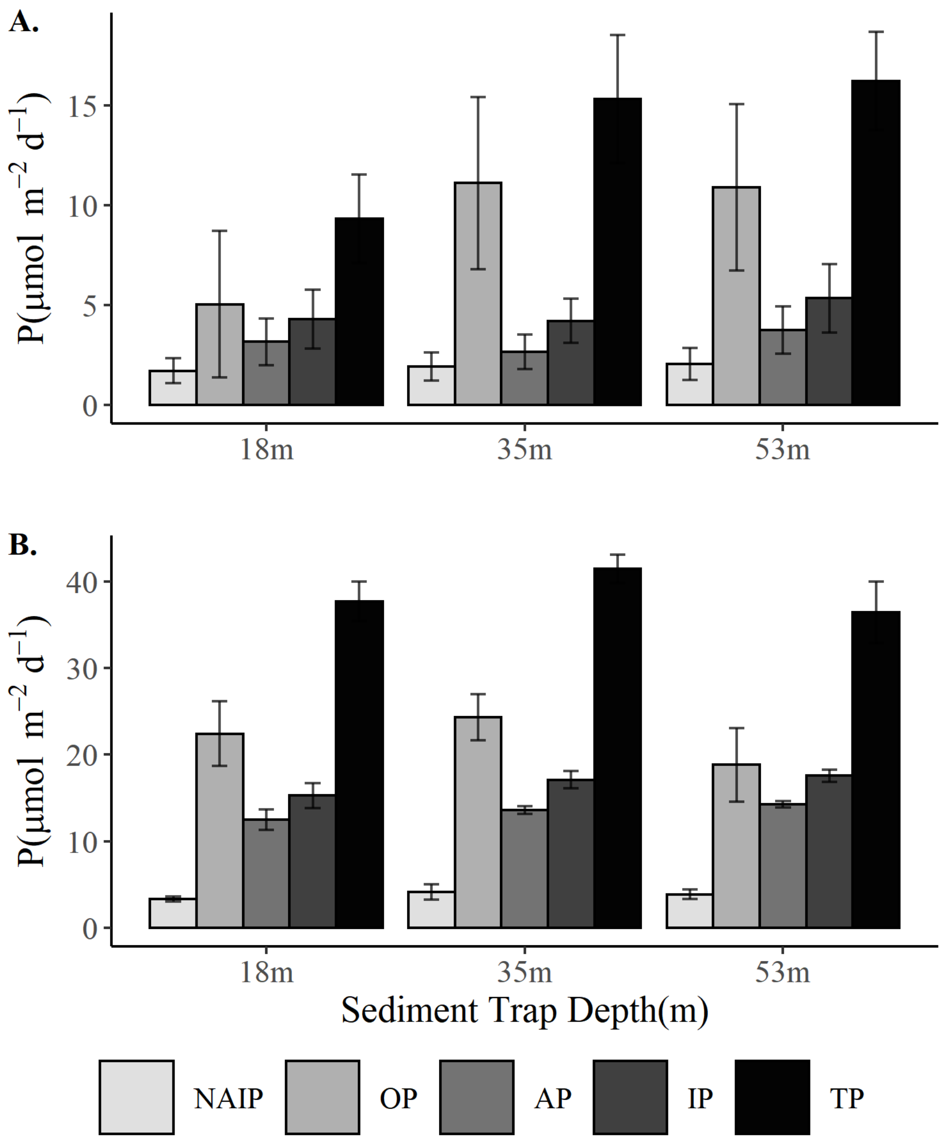

Figure 30: Phosphorus fractions in setting material sampled from sediment traps during stratification (A.) and during the mixing period sampled in April of 2018 (B.). Error bars represent standard deviation.

In April 2018, resuspension likely occurred. The particulate phosphorus and chlorophyll *a* decreased in the water column during the deployment period in April (Fig. 29), and despite the lower particulate phosphorus and chlorophyll *a*, this deployment period contained the highest about of deposited material compared to all other service periods. The sediment trap data collected during the mixed period is not included in the estimates of flux to the sediment-water interface because it does not represent passive sedimentation (Fig. 30). The NAIP portion of the sediment trap material did not differ between the stratified and mixing period, but the OP and AP portion of phosphorus were much larger during the mixing period. An increase in AP bound phosphorous is expected with resuspension of sediments because it is the primary form of phosphorus within the sediment at this site (Fig. 25). However, there was also a substantial increase in OP, which cannot be account for with phytoplankton growth because chlorophyll *a* concentrations were low during this period. Mussels live in high densities at this site producing large amounts of organic phosphorus in the form of biodeposits, which may account for some of the increase in OP if these biodeposits were also resuspended (Mosley & Bootsma 2015; See chapter 2 and 3). Assuming that only the OP and NAIP are potentially available pools for phytoplankton growth, approximately 55% of the phosphorus is potentially available in the 18 meter trap during passive sedimentation. NAIP is considered potentially available P because it describes NaOH extractable forms of P as well as Fe associated forms of P, although NAIP would overestimate the bioavailable pool because it also represents P associated with clays. The portion of available phosphorus decreased to 38 and 36% in the lower traps due to regeneration within the water column. During the resuspension event, the potentially available pool was 50-55% in the sediment traps at all depths.

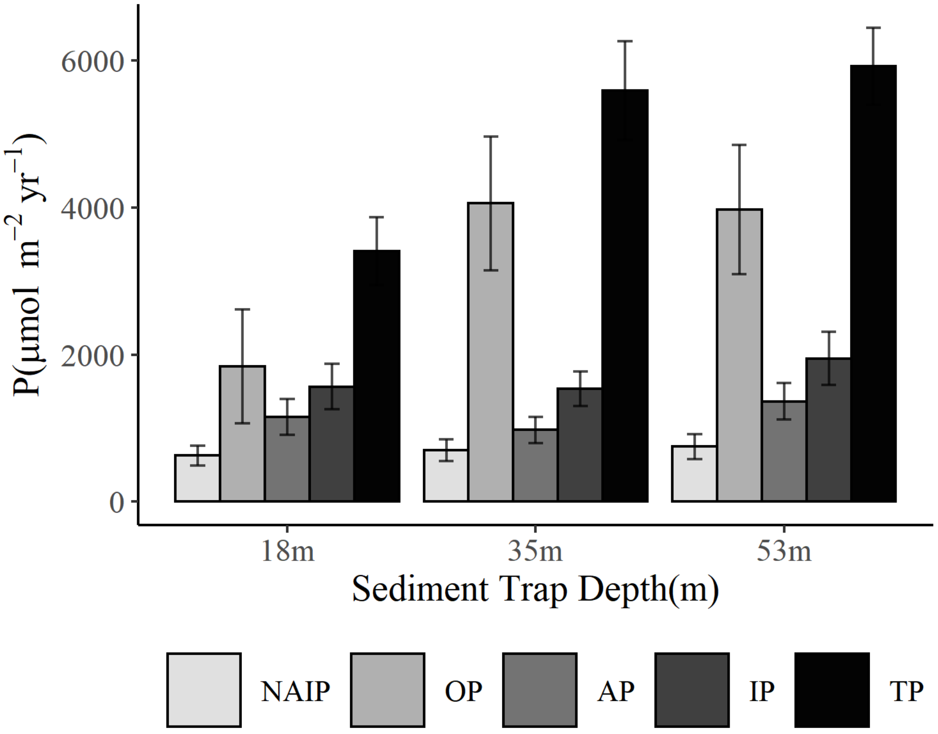

Figure 31: Phosphorus deposition rate for the three trap depths over the 2018 field season. NAIP, OP, AP, IP, and TP represent non-apatite inorganic, organic, apatite, inorganic, and total bound phosphorus respectively. The error bars represent the standard error of the triplicate replicate sediment traps for the entire deployment time (traps serviced 6 times from April 2018 to October 2018).

In order to determine the phosphorus regenerated pools at the AW55 site, the phosphorus binding fraction between the sediment trap material and the surface burial fraction of phosphorus were compared (Fig. 25 and 31). The potentially regenerated pools at the 100 meter site were determined by comparing the phosphorus mass in each fraction in the surface layers and older layers (Hupfer & Lewandowski 2005). The age of the layer is required to complete this calculation. In this method, two fluxes are calculated: rapid and slow. The rapid flux refers to the calculated flux based on the difference phosphorus masses in the surface layer and next closes layer in depth divided by the estimated age difference between the two layers. The slow flux refers to the regeneration rates calculated based on the difference phosphorus masses in the surface layer compared to layers below the oxic zone where phosphorus concentrations appear to have stabilized divided by the estimated age difference between the two layers. If the rapid and slow rates are equal, then this can be considered a reasonable estimate of the sediment regeneration rate (Hufer & Lewandowski). The flux rates at the 100 meter sites were calculated using core A because core A dating profile contained less error than core B. The rapid and slow-release at this site was similar, with a total P release of 2640 ± 430 and 2870 ± 214 μmol P m^{-2} yr^{-1} respectively, so the rapid release is represented as phosphorus regeneration at this site. The phosphorus regeneration rates at both sites are presented in Fig. 32.

The largest temporary pools of freshly deposited phosphorus at the 55 meter site were OP followed by NAIP. However, AP acts as a sink of phosphorus at the 55 meter site steadily increasing with burial with depth. At the 100 meter site, AP is an important source of phosphorus into the overlying water column. The regeneration rates and burial rates were compared to determine the percentage of deposited material that was cycled back into the water column at both sites. At the both sites, 60 ± 10% of recently deposited phosphorus was recycled annually, which is consistent with past measurements of phosphorus cycling at the sediment-water interface made by Shafer and Armstrong (1994), who estimated that 63% of the freshly deposited phosphorus was recycled every year in Southern Lake Michigan.

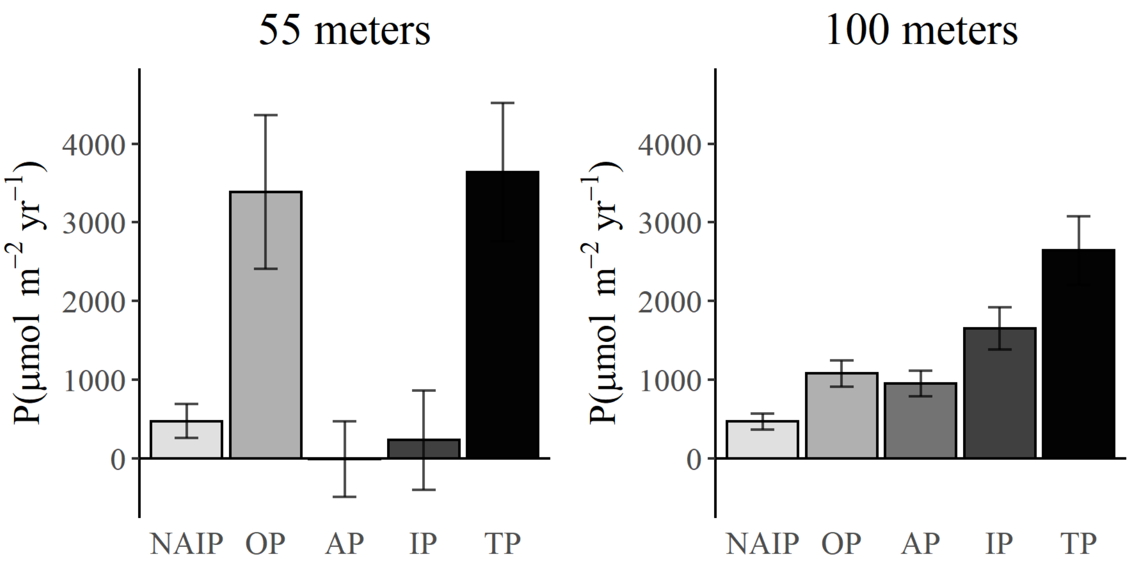

Figure 32: The potential phosphorus regeneration rates sites. The error bars represent standard error.

Discussion

Importance of Internal Loading for Lake Michigan

The SRP pore water profiles may underestimate the flux of phosphorus from the sediment. Pore water diffusive fluxes may account for less than 30% of the recycled phosphorus because these profiles cannot account for bioturbation, resuspension events, or regeneration that occurs right at the sediment-water interface (Li et al. 2018). The sampling depth intervals also limit the SRP pore water profiles diffusive flux estimates. In the case of this study, the sampling interval was 0.5 cm, which is larger than the depth of sediment deposited within the last year. Sediment incubation, as was used in Conley et al. (1988), may also underestimate the annual recycling of phosphorus in Lake Michigan. Historically, sediment release has occurred in episodic events, including resuspension during mixing periods (Eadie et al. 1984) and dissolution of apatite bound phosphorus during the spring phytoplankton bloom (Brooks and Edgington 1994). Laboratory experiments may also represent an artificially high binding of phosphorus because they typically occur over weeks to months. During that time, there is no sedimentation of fresh organic material that may enhance microbial activity (Hupfer & Lewandowski 2008). Due to these reasons, the estimates of rapid flux based on the near-surface profiles of the various sediment P fractions may be better estimates of the annual phosphorus flux from the sediment.

In Lake Michigan sediment, OP and NAIP represented temporary pools of phosphorus both near and offshore. OP represents the largest temporary pool within the sediment of Lake Michigan, which is regenerated by microbial decomposition of organic matter (Hupfer & Lewandowski 2008). The microbial activity could also cause regeneration of NAIP at the 100 meter site because the enhanced microbial activity can lead to changes in the redox potential leading to the dissolution of redox-sensitive bound phosphorous (Hupfer & Lewandowski 2008). AP was the most significant pool of phosphorus within the cores, but not all the phosphorus bound to apatite represented permanent storage. At the 100 meter site, the flux of phosphorus from the AP was larger than the NAIP. However, some of the AP loss with depth could represent the conversion of AP into other sediment pools rather or vertical movement within the core rather than flux out of the sediment. At the 55 meter site, calcite precipitated phosphorus within the pore water, making AP a further sink of phosphorus. The difference in apatite dissolution between the two sites might be due to the high excretion rate of quagga mussels (Mosley & Bootsma 2015). The 55 meter site is in the region of highest mussel density (Nalepa et al. 2010), and the mussel driven effects on benthic cycling differ based on mussel density with areas of high density experiencing more significant mussel induced changes (Callier et al. 2009; Sandwell et al. 2009). However, mussels are still expanding in the deep profundal region of Lake Michigan (Burlakova et al. 2018), which will increase the dissolved phosphorus concentration at the sediment-water interface, potentially leading to less apatite dissolution (Brooks and Edgington 1994; Mosley & Bootsma 2015).

Similar studies of phosphorus regeneration have been conducted in other Great Lakes. In Lake Erie, NAIP and OP are the primary forms of temporary phosphorus storage, and AP in sediment is relatively constant with depth (Williams et al. 1976). The reason for the difference between Lake Erie and Lake Michigan is most likely because apatite dissolution of phosphorus is not as an important source of internal loading to Lake Erie which is primarily driven by redox-sensitive and organic bound phosphorus within the sediment (Williams et al. 1976; Matisoff et al. 2016). In Lake Superior, phosphorus regeneration is primarily driven by the decomposition of organic material, however much of the regenerated material is bound by iron in the oxic layer (Li et al. 2018). This does not appear to the be case with Lake Michigan sediments because SRP concentrations within the pore water were higher in the oxic layer compared to the anoxic layer, although this may not be true in all areas of Lake Michigan. Unlike Lake Superior and Lake Erie, AP is regenerated or transformed into other forms at the deeper site. However, the majority of the regeneration of phosphorus, nitrogen, and carbon occurs in the oxic layer in Lake Michigan and is associated with decomposition of organic material.

Sediment resuspension during the mixing period represents an episodic event that may increase the availability of phosphorus in the water column (Eadie et al. 1984). A study of sediment trap material in 1978 in southern lake Michigan indicated that 15-20% of the particulate phosphorus in the material collected during the mixed period, and 30-40% collected during stratification, was potentially available for use by phytoplankton (Eadie et al. 1984). In that study, the potentially available pool was defined as the pool of phosphorus able to be extracted with NaOH, which would make it most comparable to the NAIP pool in the present study. The NAIP was approximately 15-20% of the total sediment trap phosphorus during passive sedimentation and 5-10% during the mixed period. In this study, the temporary pools of phosphorus are defined as both OP and NAIP, and during the mixing period, the portion of available phosphorus was much higher (Fig. 30). However, the increase in potentially available phosphorus did not increase the dissolved phosphorus, particulate phosphorus, or chlorophyll *a* concentration (Fig. 29). Sediment traps are biased to larger particles, and past work completed by Eadie et al. (1984) demonstrated that nearly 100% of particles under the size of 64 μm were extractable by NaOH. In this current study, the small size fraction would be accounted for in the dissolved phosphorus pool, which was low throughout the sampling period in 2018. Shafer and Armstrong (1994) determined that resuspension did not greatly increase available phosphorus, which conflicted with the results of the Eadie et al. (1984) study. The results of this study show that resuspension during mixing events does increase the potentially available pool of phosphorus, but that did not seem to increase phytoplankton growth.

The amount of regeneration of freshly deposited material at both sites are in the range of rates estimated by Shafer and Armstrong (1994), who estimated annual regeneration fluxes of 2645-4032 μmol m^{-2} $year^{-1}$ using samples collected in 1982 (Fig. 32). It might be expected that the sedimentation rates of phosphorus and renewal of fresh material would be much lower now due to decreases in water column total phosphorus and decreases in phosphorus loading (Mida et al. 2010, Dolan & Chapra 2012; Katsev 2017). However, if mussels increase the effective settling rate of phosphorus, as has been suggested by Chapra and Dolan (2012), then the delivery to the sediment would be greater than expected based on water column concentrations.

The permanent sediment burial rates calculated at both sites agreed well with the southern basin phosphorus loading estimate of 2480 ± 645 μmol m^{-2} yr^{-1} from 1994 through 2008 (Dolan & Chapra 2012) calculated using the area of southern Lake Michigan which was determined using the bathymetry map for southern lake Michigan with Sheboygan, WI as the border

(National Geophysical Data Center 1996). The annual burial rates were 2285 ± 361 and 1800 ± 660 μmol m^{-2} yr^{-1} at the 55 meter and 100 meter sites respectively. The permanent burial rate at the100 meter site was calculated as the difference between the surface burial and regeneration rate. The mean water column total phosphorus concentration measured at the 55 meter site through the 2018 field season was 2.93 ± 1.04 μg/L, which is in range of other studies that determined offshore phosphorus concentrations post mussel invasion (Mida et al. 2010). Using the phosphorus loading estimates (Dolan & Chapra 2012) and the average total water column phosphorus concentration measured in 2018, the residence time of phosphorus in southern Lake Michigan is 3.2 ± 1.4 years, assuming steady-state conditions and a mean depth of 85 meters. This estimate is lower than the 5-6 year ranged determined by past studies prior to mussel establishment (Sonzogni et al. 1976; Shafer & Armstrong 1994). The lower estimate in this study is likely due to the rapid removal of P from the water column by dreissenid mussel grazing.

Phosphorus Cycle Changes

Dreissenid mussels invaded the Great Lakes in the 1980s, altering ecosystem functions, including nutrient cycling (Zhang et al. 2011; Mosley & Bootsma 2015). We are not aware of any other studies that have examined sediment phosphorus regeneration since the expansion of quagga mussels into the profundal regions of Lake Michigan. Based on the results presented here, a conceptual model was constructed to illustrate the effect of dreissenid mussels on the Lake Michigan P cycle (Fig. 33). While the results from this study indicate that mussels have little effect on the magnitude of P recycle within the sediment, the post mussels' conceptual model demonstrates that mussels have greatly increased the importance of the benthos as a P recycling site.

The 55 meter depth was chosen to model because the sediment traps were deployed at the 55 meter site, and near in situ measurements of mussel excretion and egestion are available for this depth (See Chapter 2). Phytoplankton C:P prior to mussel invasion was set to 150:1 based on measurements of C:P during late summer in southern Lake Michigan (Pothoven & Fahnenstiel 2013). The C:P ratio was set to 200:1 after dreissenid establishment based on seston measurements offshore taken during the 2016-2017 field season (Bockwoldt 2018). The phytoplankton production rates for mid-depth regions before and after mussel are from Fahnenstiel et al. (2010) and converted into phosphorus uptake rates using the C:P ratios indicated above.

Zooplankton grazing rates of phosphorus were determined using the estimated clearance rates of zooplankton (Scavia & Fahnenstiel 1987), the zooplankton biomass before and after the mussel invasion (Vanderploeg et al. 2012), the particulate phosphorus concentration before mussel establishment (Pothoven & Fahnenstiel 2013) and after mussel establishment. The water column particulate and dissolved phosphorus concentrations after mussel establishment were determined from periodic water column sampling during the 2018-2019 field seasons at the same location the 55 meter cores were collected (See chapters 2 and 3). The dissolved phosphorus concentrations prior to mussel establishment were determined using the total phosphorus concentrations and total phosphorus to particulate phosphorus ratios measured by Pothoven and Fahnenstiel (2013).

The river inputs of phosphorus were obtained from Mida et al. (2010), normalized to the area of southern Lake Michigan (2.5×10^{10} m^2). Pre-mussel sedimentation rates of phosphorus were taken from Eadie et al. (1984) and Shafer and Armstrong (1994), and the sediment burial and sediment-water flux rates were extracted from Shafer and Armstrong (1994). The arrow connecting sedimentation to dissolved phosphorus represents calcite precipitation in the fall (Strong & Eadie 1978; Shafer & Armstrong 1994) and is only included prior to mussel establishment because of the occurrence of these precipitation events has decreased (Watkins et al. 2007). Atmospheric P deposition is from Dolan and Chapra (2012) and was assumed to be the same for both the period before and after the dreissenid invasion. Sediment burial, passive sedimentation, and sediment-water flux were determined by comparing sediment core accumulation rates and sediment trap deposition described above.

Diporeia were the most abundant benthic invertebrate prior to the mussel invasion (Nalepa et al. 2009). *Diporeia* uptake rates were determined using carbon uptake rates (Fitzgerald & Gardner 1993), and the C:P ratio of phytoplankton, assuming this was the primary food source of *Diporeia*. *Diporeia* are not included in the post mussel model due to their population decline (Nalepa et al. 2009). Mussel egestion and excretion rates were measured at 55 meter site offshore of Milwaukee during the 2018-2019 field season (see Chapter 2), and P assimilation by mussels was determined as 10% of captured phosphorus (Stoeckmann & Garton 1997). Pre-mussel bacteria uptake rates of carbon are from Fitzgerald and Gardner (1993) and converted into phosphorus uptake rates using the average C:P ration found in pelagic bacteria (Cotner et al. 2010). Post-mussel heterotrophic bacteria uptake rates were determined from measured bacteria uptake of dissolved phosphorus in incubation experiments (See chapter 3). In these incubation experiments, uptake rates of nutrients by bacteria growing on mussel biodeposits was monitored. The uptake rates were normalized to biodeposit mass. These rates were converted to areal rates using the mussel production of biodeposits per day (See chapter 2). Mussel biodeposits are returned to the dissolved pool via microbial decomposition, and this process is depicted as protozoan recycling in the model. This model assumes 100% of biodeposits P is recycled.

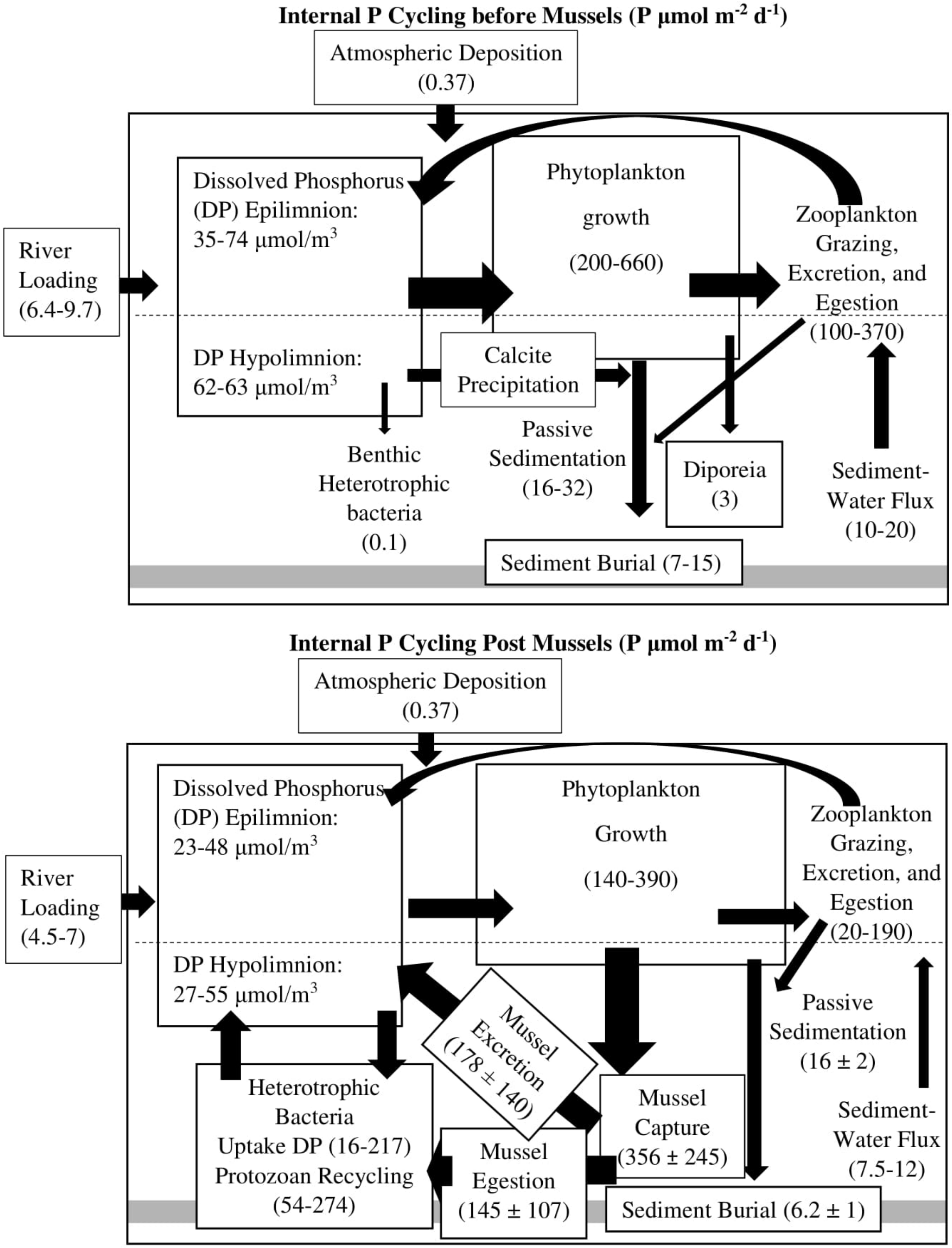

Internal P Cycling before Mussels (P µmol m^{-2} d^{-1})

Internal P Cycling Post Mussels (P µmol m^{-2} d^{-1})

Figure 33: Conceptual model of phosphorus cycling at a 55 meter site before and after the establishment of dreissenid mussels. Components of the model are described in the text.

Summary

Quagga mussels have increased the importance of the benthos as a phosphorus recycling site through the capture and recycling of phosphorus in both the dissolved and particulate form. In this study, the mussel effects on the internal loading of phosphorus were examined at two sites: one where mussel densities are highest (55m) and one where deposition rates are greater (100m). At both sites, portions of organic phosphorus and non-apatite inorganic P were recycled within the sediment. Apatite represented a further sink of P at the 55 meter site, increasing with depth. However, at the 100 meter site, apatite dissolution was a source of P to the water column, or apatite bound P was converted into some other form. The difference in apatite cycling at the two sites could be due to the increase in benthic dissolved phosphorus concentrations caused by mussels. The increase in dissolved phosphorus could cause greater adsorption or precipitation of apatite within the sediment. More work is needed to determine basin loading of phosphorus from sediments because the loading mechanisms are heterogeneous, and more sites are needed to determine which processes are prominent at different locations in Lake Michigan.

. Despite lower water column phosphorus concentrations, burial rates of phosphorus have not changed causing a shorter residency time of P. The burial rates of phosphorus did not decrease with water column P concentrations because mussels may have increased the effective settling rate of phosphorus by filtering out smaller particles that typically would have remained suspended in the water column. Decreased residency time of phosphorus may mean that low phosphorus concentrations may persist even as mussel populations stabilize.

The processes that dictate the internal cycling of phosphorus have changed with the expansion of mussels, including increased bacterial mediated recycling of phosphorus at the benthos and reduced phosphorus cycling in the epilimnion. More phosphorus cycling is occurring in the benthos compared to the water column. These changes helped support the resurgence of nuisance *Cladophora* nearshore (Auer et al. 2010; Bootsma et al. 2015). Offshore these changes may increase bacterial abundance and the importance of the microbial food web for energy transfer (Heath et al. 2003; Chapter 3). Future studies should examine the relationship between mussels and microbial communities in the profundal regions.

CHAPTER 5: Summary

Quagga mussels have fundamentally altered phosphorus cycling in the Great Lakes, leading to a decrease in phosphorus residency time within the water column and increase cycling within the benthos. Mussels are able to colonize a large portion of the nearshore substrate near Milwaukee, capturing large amounts of phosphorus. Unlike the region offshore of Muskegon, the nearshore area captures the highest about of nutrients and phytoplankton, but capture rates remain high moving into the mid-depth region. This area may act as both nearshore and mid-depth sink of nutrients, decreasing the offshore transfer of nutrients (Hecky et al. 2004; Vanderploeg et al. 2010). At the same time, mussels in this region are excreting phosphorus at a rate that far exceeds loading from the Milwaukee river leading to the resurgence of Nuisance *Cladophora* in the 0-10 m depth zone (Bootsma et al. 2012; Bootsma et al. 2015). Offshore, excreted phosphorus may be utilized by heterotrophic bacteria, as demonstrated with the biodeposit incubations.

Biodeposit deposition of phosphorus is approximately nine times greater than the passive sedimentation rate of phosphorus. The fate of the pool of phosphorus has important implications for Lake Michigan's phosphorus cycled. Modeling of water column offshore phosphorus concentration under mixing conditions demonstrated that at least a portion of biodeposits must be recycled within days of deposition, or phosphorus concentration would be much lower in the water column. The potential role of bacteria in recycling biodeposits was demonstrated through a series of incubations. Bacteria abundance increased on the biodeposits during the incubation, and as bacteria grew, they utilized dissolved forms of P, making biodeposits a further sink of phosphorus over the course of two weeks. After two weeks, the P bound within the biodeposit started to be released. The incubation likely represented a much slower release than would occur in the natural environment because the number of protozoans was limited by using filtered lake water. The model demonstrated that portions of biodeposits must be recycled within days and not weeks in order to maintain current phosphorus concentrations. Other organisms, such as oligochaetes, may also directly feed upon biodeposits increasing the recycling rates of biodeposit bound nutrients.

Along with increasing bacteria abundance, other indirect effects of mussels could alter phosphorus cycling. At 55m site, apatite was a sink of dissolve P. Excreted phosphorus at the sediment-water interface may promote higher precipitation and adsorption of dissolved P to apatite. However, apatite dissolution did occur at the 100 meter site, supporting previous work showing that apatite P may be an important source of phosphorus in Lake Michigan (Brooks & Edgington 1994). While apatite dissolution may be affected by mussels, the burial rate of phosphorus was similar to rates measured prior to the mussel invasion despite lower P concentrations within the water column leading to a lower residence time of phosphorus in the water column with an estimate of about 3.2 years. Burial rates might be similar despite lower P concentrations because mussels may increase the effective settling rates of phosphorus by filtering smaller particles out of the water column that typically would have longer residence times.

Figure 33 provides a good summary of the internal cycling of phosphorus changes since the expansion of mussels. Mussels have greatly increased the importance of the benthos as a P recycling site. Currently, more phosphorus is cycled in the benthos than by zooplankton within the water column. Increasing benthic recycling nearshore has led to higher rates of benthic macrophyte growth (Bootsma et al. 2004; Bootsma 2009; Auer et al. 2010; Bootsma et al. 2012). Offshore these changes may increase bacterial abundance and the importance of the microbial food web for energy transfer. Future work should focus on profundal benthic bacteria and their role in nutrient cycling.

References

Arnott, D. L., & Vanni, M. J. (1996). Nitrogen and phosphorus recycling by the zebra mussel (*Dreissena polymorpha)* in the western basin of Lake Erie. *Can. J. of Fish. and Aquat. Sci., 53*(3), 646–659. https://doi.org/10.1139/cjfas-53-3-646

Arar, E., & Collins, G. (1997). In Vitro Determination of Chlorophyll *a* and Pheophytin *a* in Marine and Freshwater Algae by Fluorescence. Method 445.0. National Exposure Research Laboratory Office of Research and Development U.S. Environmental Protection Agency, Cincinnati, Ohio 45268.

Auer, M., Tomlinson, L., Higgins, S., Malkin, S., Howell, E., Bootsma, H. 2010. Great Lakes *Cladophora* in the 21st century: same algae—different ecosystem. *J. Great Lakes Res.*, 36, 248-255.

Baldwin, B. S., Mayer, M. S., Dayton, J., Pau, N., Medilla, J., Sullivan, M., Moore, A., Ma, A., Mills, E. L. (2002). Comparative growth and feeding in zebra and quagga mussels (*Dreissena polymorpha* and *Dreissena bugensis*): implication for North American lakes. *Can. J. of Fish. and Aquat. Sci.*, 59, 680–694.

Baskaran, M., Nix, J., Kuyper, C., & Karunakara, N. (2014). Problems with the dating of sediment core using excess210Pb in a freshwater system impacted by large scale watershed changes. *J. Environ. Radioact*., 138, 355–363. https://doi.org/10.1016/j.jenvrad.2014.07.006

Bially, A., & MacIsaac, H. J. (2000). Fouling mussels (*Dreissena spp*.) colonize soft sediments in Lake Erie and facilitate benthic invertebrates. *Freshw. Biol.*, 43 (1), 85–97. https://doi.org/10.1046/j.1365-2427.2000.00526.x

Bockwoldt, K., Bootsma, H. A. (2018). Spatial and temporal variation of phytoplankton production in Lake Michigan. Master's Thesis. University of Wisconsin Milwaukee.

Bootsma, H.A., Young, E.B., Berges, J.A., 2004. Temporal and spatial patterns of Cladophora biomass and nutrient stoichiometry in Lake Michigan. In: Bootsma,H.A., Jenson, E.T., Young, E.B., Berges, J.A. (Eds.), CladophoraResearch and Mana-gement in the Great Lakes,Proceedings of a workshop held at the Great Lakes WATER Institute, University of Wisconsin-Milwaukee, December, 2004, 81–88.

Bootsma, H.A., 2009. Causes, consequences and management of nuisance Cladophora Milwaukee, WI Report submitted to the U.S. Environmental Protection Agency. Great Lakes National Program Office, Chicago, IL.

Bootsma, H. A., Waples, J. T., & Liao, Q. (2012). Identifying major phosphorus pathways in the Lake Michigan nearshore zone. Final Report MMSD Contract M03029P05.

Bootsma, H., Liao, Q. 2014. Nutrient Cycling by Dreissenid Mussels controlling factors and ecosystem response. *Quagga and zebra mussels: biology, impacts, and control*. Chapter

35, 555-574.

Bootsma, H., Rowe, M., Brooks, C., Vanderploeg, H. 2015. Commentary: The need for model development related to *Cladophora* and nutrient management in Lake Michigan. *J. Great Lakes Res*, 41, 7-15.

Breffle, W. S., Muralidharan, D., Donovan, R. P., Liu, F., Mukherjee, A., & Jin, Y. (2013). Socioeconomic evaluation of the impact of natural resource stressors on human-use services in the Great Lakes environment: A Lake Michigan case study. *Resour. Policy*, 38 (2), 152–161. https://doi.org/10.1016/j.resourpol.2012.10.004

Brodie, C. R., Casford, J. S. L., Lloyd, J. M., Leng, M. J., Heaton, T. H. E., Kendrick, C. P., & Yongqiang, Z. (2011). Evidence for bias in C/N, δ13C and δ15N values of bulk organic matter, and on environmental interpretation, from a lake sedimentary sequence by pre-analysis acid treatment methods. *Quat. Sci. Rev.*, 30 (21–22), 3076–3087. https://doi.org/10.1016/j.quascirev.2011.07.003

Brooks, A. S., & Edgington, D. (1994). Biogeochemical control of phosphorus production in Lake Michigan. *Limnol. Oceanogr.*, 39 (4), 961–968.

Bunnell, D. B., Madenjian, C. P., Holuszko, J. D., Adams, J. V., & French, J. R. P. (2009). Expansion of Dreissena into offshore waters of Lake Michigan and potential impacts on fish populations. *J. Great Lakes Res.*, 35 (1), 74–80. https://doi.org/10.1016/j.jglr.2008.10.002

Burlakova, L. E., Barbiero, R. P., Karatayev, A. Y., Daniel, S. E., Hinchey, E. K., & Warren, G. J. (2018). The benthic community of the Laurentian Great Lakes: Analysis of spatial gradients and temporal trends from 1998 to 2014. *J. Great Lakes Res*., 44 (4), 600–617. https://doi.org/10.1016/j.jglr.2018.04.008

Callier, M. D., Richard, M., McKindsey, C. W., Archambault, P., & Desrosiers, G. (2009). Responses of benthic macrofauna and biogeochemical fluxes to various levels of mussel biodeposition: An in situ "benthocosm" experiment. *Mar. Pollut. Bull.*, 58 (10), 1544–1553. https://doi.org/10.1016/j.marpolbul.2009.05.010

Carlsson, M. S., Glud, R. N., & Petersen, J. K. (2010). Degradation of mussel (*mytilus edulis*) fecal pellets released from hanging long-lines upon sinking and after settling at the sediment. *Can. J. of Fish. and Aquat. Sci.*, 67 (9), 1376–1387. https://doi.org/10.1139/F10-067

Carrick, H. J., Fahnenstiel, G. L., & Taylor, W. D. (1992). Growth and production of planktonic protozoa in Lake Michigan: In situ versus in vitro comparisons and importance to food web dynamics. *Limnol. Oceanogr.*, *37*(6), 1221–1235. https://doi.org/10.4319/lo.1992.37.6.1221

Carrick, H. J. (2005). An under-appreciated component of biodiversity in plankton communities: The role of protozoa in Lake Michigan (a case study). *Hydrobiologia*, 551 (1), 17–32. https://doi.org/10.1007/s10750-005-4447-0

Chapra, S. C., & Dolan, D. M. (2012). Great Lakes total phosphorus revisited: 2. Mass balance modeling. *J. Great Lakes Res*., 38 (4), 741–754. https://doi.org/10.1016/j.jglr.2012.10.002

Chen, M., Ding, S., Liu, L., Xu, D., Gong, M., Tang, H., & Zhang, C. (2016). Kinetics of phosphorus release from sediments and its relationship with iron speciation influenced by the mussel (*Corbicula fluminea*) bioturbation. *Sci. Total Environ.*, 542, 833–840. https://doi.org/10.1016/j.scitotenv.2015.10.155

Conley, D. J., Quigley, M. A., & Schelske, C. L. (1988). Silica and phosphorus flux from sediments: importance of internal recycling in Lake Michigan. *Can. J. of Fish. and Aquat. Sci.*, 45 (6), 1030–1035. https://doi.org/10.1139/f88-126

Corkum, L., Sapota, M., & Skora, K. (2004). The round goby, *Neogobius melanostomus*, a fish invader on both sides of the Atlantic Ocean. *Biol. Invasions*, 6 (1), 173–181.

Cotner, J. B., & Wetzel, R. G. (1992). Uptake of dissolved inorganic and organic phosphorus compounds by phytoplankton and bacterioplankton. *Limnol. Oceanogr.*, 37 (2), 232–243. https://doi.org/10.4319/lo.1992.37.2.0232

Cotner, J. B., Hall, E. K., Scott, J. T., & Heldal, M. (2010). Freshwater bacteria are stoichiometrically flexible with a nutrient composition similar to seston. *Front. Microbiol.*, 1, 1–11. https://doi.org/10.3389/fmicb.2010.00132

Creque, S. M., Stainbrook, K. M., Glover, D. C., Czesny, S. J., & Dettmers, J. M. (2010). Mapping bottom substrate in Illinois waters of Lake Michigan: Linking substrate and biology. *J. Great Lakes Res*., *36* (4), 780–789. https://doi.org/10.1016/j.jglr.2010.08.010

Crisp, D.J., 1984. Energy flow measurements. In: Holme, N.A., McIntyre, A.D. (Eds.), Methods for the study of marine benthos. Blackwell Scientific Publications, Palo Alto, pp. 284–372.

Dolan, D. M., & Chapra, S. C. (2012). Great Lakes total phosphorus revisited: 1. Loading analysis and update (1994-2008). *J. Great Lakes Res*., 38 (4), 730–740. https://doi.org/10.1016/j.jglr.2012.10.001

Dermott, R., Munawar, M., 1993. Invasion of Lake Erie offshore sediments by *Dreissena* and its ecological implications. *Can. J. Fish. Aquat. Sci*., 50, 2298–2304.

Dittrich, M., Casper, P., & Koschel, R. (2000). Changes in the porewater chemistry of profundal sediments in response to artificial hypolimnetic calcite precipitation. *Arch. Hydrobiol. Spec. Issues Advanc. Limnol.*, 55, 421–432.

Dolan, D. M., & Chapra, S. C. (2012). Great Lakes total phosphorus revisited: 1. Loading analysis and update (1994-2008). *J. Great Lakes Res., 3*8 (4), 730–740. https://doi.org/10.1016/j.jglr.2012.10.001

Eadie, B., Chamber, R., Gardner, W., & Bell, G. (1984). Sediment Trap Studies in Lake Michigan: Resuspension and Chemical Fluxes in the Southern Basin. *J. Great Lakes Res.*, 10 (3), 307–321.

Eadie, B., Robbins, J., Klump, J. V., Schwab, D., & Edgington, D. (2008). Winter-Spring Storms and Their Influence on Sediment Resuspension, Transport, and Accumulation Patterns in Southern Lake Michigan. *Oceanography*, 21 (4), 118–135. https://doi.org/10.5670/oceanog.2008.09

Fahnenstiel, G., Pothoven, S., Vanderploeg, H., Klarer, D., Nalepa, T., & Scavia, D. (2010). Recent changes in primary production and phytoplankton in the offshore region of southeastern Lake Michigan. *J. Great Lakes Res.*, 36 (3), 20–29. https://doi.org/10.1016/j.jglr.2010.03.009

Fahnenstiel, G. L., Sayers, M. J., Shuchman, R. A., Yousef, F., & Pothoven, S. A. (2016). Lake-wide phytoplankton production and abundance in the Upper Great Lakes: 2010-2013. *J. Great Lakes Res.,* 42 (3), 619-629. https://doi.org/10.1016/j.jglr.2016.02.004

Finlay, B. J., & Esteban, G. (1998). Freshwater protozoa: Biodiversity and ecological function. *Entomologia Experimentalis et Applicata*, 7, 1163–1186. https://doi.org/10.1023/A

Fitzgerald, S. A., & Gardner, W. S. (1993). An algal carbon budget for pelagic-benthic coupling in Lake Michigan. *Limnol. Oceanogr.*, 38 (3), 547–560. https://doi.org/10.4319/lo.1993.38.3.0547

Giles, H., & Pilditch, C. A. (2004). Effects of diet on sinking rates and erosion thresholds of mussel *Perna canaliculus* biodeposits. *Mar. Ecol. Prog. Ser.*, 282, 205–219. https://doi.org/10.3354/meps282205

Giles, H., & Pilditch, C. A. (2006). Effects of mussel (*Perna canaliculus*) biodeposit decomposition on benthic respiration and nutrient fluxes. *Mar. Biol.,* 150 (2), 261–271. https://doi.org/10.1007/s00227-006-0348-7

Glyshaw, P. W., Riseng, C. M., Nalepa, T. F., & Pothoven, S. A. (2015). Temporal trends in condition and reproduction of quagga mussels (*Dreissena rostriformis bugensis)* in southern Lake Michigan. *J. Great Lakes Res.*, 41, 16–26. https://doi.org/10.1016/j.jglr.2015.08.006

Goldhammer, T., Brüchert, V., Ferdelman, T. G., & Zabel, M. (2010). Microbial sequestration of phosphorus in anoxic upwelling sediments. *Nat. Geosci.*, 3 (8), 557–561. https://doi.org/10.1038/ngeo913

Gonsiorczyk, T., Casper, P., & Koschel, R. (1998). Phosphorus-Binding forms in the sediment of an oligotrophic and an eutrophic hardwater lake of the Baltic Lake District (Germany). *Water Sci. and Technol.*, 37 (3), 51–58.

Grenz, C., Hermin, M. N., Baudinet, D., & Daumas, R. (1990). In situ biochemical and bacterial variation of sediments enriched with mussel biodeposits. *Hydrobiologia*, 207 (1), 153–160. https://doi.org/10.1007/BF00041452

Halvorson, H. M., & Atkinson, C. L. (2019). Egestion Versus Excretion: A Meta-Analysis. *Diversity*, 11 (189). https://doi.org/10.3390/d11100189

Heath, R. T., Hwang, S. J., & Munawar, M. (2003). A hypothesis for the assessment of the importance of microbial food web linkages in nearshore and offshore habitats of the Laurentian Great Lakes. *Aquat. Ecosyst. Health Manag*, 6 (3), 231–239. https://doi.org/10.1080/14634980301495

Hecky, R. E., Smith, R. E., Barton, D. R., Guildford, S. J., Taylor, W. D., Charlton, M. N., & Howell, T. (2004). The nearshore phosphorus shunt: a consequence of ecosystem engineering by dreissenids in the Laurentian Great Lakes. *Can. J. Fish. Aquat. Sci*., 61 (7), 1285–1293. https://doi.org/10.1139/f04-065

Hupfer, M., & Lewandowski, J. (2005). Retention and early diagenetic transformation of phosphorus in Lake Arendsee (Germany) - Consequences for management strategies. *Archiv Fur Hydrobiologie*, 164 (2), 143–167. https://doi.org/10.1127/0003-9136/2005/0164-0143

Hupfer, M., Lewandowski, J. 2008. Oxygen controls the phosphorus release from Lake Sediments- a Long-Lasting Paradigm in Limnology. *Internat. Rev. Hydrobiol.* 93, 415-432.

ITTC. 2011. Freshwater and Saltwater properties. International Towing Tank conference-Recommended Procedures.

Jansen, H. M., Verdegem, M. C. J., Strand, & Smaal, A. C. (2012). Seasonal variation in mineralization rates (C-N-P-Si) of mussel *Mytilus edulis* biodeposits. *Mar. Biol.*, 159 (7), 1567–1580. https://doi.org/10.1007/s00227-012-1944-3

Jin, T., Liao, Q., (2019). Underwater Particle Image Velocimetry (PIV) Measurements of Turbulence over Mussel Bed in the Deep site of Lake Michigan. PhD Thesis. University of Wisconsin Milwaukee.

Johengen, T., Vanderploeg, H., & Liebig, J. (2013). Effects of Algal Composition, Seston Stoichiometry, and Feeding Rate on Zebra Mussel (*Dreissena polymorpha*) Nutrient Excretion in Two Laurentian Great Lakes. *Quagga and zebra mussels: biology, impacts, and control*, 445–460. https://doi.org/10.1201/b15437-34

Katsev, S. (2017). When large lakes respond fast: A parsimonious model for phosphorus dynamics. *J. Great Lakes Res.,* 43 (1), 199–204. https://doi.org/10.1016/j.jglr.2016.10.012

Katsev, S., Tsandev, I., L'Heureux, I., & Rancourt, D. G. (2006). Factors controlling long-term phosphorus efflux from lake sediments: Exploratory reactive-transport modeling. *Chem. Geol.*, 234 (1–2), 127–147. https://doi.org/10.1016/j.chemgeo.2006.05.001

Kirchman, D. 1994. The uptake of inorganic nutrients by heterotrophic bacteria. *Microb. Ecol.*, 28, 255-271

Komada, T., Anderson, M. R., & Dorfmeier, C. L. (2008). Carbonate removal from coastal sediments for the determination of organic carbon and its isotopic signatures, δ 13 C and Δ 14 C: comparison of fumigation and direct acidification by hydrochloric acid. *Limnol. Oceanogr.Methods,* 6 (6), 254–262. https://doi.org/10.4319/lom.2008.6.254

Kuhns, L. A., & Berg, M. B. (1999). Benthic invertebrate community responses to round goby (*Neogobius melanostomus*) and zebra mussel (*Dreissena polymorpha*) invasion in southern Lake Michigan. *J. Great Lakes Res.*, 25 (4), 910–917. https://doi.org/10.1016/S0380-1330(99)70788-4

Lauringson, V., Mälton, E., Kotta, J., Kangur, K., Orav-Kotta, H., & Kotta, I. (2007). Environmental factors influencing the biodeposition of the suspension feeding bivalve *Dreissena polymorpha* (Pallas): Comparison of brackish and freshwater populations. *Estuar. Coast. Shelf Sci.*, 75 (4), 459–467. https://doi.org/10.1016/j.ecss.2007.05.037

Lavrentyev, P. J., Gardner, W. S., & Yang, L. (2000). Effects of the zebra mussel on nitrogen dynamics and the microbial community at the sediment-water interface. *Aquat. Microb. Ecol.*, 21 (2), 187–194.

Li, J., Zhang, Y., & Katsev, S. (2018). Phosphorus recycling in deeply oxygenated sediments in Lake Superior controlled by organic matter mineralization. *Limnol. Oceanogr.*, 63 (3), 1372–1385. https://doi.org/10.1002/lno.10778

Lohner, R. N., Sigler, V., Mayer, C. M., & Balogh, C. (2007). A comparison of the benthic bacterial communities within and surrounding Dreissena clusters in lakes. *Microb. Ecol.*, 54 (3), 469–477. https://doi.org/10.1007/s00248-007-9211-8

López-Lara, I. M., Sohlenkamp, C., & Geiger, O. (2003). Membrane lipids in plant-associated bacteria: Their biosyntheses and possible functions. *Mol. Plant-Microbe Interact.*, 16 (7), 567–579. https://doi.org/10.1094/MPMI.2003.16.7.567

MacKenzie, A. B., & Scott, R. D. (1979). Separation of bismuth-210 and polonium-210 from aqueous solutions by spontaneous adsorption on copper foils. *Analyst*, 104 (1245), 1151–1158. https://doi.org/10.1039/an9790401151

Madenjian, C. P., Bunnell, D. B., Warner, D. M., Pothoven, S. A., Fahnenstiel, G. L., Nalepa, T. F., Vanderploeg, H., Tsehay, I, Claramunt, R., Clark, R. D. (2015). Changes in the Lake Michigan food web following dreissenid mussel invasions: A synthesis. *J. of Great Lakes Res.*, 41, 217–231. https://doi.org/10.1016/j.jglr.2015.08.009

Makino, W., Cotner, J. B., Sterner, R. W., & Elser, J. J. (2003). Are bacteria more like plants or animals? Growth rate and resource dependence of bacterial C:N:P stoichiometry. *Funct. Ecol.*, 17 (1), 121–130. https://doi.org/10.1046/j.1365-2435.2003.00712.x

Martin, S., Thouzeau, G., Chauvaud, L., Jean, F., Guérin, L., & Clavier, J. (2006). Respiration, calcification, and excretion of the invasive slipper limpet, *Crepidula fornicata L.*: Implications for carbon, carbonate, and nitrogen fluxes in affected areas. *Limnol. Oceanogr.*, 51 (5), 1996–2007. https://doi.org/10.4319/lo.2006.51.5.1996

Martin, S., Thouzeau, G., Richard, M., Chauvaud, L., Jean, F., & Clavier, J. (2007). Benthic community respiration in areas impacted by the invasive mollusk *Crepidula fornicata*. *Mar. Ecol. Prog. Ser.*, 347, 51–60. https://doi.org/10.3354/meps07000

Mathay, C., Hamot, G., Henry, E., Georges, L., Bellora, C., Lebrun, L., de Witt, B., Ammerlaan, W., Buschart, A., Wilmes, P., Betsou, F. (2015). Method optimization for fecal sample collection and fecal DNA extraction. *Biopreserv. and Biobank.*, 13 (2), 79–93. https://doi.org/10.1089/bio.2014.0031

Matisoff, G., Kaltenberg, E. M., Steely, R. L., Hummel, S. K., Seo, J., Gibbons, K. J., Gibbons, K., Bridgeman, T., Seo, Y., Behbahani, M., James, W., Johnson, L., Doan, P., Dittrich, M., Evans, M., Chaffin, J. D. (2016). Internal loading of phosphorus in western Lake Erie. *J. Great Lakes Res.*, 42 (4), 775–788. https://doi.org/10.1016/j.jglr.2016.04.004

Mehler, K., Burlakova, L. E., Karatayev, A. Y., Elgin, A. K., Nalepa, T. F., Madenjian, C. P., & Hinchey, E. (2020). Long-term trends of Lake Michigan benthos with emphasis on the southern basin. *J. Great Lakes Res*. https://doi.org/10.1016/j.jglr.2020.03.011

Mermillod-Blondin, F., & Rosenberg, R. (2006). Ecosystem engineering: The impact of bioturbation on biogeochemical processes in marine and freshwater benthic habitats. *Aquat. Sci.*, 68 (4), 434–442. https://doi.org/10.1007/s00027-006-0858-x

Mida, J. L., Scavia, D., Fahnenstiel, G. L., Pothoven, S. A., Vanderploeg, H. A., & Dolan, D. M. (2010). Long-term and recent changes in southern Lake Michigan water quality with implications for present trophic status. *J. of Great Lakes Res.*, 36 (SUPPL. 3), 42–49. https://doi.org/10.1016/j.jglr.2010.03.010

Mortimer, C. 1941, 1942: The exchange of dissolved substances between mud and water in lakes. *J. Ecology* 29: 280–329. *J. Ecol.*, 30, 147–201.

Mosley, C., Bootsma, H.A., 2015. Phosphorus recycling by profundal Quagga mussels (*Dreissena rostriformis bugensis*) in Lake Michigan. *J. Great Lakes Res*., 41, 38-48.

Nagul, E., McKelvie, I., Worsfold, P., Kolev, S. 2015. The molybdenum blue reaction for the determination of orthophosphate revisited: Opening the black box. *Anal. Chim. Acta,* 890, 60-82.

Nalepa, T. F., Gardner, W. S., & Malczyk, J. M. (1991). Phosphorus cycling by mussels (Unionidae : Bivalvia) in Lake St. Clair. *Hydrobiologia*, 219 (1), 239–250. https://doi.org/10.1007/BF00024758

Nalepa, T. F., Cavaletto, J. F., Ford, M., Gordon, W. M., & Wimmer, M. (1993). Seasonal and Annual Variation in Weight and Biochemical Content of the Zebra Mussel, *Dreissena polymorpha*, in Lake St. Clair. *J. Great Lakes Res.*, 19 (3), 541–552. https://doi.org/10.1016/S0380-1330(93)71240-X

Nalepa, T. F., Fanslow, D. L., & Lang, G. A. (2009). Transformation of the offshore benthic community in Lake Michigan: Recent shift from the native amphipod *Diporeia spp.* to the invasive mussel *Dreissena rostriformis bugensis. Freshw. Biol.*, 54 (3), 466–479. https://doi.org/10.1111/j.1365-2427.2008.02123.x

Nalepa, T., Fanslow, D., Pothoven, S. 2010. Recent changes in density, biomass, recruitment, size structure, and nutritional state of *Dreissena* populations in southern Lake Michigan. *J. Great Lakes Res.*, 36, 5-19.

Nalepa, T. F., Burlakova, L. E., Elgin, A. K., Karatayev, A. Y., Lang, G. A., Mehler, K. 2020. Abundance and Biomass of Benthic Macroinvertebrates in Lake Michigan in 2015, with a Summary of Temporal Trends. U.S. Dep. Commerce, NOAA Tech. Memo. GLERL-175. https://doi.org/10.25923/g0d3-3v41

National Research Council of the United States and the Royal Society of Canada. The Great Lakes Water Quality Agreement: an Evolving Instrument for Ecosystem Management. Washington, D.C.: Ottawa, Ontario: National Academy Press; Royal Society of Canada, 1985.

National Geophysical Data Center, 1996. Bathymetry of Lake Michigan. National Geophysical Data Center, NOAA. doi:10.7289/V5B85627 [3/4/2020].

Navarro, J. M., & Thompson, R. J. (1997). Biodeposition by the horse mussel *Modiolus modiolus* (Dillwyn) during the spring diatom bloom. *J. Exp. Mar. Biol. and Ecol.*, 209 (1–2), 1–13. https://doi.org/10.1016/0022-0981(96)02681-0

Newell, R. I. E., & Jordan, S. (1983). Preferential ingestion of organic material by the American oyster *Crassostrea virginica*. *Mar. Ecol. Prog. Ser.*, 13, 47–53.

Newell, R. (2004). Ecosystem Influences of Natural and Cultivated Populations of Suspension-Feeding Bivalve Molluscs: A Review. *J. Shellfish Res.*, 23 (1), 51–61.

Nürnberg, G. K. (1991). Phosphorus from Internal Sources in the Laurentian Great Lakes, and the Concept of Threshold External Load. *J. Great Lakes Res.*, 17 (1), 132–140. https://doi.org/10.1016/S0380-1330(91)71348-8

Ozersky, T., Evans, D. O., & Ginn, B. K. (2015). Invasive mussels modify the cycling, storage and distribution of nutrients and carbon in a large lake. *Freshw. Biol.*, 60 (4), 827–843. https://doi.org/10.1111/fwb.12537

Pardo, P., Rauret, G., & López-Sánchez, J. F. (2003). Analytical approaches to the determination of phosphorus partitioning patterns in sediments. *J. Environ. Monitor.*, 5 (2), 312–318. https://doi.org/10.1039/b210354k

Platt, T., Irwin, B., 1973. Caloric content of phytoplankton. *Limnol. Oceanogr.* 18, 306–310.

Pothoven, S. A., & Madenjian, C. P. (2008). Changes in Consumption by Alewives and Lake Whitefish after *Dreissenid* Mussel Invasions in Lakes Michigan and Huron. *N. Am. J. Fish. Manag.*, 28 (1), 308–320. https://doi.org/10.1577/m07-022.1

Pothoven, S. A., & Fahnenstiel, G. L. (2013). Recent change in summer chlorophyll a dynamics of southeastern Lake Michigan. *J. Great Lakes Res.*, 39 (2). https://doi.org/10.1016/j.jglr.2013.02.005

Pothoven, S. A., & Vanderploeg, H. A. (2020). Seasonal patterns for Secchi depth, chlorophyll a, total phosphorus, and nutrient limitation differ between nearshore and offshore in Lake Michigan. *J. Great Lakes Res*. https://doi.org/10.1016/j.jglr.2020.03.013

Pomeroy, L. (1974). The Ocean's Foodweb, A Changing Paradigm. *J. Biosci.*, 24 (9), 499-504.

Porter, K. G., & Feig, Y. S. (1980). The use of DAPI for identifying and counting aquatic microflora 1. *Limnol. Oceanogr.*, 25 (5), 943-948.

Ray, W., & Corkum, L. (1997). Predation of zebra mussels by round gobies. *Environmental Biology of Fishes*, 267–273.

Robbins, J. A., & Edgington, D. N. (1975). Determination of recent sedimentation rates in Lake Michigan using Pb-210 and Cs-137. *Geochim. Cosmochim. Acta*, 39 (3), 285–304. https://doi.org/10.1016/0016-7037(75)90198-2

Roditi, H. A., Strayer, D. L., & Findlay, S. E. G. (1997). Characteristics of zebra mussel (*Dreissena polymorpha*) biodeposits in a freshwater estuary. *Archiv fur Hydrobiologie*, 140 (2), 207-219.

Roe, S. L., & MacIsaac, H. J. (1997). Deepwater population structure and reproductive state of quagga mussels (*Dreissena bugensis*) in Lake Erie. *Can. J. of Fish. and Aquat. Sci*, 54 (10), 2428–2433. https://doi.org/10.1139/f97-151

Roley, S. S., & Tank, J. L. (2016). Pore water physicochemical constraints on the endangered clubshell mussel (*Pleurobema clava*). *Can. J. of Fish. and Aquat. Sci.*, 73 (12), 1712–1722. https://doi.org/10.1139/cjfas-2015-0442

Rothlisberger, J. D., Finnoff, D. C., Cooke, R. M., & Lodge, D. M. (2012). Ship-borne Nonindigenous Species Diminish Great Lakes Ecosystem Services. *Ecosystems*, 15 (3), 462–476. https://doi.org/10.1007/s10021-012-9522-6

Rowe, M. D., Kreis, R. G., & Dolan, D. M. (2014). A reactive nitrogen budget for Lake Michigan. *J. Great Lakes Res.*, 40 (1), 192–201. https://doi.org/10.1016/j.jglr.2013.11.005

Rowe, M. D., Anderson, E. J., Vanderploeg, H. A., Pothoven, S. A., Elgin, A. K., Wang, J., & Yousef, F. (2017). Influence of invasive quagga mussels, phosphorus loads, and climate on spatial and temporal patterns of productivity in Lake Michigan: A biophysical modeling study. *Limnol. Oceanogr.* ps://doi.org/10.1002/lno.10595

Ruban, V., Lopez-Sanchez F., J., Pardo, P., Rauret, G., Muntau, H., & Quevauviller, P. (1999). Selection and evaluation of sequential extraction procedures for the determination of phosphorus forms in lake sediment. *J. Environ. Monitor.*, 1 (1), 51–56. https://doi.org/10.1039/A807778I

Ruginis, T., Bartoli, M., Petkuviene, J., Zilius, M., Lubiene, I., Laini, A., & Razinkovas-Baziukas, A. (2014). Benthic respiration and stoichiometry of regenerated nutrients in lake sediments with *Dreissena polymorpha*. *Aquat. Sci.*, 76 (3), 405–417. https://doi.org/10.1007/s00027-014-0343-x

Sandwell, D. R., Pilditch, C. A., & Lohrer, A. M. (2009). Density dependent effects of an infaunal suspension-feeding bivalve (*Austrovenus stutchburyi*) on sandflat nutrient fluxes and microphytobenthic productivity. *Journal Exp. Mar. Biol. Ecol.*, 373 (1), 16–25. https://doi.org/10.1016/j.jembe.2009.02.015

Scavia, D., & Fahnenstiel, G. (1987). Dynamics of Lake Michigan Phytoplankton: Mechanisms Controlling Epilimnetic Communities. *J. Great Lakes Res.*, 13 (2), 103–120.

Schaeffer, J. S., Bowen, A., Thomas, M., French, J. R. P., & Curtis, G. L. (2005). Invasion history, proliferation, and offshore diet of the round goby *Neogobius melanostomus* in Western Lake Huron, USA. *J. Great Lakes Res.*, 31 (4), 414–425. https://doi.org/10.1016/S0380-1330(05)70273-2

Schneider, C. A.; Rasband, W. S. & Eliceiri, K. W. (2012), NIH Image to ImageJ: 25 years of image analysis, *Nat. Methods*, 9 (7), 671-675.

Shafer, M.M., Armstrong, D.E., 1994. Mass fluxes and recycling of phosphorus in Lake Michigan: The role of major particle phases in regulating the annual cycle. *Environmental Chemistry of Lakes and Reservoirs*. pp. 287–322.

Shen, C., Liao, Q., Bootsma, H. A., Troy, C. D., & Cannon, D. (2018). Regulation of plankton and nutrient dynamics by profundal quagga mussels in Lake Michigan: a one-dimensional model. *Hydrobiologia*. https://doi.org/10.1007/s10750-018-3547-6

Shen, C., Liao, Q., & Bootsma, H. A. (2020). Modelling the influence of invasive mussels on phosphorus cycling in Lake Michigan. *Ecol. Model.*, 416 , 108920. https://doi.org/10.1016/j.ecolmodel.2019.108920

Sisma-Ventura, G., & Rahav, E. (2019). DOP stimulates heterotrophic bacterial production in the oligotrophic southeastern Mediterranean coastal waters. *Front. Microbiol.*, 10 , 1–10. https://doi.org/10.3389/fmicb.2019.01913

Sø, H. U., Postma, D., Jakobsen, R., & Larsen, F. (2011). Sorption of phosphate onto calcite; results from batch experiments and surface complexation modeling. *Geochimica et Cosmochimica Acta*, 75 (10), 2911–2923. https://doi.org/10.1016/j.gca.2011.02.031

Sonzogni, W. C., Uttormark, P. C., & Lee, G. F. (1976). A phosphorus residence time model: Theory and application. *Water Res.*, 10 (5), 429–435. https://doi.org/10.1016/0043-1354(76)90061-0

Stainton, M.P., Capel, M.J., Armstrong, F.A.J., 1974. The chemical analysis of fresh water.

Stoeckmann, A., & Garton, D. (1997). A seasonal energy budget for zebra mussels (*Dreissena polymorpha*) in western Lake Erie. *Can. J. Fish. Aquat. Sci.*, 54 (12), 2743–2751. https://doi.org/10.1139/cjfas-54-12-2743

Stoeckmann, A., 2003. Physiological energetics of Lake Erie dreissenid mussels: a basis for the displacement of *Dreissena polymorpha* by *Dreissena bugensis*. *Can. J. Fish. Aquat. Sci*., 60, 126–134.

Strayer, D. L. (2009). Twenty years of zebra mussels: Lessons from the mollusk that made headlines. *Front. Ecol. Environ.*, 7 (3), 135–141. https://doi.org/10.1890/080020

Strayer, D. L. (2014). Understanding how nutrient cycles and freshwater mussels (*Unionoida*) affect one another. *Hydrobiologia*, 735 (1), 277–292. https://doi.org/10.1007/s10750-013-1461-5

Strong, A. E., & Eadie, B. J. (1978). Satellite observations of calcium carbonate precipitations in the Great Lakes. *Limnol. Oceanogr.*, 23 (5), 877–887.

Summers, B., Thorp, J. H., Alexander, J. E., & Fell, R. D. (1996). Respiratory adjustment of dreissenid mussels (*Dreissena polymorpha* and *Dreissena bugensis*) in response to chronic turbidity. *Can. J. Fish. Aquat. Sci*., 53 (7), 1626–1631. https://doi.org/10.1139/f96-096

Turner, C. B. (2010). Influence of zebra (*Dreissena polymorpha*) and quagga (*Dreissena rostriformis*) mussel invasions on benthic nutrient and oxygen dynamics. *Can. J. Fish. Aquat. Sci*., 67 (12), 1899–1908. https://doi.org/10.1139/F10-107

Turschak, B. A., Bunnell, D., Czesny, S., Höök, T. O., Janssen, J., Warner, D., & Bootsma, H. A. (2014). Nearshore energy subsidies support Lake Michigan fishes and invertebrates following major changes in food web structure. *Ecology*, 95 (5), 1243–1252. https://doi.org/10.1890/13-0329.1

Tyner, E. H., Bootsma, H. A., & Lafrancois, B. M. (2015). Dreissenid metabolism and ecosystem-scale effects as revealed by oxygen consumption. *J. Great Lakes Res.,* 41, 27–37. https://doi.org/10.1016/j.jglr.2015.05.009

Van Broekhoven, W., Jansen, H., Verdegem, M., Struyf, E., Troost, K., Lindeboom, H., & Smaal, A. (2015). Nutrient regeneration from feces and pseudofeces of mussel *mytilus edulis* spat. *Mar. Ecol. Prog. Ser.*, 534, 107–120. https://doi.org/10.3354/meps11402

Vanderploeg, H. A., Nalepa, T. F., Jude, D. J., Mills, E. L., Holeck, K. T., Liebig, J. R., Grigorovich, I., Ojaveer, H. (2002). Dispersal and emerging ecological impacts of Ponto-Caspian species in the Laurentian Great Lakes. *Can. J. Fish. Aquat. Sci*., 59 (7), 1209–1228. https://doi.org/10.1139/f02-087

Vanderploeg, H., Liebig, J., Nalepa, T., Fahnenstiel, G., Pothoven, S. 2010. *Dreissena* and the disappearance of the spring phytoplankton bloom in Lake Michigan. *J. Great Lakes Res.*, 36 (3), 50-59.

Vanderploeg, H. A., Pothoven, S. A., Fahnenstiel, G. L., Cavaletto, J. F., Liebig, J. R., Stow, C. A., Nalepa, T., Madenjian, T., Charles, P., Bunnell, D. B. (2012). Seasonal zooplankton dynamics in Lake Michigan: Disentangling impacts of resource limitation, ecosystem engineering, and predation during a critical ecosystem transition. *J. Great Lakes Res.*, 38 (2), 336–352. https://doi.org/10.1016/j.jglr.2012.02.005

Vanderploeg, H. A., Sarnelle, O., Liebig, J. R., Morehead, N. R., Robinson, S. D., Johengen, T. H., & Horst, G. P. (2017). Seston quality drives feeding, stoichiometry and excretion of zebra mussels. *Freshw. Biol.*, 62 (4), 664–680. https://doi.org/10.1111/fwb.12892

Vaughn, C. C., & Hoellein, T. J. (2018). Bivalve Impacts in Freshwater and Marine Ecosystems. *Annu. Rev. Ecol. Evol. Syst.*, 49 (1), 183–208. https://doi.org/10.1146/annurev-ecolsys-110617-062703

Vlčková, K., Mrázek, J., Kopečný, J., & Petrželková, K. J. (2012). Evaluation of different storage methods to characterize the fecal bacterial communities of captive western lowland gorillas (*Gorilla gorilla gorilla*). *Journal Microbiol. Methods*, 91 (1), 45–51. https://doi.org/10.1016/j.mimet.2012.07.015

Walsh, M. G., Dittman, D. E., & O'Gorman, R. (2007). Occurrence and food habits of the round goby in the profundal zone of southwestern Lake Ontario. *J. Great Lakes Res.*, *33*(1), 83–92.

Waples, J. T., Paddock, R., Janssen, J., Lovalvo, D., Schulze, B., Kaster, J., & Val Klump, J. (2005). High Resolution Bathymetry and Lakebed Characterization in the Nearshore of

Western Lake Michigan. *J. Great Lakes Res.*, 31, 64–74. https://doi.org/10.1016/S0380-1330(05)70290-2

Waples, J. T. (2020). Measuring bismuth-210, its parent, and daughter in aquatic systems. *Limnol. Oceanogr.: Methods*. https://doi.org/10.1002/lom3.10352

Watkins, J. M., Dermott, R., Lozano, S. J., Mills, E. L., Rudstam, L. G., & Scharold, J. V. (2007). Evidence for Remote Effects of Dreissenid Mussels on the Amphipod *Diporeia*: Analysis of Lake Ontario Benthic Surveys, 1972 – 2003. *J. Great Lakes Res.*, 33, 642–657.

Williams, J. D. H., Murphy, T. P., & Mayer, T. (1976). Rates of Accumulation of Phosphorus Forms in Lake Erie Sediments. *Can. J. Fish. Aquat. Sci*., 33 (3), 430–439. https://doi.org/10.1139/f76-064

Wu, Y., Wen, Y., Zhou, J., & Wu, Y. (2014). Phosphorus release from lake sediments: Effects of pH, temperature, and dissolved oxygen. *KSCE Journal of Civil Engineering*, *18*(1), 323–329. https://doi.org/10.1007/s12205-014-0192-0

Zhang, H., Culver, D. A., & Boegman, L. 2011. *Dreissenids* in Lake Erie: An algal filter or a fertilizer? *Aquat. Invasions*, 6(2): 175–1

Appendix A: Mussel Excretion rates for each experiment.

Date	Site	Size	Count	Dry mass (mg)	Volume (mL)	Time (hrs)	Temp. (˚C)	SRP (µmol mgDW^{-1} d^{-1})	TDP (µmol mgDW^{-1} d^{-1})	DOP (µmol mgDW^{-1} d^{-1})	O_2 (µmol mgDW^{-1} d^{-1})
4/20/2018	AW55	S (5-11mm)	4	21.6	120	2.0	3.5	0.0018	0.0020	0.0002	1.16
4/20/2018	AW55	S (5-11mm)	4	30.2	120	2.0	3.5	0.0013	0.0022	0.0008	1.46
4/20/2018	AW55	S (5-11mm)	4	19.5	120	2.0	3.5	0.0068	NA	NA	1.50
4/20/2018	AW55	M (12-19mm)	4	90.6	120	2.0	3.5	0.0012	0.0016	0.0003	0.49
4/20/2018	AW55	M (12-19mm)	4	106.7	120	2.0	3.5	0.0008	0.0013	0.0006	0.43
4/20/2018	AW55	M (12-19mm)	4	41.3	120	2.0	3.5	0.0027	0.0021	-0.0006	0.82
4/20/2018	AW55	L (20-27mm)	4	64.5	120	2.0	3.5	0.0010	0.0042	0.0032	0.83
4/20/2018	AW55	L (20-27mm)	4	99.1	120	2.0	3.5	0.0029	0.0035	0.0006	0.40
4/20/2018	AW55	L (20-27mm)	4	83.7	120	2.0	3.5	0.0026	0.0020	-0.0006	0.59
7/24/2018	AW55	S (5-11mm)	5	19	120	2.0	3.5	0.0008	0.0053	0.0045	1.46
7/24/2018	AW55	S (5-11mm)	6	12.9	120	2.0	3.5	0.0081	NA	NA	0.73
7/24/2018	AW55	S (5-11mm)	6	26.7	120	2.0	3.5	0.0105	0.0111	0.0006	0.94
7/24/2018	AW55	M (12-19mm)	4	25	120	2.0	3.5	0.0036	0.0042	0.0006	1.06
7/24/2018	AW55	M (12-19mm)	4	31.2	120	2.0	3.5	0.0056	0.0055	-0.0001	0.71
7/24/2018	AW55	M (12-19mm)	4	39	120	2.0	3.5	0.0022	0.0047	0.0025	0.46

Date	Site	Size	Count	Dry mass (mg)	Volume (mL)	Time (hrs)	Temp. (˚C)	SRP (μmol mgDW^{-1} d^{-1})	TDP (μmol mgDW^{-1} d^{-1})	DOP (μmol mgDW^{-1} d^{-1})	O_2 (μmol mgDW^{-1} d^{-1})
7/24/2018	AW55	L (20-27mm)	4	86.8	120	2.0	3.5	0.0029	0.0033	0.0004	0.24
7/24/2018	AW55	L (20-27mm)	4	70.8	120	2.0	3.5	0.0030	0.0034	0.0003	0.39
7/24/2018	AW55	L (20-27mm)	4	94.7	120	2.0	3.5	0.0015	0.0028	0.0012	0.24
8/6/2018	AW55	S (5-11mm)	5	11.5	120	2.3	4	0.0101	0.0108	0.0007	6.65
8/6/2018	AW55	S (5-11mm)	6	13.7	120	2.3	4	0.0117	0.0089	-0.0029	3.28
8/6/2018	AW55	S (5-11mm)	5	11.9	120	2.3	4	0.0080	0.0133	0.0052	4.63
8/6/2018	AW55	M (12-19mm)	4	26.1	120	2.3	4	0.0081	0.0061	-0.0021	2.33
8/6/2018	AW55	M (12-19mm)	4	28.9	120	2.3	4	0.0033	0.0011	-0.0022	0.83
8/6/2018	AW55	M (12-19mm)	4	31.6	120	2.3	4	0.0044	0.0045	0.0002	1.82
8/6/2018	AW55	L (20-27mm)	4	50.1	120	2.3	4	0.0060	0.0052	-0.0009	0.94
8/6/2018	AW55	L (20-27mm)	4	53	120	2.3	4	0.0061	NA	NA	0.97
8/6/2018	AW55	L (20-27mm)	4	51.2	120	2.3	4	0.0023	0.0054	0.0030	1.07
8/23/2018	AW55	S (5-11mm)	6	7.8	120	2.2	4	0.0053	NA	NA	NA
8/23/2018	AW55	S (5-11mm)	6	5.7	120	2.2	4	0.0016	0.0020	0.0004	NA
8/23/2018	AW55	M (12-19mm)	4	24.3	120	2.2	4	NA	0.0043	NA	NA
8/23/2018	AW55	M (12-19mm)	4	30.1	120	2.2	4	0.0029	0.0049	0.0020	NA

Date	Site	Size	Count	Dry mass (mg)	Volume (mL)	Time (hrs)	Temp. (˚C)	SRP (µmol mgDW^{-1} d^{-1})	TDP (µmol mgDW^{-1} d^{-1})	DOP (µmol mgDW^{-1} d^{-1})	O_2 (µmol mgDW^{-1} d^{-1})
8/23/2018	AW55	M (12-19mm)	4	26.8	120	2.2	4	0.0116	0.0140	0.0024	NA
8/23/2018	AW55	L (20-27mm)	4	60.2	120	2.2	4	NA	0.0029	NA	NA
8/23/2018	AW55	L (20-27mm)	4	45.8	120	2.2	4	0.0023	0.0035	0.0012	NA
8/23/2018	AW55	L (20-27mm)	4	58.5	120	2.2	4	0.0012	0.0025	0.0014	NA
9/11/2019	AW55	S (5-11mm)	5	8.3	100	2.0	4	0.0034	0.0042	0.0008	NA
9/11/2019	AW55	M (12-19mm)	4	15	100	2.0	4	0.0066	0.0065	-0.0001	NA
9/11/2019	AW55	M (12-19mm)	4	13.3	100	2.0	4	NA	0.0009	NA	NA
9/11/2019	AW55	M (12-19mm)	4	22	100	2.0	4	0.0031	0.0013	-0.0018	NA
9/11/2019	AW55	L (20-27mm)	4	47.4	100	2.0	4	0.0041	0.0047	0.0007	NA
9/11/2019	AW55	L (20-27mm)	4	50.9	100	2.0	4	0.0032	0.0034	0.0002	NA
9/11/2019	AW55	L (20-27mm)	4	53.6	100	2.0	4	0.0029	0.0032	0.0003	NA
10/9/2018	AW55	S (5-11mm)	10	17	100	2.0	6	0.0038	0.0037	-0.0001	3.89
10/9/2018	AW55	S (5-11mm)	10	26.2	100	2.0	6	0.0023	0.0019	-0.0004	0.89
10/9/2018	AW55	S (5-11mm)	10	15.2	100	2.0	6	0.0106	0.0108	0.0003	5.24
10/9/2018	AW55	M (12-19mm)	4	34.1	100	2.0	6	0.0028	0.0004	-0.0024	1.11
10/9/2018	AW55	M (12-19mm)	4	25.5	100	2.0	6	0.0070	0.0076	0.0006	1.24

Date	Site	Size	Count	Dry mass (mg)	Volume (mL)	Time (hrs)	Temp. (˚C)	SRP (µmol mgDW^{-1} d^{-1})	TDP (µmol mgDW^{-1} d^{-1})	DOP (µmol mgDW^{-1} d^{-1})	O$_2$ (µmol mgDW^{-1} d^{-1})
10/9/2018	AW55	M (12-19mm)	4	37.8	100	2.0	6	0.0020	0.0025	0.0004	1.60
10/9/2018	AW55	L (20-27mm)	4	55.7	100	2.0	6	0.0029	0.0033	0.0004	1.62
10/9/2018	AW55	L (20-27mm)	4	56.3	100	2.0	6	0.0061	0.0055	-0.0006	1.32
10/9/2018	AW55	L (20-27mm)	4	48.8	100	2.0	6	0.0051	0.0047	-0.0004	0.96
5/2/2019	AW55	S (5-11mm)	11	10.5	100	2.0	3.5	0.0025	NA	NA	NA
5/2/2019	AW55	S (5-11mm)	9	14.9	100	2.0	3.5	0.0021	0.0016	-0.0005	NA
5/2/2019	AW55	S (5-11mm)	10	14.2	100	2.0	3.5	0.0034	0.0030	-0.0003	NA
5/2/2019	AW55	M (12-19mm)	5	35.6	100	2.0	3.5	0.0017	0.0029	0.0012	NA
5/2/2019	AW55	M (12-19mm)	4	26.9	100	2.0	3.5	0.0032	0.0037	0.0005	NA
5/2/2019	AW55	M (12-19mm)	4	19.6	100	2.0	3.5	0.0066	0.0058	-0.0009	NA
5/2/2019	AW55	L (20-27mm)	5	84.8	100	2.0	3.5	0.0032	0.0034	0.0002	NA
5/2/2019	AW55	L (20-27mm)	4	63.1	100	2.0	3.5	0.0056	0.0052	-0.0005	NA
5/2/2019	AW55	L (20-27mm)	5	62.6	100	2.0	3.5	0.0044	0.0038	-0.0007	NA
7/1/2019	AW55	S (5-11mm)	8	12.1	100	2.0	4	0.0044	0.0059	0.0015	2.76
7/1/2019	AW55	S (5-11mm)	10	13.2	100	2.0	4	0.0024	0.0036	0.0012	3.21
7/1/2019	AW55	M (12-19mm)	5	49.6	100	2.0	4	0.0074	0.0070	-0.0003	NA

Date	Site	Size	Count	Dry mass (mg)	Volume (mL)	Time (hrs)	Temp. (˚C)	SRP (µmol mgDW^{-1} d^{-1})	TDP (µmol mgDW^{-1} d^{-1})	DOP (µmol mgDW^{-1} d^{-1})	O_2 (µmol mgDW^{-1} d^{-1})
7/1/2019	AW55	M (12-19mm)	5	26.1	100	2.0	4	0.0054	0.0032	-0.0022	2.48
7/1/2019	AW55	M (12-19mm)	5	31.6	100	2.0	4	0.0029	0.0039	0.0010	0.28
7/1/2019	AW55	L (20-27mm)	4	65.6	100	2.0	4	0.0030	0.0036	0.0005	0.11
7/1/2019	AW55	L (20-27mm)	4	56.8	100	2.0	4	0.0039	0.0038	0.0000	0.59
7/1/2019	AW55	L (20-27mm)	4	43	100	2.0	4	0.0051	0.0059	0.0008	0.78
12/5/2019	AW55	M (12-19mm)	5	31.5	70	1.3	3.5	0.0051	0.0107	0.0055	NA
12/5/2019	AW55	M (12-19mm)	5	39	70	1.3	3.5	0.0050	0.0105	0.0055	NA
12/5/2019	AW55	M (12-19mm)	5	43.2	70	1.3	3.5	0.0040	0.0073	0.0033	NA
7/17/2018	AW25	S (5-11mm)	4	13.2	120	2.0	4	0.0076	0.0122	0.0047	5.49
7/17/2018	AW25	S (5-11mm)	4	18.8	120	2.0	4	0.0011	0.0005	-0.0006	5.24
7/17/2018	AW25	S (5-11mm)	4	4.9	120	2.0	4	NA	NA	NA	8.99
7/17/2018	AW25	M (12-19mm)	4	50	120	2.0	4	0.0010	0.0009	-0.0001	0.97
7/17/2018	AW25	M (12-19mm)	4	33.6	120	2.0	4	0.0013	0.0021	0.0007	0.91
7/17/2018	AW25	M (12-19mm)	4	42.9	120	2.0	4	0.0027	NA	NA	2.02
7/17/2018	AW25	L (20-27mm)	4	66	120	2.0	4	0.0020	0.0017	-0.0004	0.79
7/17/2018	AW25	L (20-27mm)	4	76	120	2.0	4	0.0019	0.0022	0.0003	0.63

Date	Site	Size	Count	Dry mass (mg)	Volume (mL)	Time (hrs)	Temp. (˚C)	SRP (µmol mgDW^{-1} d^{-1})	TDP (µmol mgDW^{-1} d^{-1})	DOP (µmol mgDW^{-1} d^{-1})	O_2 (µmol mgDW^{-1} d^{-1})
7/17/2018	AW25	L (20-27mm)	4	91.7	120	2.0	4	0.0032	0.0046	0.0014	0.48
8/16/2018	AW25	S (5-11mm)	4	10.2	100	2.0	6	NA	0.0027	NA	8.98
8/16/2018	AW25	S (5-11mm)	4	8.6	100	2.0	6	NA	0.0047	NA	10.48
8/16/2018	AW25	S (5-11mm)	4	10	100	2.0	6	0.0024	0.0095	0.0072	6.91
8/16/2018	AW25	M (12-19mm)	4	49.6	100	2.0	6	0.0037	0.0050	0.0013	2.46
8/16/2018	AW25	M (12-19mm)	4	29.5	100	2.0	6	0.0077	0.0092	0.0014	2.81
8/16/2018	AW25	M (12-19mm)	4	83.1	100	2.0	6	0.0024	0.0032	0.0008	1.55
8/16/2018	AW25	L (20-27mm)	4	103.6	100	2.0	6	0.0019	0.0027	0.0007	1.27
8/16/2018	AW25	L (20-27mm)	4	115.2	100	2.0	6	0.0039	0.0055	0.0015	1.14
8/16/2018	AW25	L (20-27mm)	4	77.1	100	2.0	6	0.0023	0.0031	0.0008	1.33
9/4/2018	AW25	S (5-11mm)	4	5.7	100	2.2	7.5	0.0346	0.0317	-0.0029	NA
9/4/2018	AW25	S (5-11mm)	4	6.9	100	2.2	7.5	0.0223	0.0157	-0.0066	NA
9/4/2018	AW25	S (5-11mm)	4	9.7	100	2.2	7.5	0.0241	0.0257	0.0016	NA
9/4/2018	AW25	M (12-19mm)	4	43.8	100	2.2	7.5	0.0062	0.0070	0.0008	NA
9/4/2018	AW25	M (12-19mm)	4	51.2	100	2.2	7.5	0.0058	0.0063	0.0005	NA
9/4/2018	AW25	M (12-19mm)	4	29.2	100	2.2	7.5	0.0105	0.0148	0.0044	NA

Date	Site	Size	Count	Dry mass (mg)	Volume (mL)	Time (hrs)	Temp. (˚C)	SRP (µmol mgDW^{-1} d^{-1})	TDP (µmol mgDW^{-1} d^{-1})	DOP (µmol mgDW^{-1} d^{-1})	O$_2$ (µmol mgDW^{-1} d^{-1})
9/4/2018	AW25	L (20-27mm)	4	92	100	2.2	7.5	0.0077	0.0077	0.0000	NA
9/4/2018	AW25	L (20-27mm)	4	134.9	100	2.2	7.5	0.0079	0.0106	0.0027	NA
9/4/2018	AW25	L (20-27mm)	4	96.2	100	2.2	7.5	0.0053	0.0057	0.0004	NA
10/18/2018	AW25	S (5-11mm)	4	12.6	100	2.0	7	0.0335	0.0287	-0.0048	NA
10/18/2018	AW25	S (5-11mm)	4	30.8	100	2.0	7	0.0131	0.0121	-0.0010	NA
10/18/2018	AW25	M (12-19mm)	4	37.4	100	2.0	7	0.0015	0.0002	-0.0013	NA
10/18/2018	AW25	M (12-19mm)	4	32.3	100	2.0	7	0.0034	0.0027	-0.0007	NA
10/18/2018	AW25	M (12-19mm)	4	43.7	100	2.0	7	0.0047	0.0041	-0.0006	NA
10/18/2018	AW25	L (20-27mm)	4	96.8	100	2.0	7	0.0071	0.0067	-0.0005	NA
10/18/2018	AW25	L (20-27mm)	4	124.7	100	2.0	7	0.0057	0.0054	-0.0003	NA
10/18/2018	AW25	L (20-27mm)	4	82.7	100	2.0	7	0.0054	0.0051	-0.0004	NA
4/25/2019	AW25	S (5-11mm)	4	12.6	100	2.2	3.5	0.0115	0.0207	0.0093	0.99
4/25/2019	AW25	S (5-11mm)	4	16.2	100	2.2	3.5	0.0065	0.0139	0.0075	0.56
4/25/2019	AW25	M (12-19mm)	4	35.5	100	2.2	3.5	0.0094	0.0090	-0.0005	1.19
4/25/2019	AW25	M (12-19mm)	4	53.7	100	2.2	3.5	0.0036	0.0036	0.0000	1.09
4/25/2019	AW25	M (12-19mm)	4	37.3	100	2.2	3.5	0.0041	0.0060	0.0018	0.57

Date	Site	Size	Count	Dry mass (mg)	Volume (mL)	Time (hrs)	Temp. (˚C)	SRP (µmol mgDW^{-1} d^{-1})	TDP (µmol mgDW^{-1} d^{-1})	DOP (µmol mgDW^{-1} d^{-1})	O_2 (µmol mgDW^{-1} d^{-1})
4/25/2019	AW25	L (20-27mm)	4	99.4	100	2.2	3.5	0.0023	0.0021	-0.0002	0.73
4/25/2019	AW25	L (20-27mm)	4	105.1	100	2.2	3.5	0.0050	0.0049	-0.0001	0.51
4/25/2019	AW25	L (20-27mm)	4	94	100	2.2	3.5	0.0060	0.0062	0.0002	0.60
9/20/2019	AW25	S (5-11mm)	4	13	100	2.0	8	0.0026	NA	NA	NA
9/20/2019	AW25	S (5-11mm)	4	10	100	2.0	8	0.0048	0.0065	0.0018	NA
9/20/2019	AW25	M (12-19mm)	4	24.4	100	2.0	8	0.0060	0.0059	-0.0001	NA
9/20/2019	AW25	M (12-19mm)	4	30.5	100	2.0	8	0.0113	NA	NA	NA
9/20/2019	AW25	M (12-19mm)	4	39.4	100	2.0	8	0.0056	0.0063	0.0007	NA
9/20/2019	AW25	L (20-27mm)	4	92.9	100	2.0	8	0.0016	0.0030	0.0015	NA
9/20/2019	AW25	L (20-27mm)	4	90.1	100	2.0	8	0.0032	0.0033	0.0001	NA
9/20/2019	AW25	L (20-27mm)	4	98.2	100	2.0	8	0.0050	0.0048	-0.0002	NA

Appendix B: Mussel Egestion rates for each experiment.

Date	Site	Size	Time (hr)	Temp. (˚C)	Dry Mass (mg)	P (µmol mgDW^{-1} d^{-1})	C (µmol mgDW^{-1} d^{-1})	N (µmol mgDW^{-1} d^{-1})
7/17/2018	AW25	L (15-25mm)	2	4	508.70	0.0025	0.9118	0.1162
7/17/2018	AW25	L (15-25mm)	2	4	513.20	0.0062	0.8602	0.0734
7/17/2018	AW25	L (15-25mm)	2	4	586.10	NA	0.2066	0.0504
7/17/2018	AW25	S (5-14mm)	2	4	192.80	0.0037	0.2578	NA
8/16/2018	AW25	L (15-25mm)	2	6	673.80	0.0031	0.5356	0.0330
8/16/2018	AW25	L (15-25mm)	2	6	1004.40	0.0018	0.5761	0.0460
8/16/2018	AW25	L (15-25mm)	2	6	664.40	0.0021	1.2987	0.1237
8/16/2018	AW25	S (5-14mm)	2	6	36.00	0.0081	2.9512	NA
8/16/2018	AW25	S (5-14mm)	2	6	29.20	0.0078	4.6865	NA
8/16/2018	AW25	S (5-14mm)	2	6	49.60	0.0053	NA	NA
9/4/2018	AW25	L (15-25mm)	2	7.5	419.20	0.0037	0.4814	0.0436
9/4/2018	AW25	L (15-25mm)	2	7.5	492.70	0.0037	0.8296	0.0816
9/4/2018	AW25	L (15-25mm)	2	7.5	497.70	0.0033	0.4775	0.0478
9/4/2018	AW25	S (5-14mm)	2	7.5	33.50	0.0073	1.3811	NA

Date	Site	Size	Time (hr)	Temp. (˚C)	Dry Mass (mg)	P (μmol mgDW^{-1} d^{-1})	C (μmol mgDW^{-1} d^{-1})	N (μmol mgDW^{-1} d^{-1})
9/4/2018	AW25	S (5-14mm)	2	7.5	38.30	0.0019	1.6231	NA
9/4/2018	AW25	S (5-14mm)	2	7.5	51.00	0.0052	0.4880	NA
10/18/2018	AW25	L (15-25mm)	2	7	430.10	0.0048	0.7058	0.0281
10/18/2018	AW25	L (15-25mm)	2	7	347.80	0.0034	1.0025	0.0276
10/18/2018	AW25	L (15-25mm)	2	7	428.30	0.0032	0.6709	0.0148
4/25/2019	AW25	L (15-25mm)	2	4	505.7	0.0080	1.2431	0.0599
4/25/2019	AW25	L (15-25mm)	2	4	617.6	0.0053	0.9454	0.0630
4/25/2019	AW25	L (15-25mm)	2	4	646.3	0.0036	0.5790	0.0424
4/25/2019	AW25	S (5-14mm)	2	4	31.3	0.0198	0.9283	NA
4/25/2019	AW25	S (5-14mm)	2	4	77.2	0.0035	0.6741	NA
4/25/2019	AW25	S (5-14mm)	2	4	44.4	0.0142	1.0795	NA
9/20/2019	AW25	L (15-25mm)	2	8	750	0.0064	0.9530	0.0690
9/20/2019	AW25	L (15-25mm)	2	8	1011.4	0.0169	2.7617	0.1855
9/20/2019	AW25	L (15-25mm)	2	8	522.3	0.0108	1.7524	0.1092
4/20/2018	AW55	L (15-25mm)	2	3.5	945.7	0.0020	0.4060	0.0271

Date	Site	Size	Time (hr)	Temp. (˚C)	Dry Mass (mg)	P (µmol mgDW^{-1} d^{-1})	C (µmol mgDW^{-1} d^{-1})	N (µmol mgDW^{-1} d^{-1})
4/20/2018	AW55	L (15-25mm)	2	3.5	1458.2	0.0027	0.2947	0.0160
4/20/2018	AW55	L (15-25mm)	2	3.5	590.2	0.0058	0.6038	0.0576
4/20/2018	AW55	L (15-25mm)	2	3.5	813.8	0.0011	1.6022	0.0562
4/20/2018	AW55	L (15-25mm)	2	3.5	2343.6	0.0011	0.2350	0.0157
8/6/2018	AW55	L (15-25mm)	2	4	398.9	0.0028	0.7567	0.0653
8/6/2018	AW55	L (15-25mm)	2	4	386.60	0.0023	0.8036	0.0687
8/6/2018	AW55	L (15-25mm)	2	4	338.20	0.0015	0.2476	0.0261
8/6/2018	AW55	S (5-14mm)	2	4	122.1	0.0043	1.0001	NA
8/6/2018	AW55	S (5-14mm)	2	4	115.7	0.0142	1.2715	NA
8/6/2018	AW55	S (5-14mm)	2	4	108.7	0.0056	1.0152	NA
8/23/2018	AW55	L (15-25mm)	2	4	349.4	0.0022	0.2543	0.0680
8/23/2018	AW55	L (15-25mm)	2	4	394.4	0.0052	0.9005	0.1099
8/23/2018	AW55	L (15-25mm)	2	4	342.6	0.0073	1.1327	0.1695
8/23/2018	AW55	S (5-14mm)	2	4	33	0.0016	0.6153	NA
8/23/2018	AW55	S (5-14mm)	2	4	45.3	0.0013	0.3400	NA

Date	Site	Size	Time (hr)	Temp. (˚C)	Dry Mass (mg)	P (µmol mgDW^{-1} d^{-1})	C (µmol mgDW^{-1} d^{-1})	N (µmol mgDW^{-1} d^{-1})
8/23/2018	AW55	S (5-14mm)	2	4	46.2	0.0014	NA	NA
9/11/2018	AW55	L (15-25mm)	2	4	438.00	0.0021	0.2762	
9/11/2018	AW55	L (15-25mm)	2	4	485.90	0.0012	0.3280	0.0405
9/11/2018	AW55	L (15-25mm)	2	4	366.4	0.0018	0.4642	0.0581
9/11/2018	AW55	S (5-14mm)	2	4	56.6	0.0020	1.0928	NA
9/11/2018	AW55	S (5-14mm)	2	4	64.4	0.0028	0.6574	NA
10/9/2018	AW55	L (15-25mm)	2	6	406.6	0.0041	0.5797	0.0472
10/9/2018	AW55	L (15-25mm)	2	6	419.7	0.0030	0.5486	0.0320
10/9/2018	AW55	L (15-25mm)	2	6	409.2	0.0039	1.0519	0.0800
10/9/2018	AW55	S (5-14mm)	2	6	85.5	0.0055	0.8117	NA
10/9/2018	AW55	S (5-14mm)	2	6	79.7	0.0081	0.9781	NA
10/9/2018	AW55	S (5-14mm)	2	6	90.1	0.0041	0.6124	NA
5/2/2019	AW55	L (15-25mm)	2	3.5	366	0.0019	2.0750	0.1284
5/2/2019	AW55	L (15-25mm)	2	3.5	322.3	0.0010	1.2888	0.1000
5/2/2019	AW55	L (15-25mm)	2	3.5	386.7	0.0003	0.8287	0.1201

Date	Site	Size	Time (hr)	Temp. (˚C)	Dry Mass (mg)	P (μmol mgDW^{-1} d^{-1})	C (μmol mgDW^{-1} d^{-1})	N (μmol mgDW^{-1} d^{-1})
5/2/2019	AW55	S (5-14mm)	2	3.5	38.2	NA	1.0418	NA
5/2/2019	AW55	S (5-14mm)	2	3.5	50.5	0.0034	0.5868	NA
5/2/2019	AW55	S (5-14mm)	2	3.5	48.3	0.0008	1.1537	NA
7/1/2019	AW55	L (15-25mm)	2	4	378.9	0.0081	1.0055	0.0961
7/1/2019	AW55	L (15-25mm)	2	4	473	0.0064	0.6215	0.0576
7/1/2019	AW55	L (15-25mm)	2	4	449.1	0.0027	0.3591	0.0276
7/1/2019	AW55	S (5-14mm)	2	4	88.2	0.0023	0.5117	NA
7/1/2019	AW55	S (5-14mm)	2	4	57.5	0.0021	0.4377	NA
7/1/2019	AW55	S (5-14mm)	2	4	53.1	0.0052	0.5336	NA
12/5/2019	AW55	L (15-25mm)	2	3.5	422.6	0.0190	NA	NA
12/5/2019	AW55	L (15-25mm)	2	3.5	418.1	0.0059	NA	NA
12/5/2019	AW55	L (15-25mm)	2	3.5	453.1	0.0008	NA	NA

Appendix C: Mussel Clearance Rates Calculations

Date	Site	Biomass (mg m^{-2})	St. Error	PP (µmol L^{-1})	P capture (µmol m^{-2} d^{-1})	St. Error	Clearance (L $mgDW^{-1}$ d^{-1})	St. Error
4/20/2018	AW55	41500	3765	0.03	203.11	49.14	0.19	0.05
8/6/2018	AW55	41500	3765	0.05	470.04	132.85	0.24	0.07
8/23/2018	AW55	41500	3765	0.07	331.07	114.04	0.11	0.04
9/11/2018	AW55	41500	3765	0.02	243.25	42.42	0.26	0.05
10/9/2018	AW55	41500	3765	0.04	385.28	77.80	0.24	0.05
5/14/2019	AW55	41500	3765	0.02	213.75	43.53	0.24	0.05
7/1/2019	AW55	41500	3765	0.02	376.40	68.06	0.55	0.11
7/17/2018	AW25	20926	6128	0.06	141.34	52.83	0.11	0.05
8/16/2018	AW25	20926	6128	0.03	171.35	62.08	0.28	0.13
9/4/2018	AW25	20926	6128	0.04	376.83	138.93	0.42	0.20
10/18/2018	AW25	20926	6128	0.04	274.13	116.14	0.31	0.16
4/25/2019	AW25	20926	6128	0.03	316.13	118.40	0.53	0.25
9/20/2019	AW25	20926	6128	0.05	342.36	124.58	0.31	0.14

Appendix D: Biodeposit Composition After Incubation for the Batch Experiments

Exp. A Biodeposit Composition Report

Duration (days)	Volume (L)	Biodeposit		Mass (mg)	P (µmol)	N (µmol)	C (µmol)	C:P	C:N
14	0.5	Starting (S) (n=2)	Mean	1.95	0.13	0.5	9.5	73.2	18.3
			Standard Deviation	0.85	0.06	0.1	0.9	32.6	8.4
		Biodeposit Treatment (BE) (n=3)	Mean	3	0.22	2.9	33.8	160.7	11.5
			Standard Deviation	0.08	0.04	0.1	2.4	41.1	0.4
		Biodeposit with added P Treatment (B+E) (n=3)	Mean	2.53	0.43	3.9	39.1	114.0	9.9
			Standard Deviation	0.41	0.23	0.2	4.5	45.5	0.9
		Biodeposit: Starting t-test p value		0.43	0.30	0.0010	0.0003	0.2	0.06
		Biodeposit + P: Starting t-test p value		0.62	0.19	0.01	0.0007	0.98	0.017

Exp. B Biodeposit Composition Report

Duration (days)	Volume (L)	Biodeposit		Mass (mg)	P (µmol)	N (µmol)	C (µmol)	C:P	C:N
17	0.5	Starting (S) (n=3)	Mean	13	0.60	4.6	75.0	125.9	16.4
			Standard Deviation	0.4	0.02	0.1	2.2	5.1	0.7
		Biodeposit Treatment (BE) (n=3)	Mean	12.2	0.70	5.4	82.4	117.3	15.4
			Standard Deviation	0.4	0.10	0.7	5.7	17.9	2.9
		Biodeposit with added P Treatment (B+E) (n=3)	Mean	11.9	0.79	11.1	133.3	168.8	12.0
			Standard Deviation	0.9	0.09	4.0	34.2	46.9	4.5
		Biodeposit: Starting t-test p value		0.11	0.25	0.25	0.20	0.6	0.32
		Biodeposit + P: Starting t-test p value		0.22	0.08	0.35	0.34	0.57	0.23

Exp. C Biodeposit Composition Report

Duration (days)	Volume (L)	Biodeposit		Mass (mg)	P (μmol)	N (μmol)	C (μmol)	C:P	C:N
22	3	Starting (S) (n=4)	Mean	10.35	0.63	5.4	73.2	116.0	13.5
			Standard Deviation	0.89	0.06	0.4	6.6	14.9	1.7
		Biodeposit Treatment (BE) (n=2)	Mean	8.58	0.57	9.5	94.9	165.2	10.0
			Standard Deviation	0.25	0.05	0.1	1.3	14.1	0.8
		Biodeposit with added P Treatment (B+E) (n=3)	Mean	15.78	1.84	43.2	411.2	223.0	9.5
			Standard Deviation	1.42	0.17	7.6	53.3	35.6	1.9
		Biodeposit: Starting t-test p value		0.03	0.29	0.0003	0.02	0.20	0.006
		Biodeposit + P: Starting t-test p value		0.02	0.007	0.02	0.01	0.08	0.001

Appendix E: Biofilm Composition for Batch Experiment 3

Exp. C Biofilm Composition Report

Biodeposit		P (μmol)	N (μmol)	C (μmol)	C:P	C:N
FW+ (n=3)	Mean	1.71	20.89	110.34	64.77	5.30
	Standard Deviation	0.08	3.34	15.48	10.88	0.15
B (n=2)	Mean	0.02	1.18	10.59	451.20	9.11
	Standard Deviation	0.01	0.71	6.12	12.25	0.27
B+ (n=3)	Mean	0.52	11.26	111.94	216.32	9.98
	Standard Deviation	0.07	3.10	30.72	43.53	0.68
One-way ANOVA P Value		0.00001	0.005	0.016	0.000	0.0003
Tukey HSD P values		FW+-B :0.00001	FW+-B :0.004	FW+-B :0.02	FW+-B :0.0002	FW+-B :0.002
		FW+-B+: 0.00003	FW+-B+: 0.046	FW+-B+: 0.99	FW+-B+: 0.008	FW+-B+: 0.0004
		B-B+: 0.003	B-B+: 0.059	B-B+: 0.02	B-B+: 0.002	B-B+: 0.29

Appendix F: Biodeposit and Biofilm Composition for the Flow-Through Biodeposit Experiment

Flow Exp. Biodeposit Composition Report									
Duration (days)	Volume (L)	Biodeposit		Mass (mg)	P (µmol)	N (µmol)	C (µmol)	C:P	C:N
12	1	Starting (S) (n=4)	Mean	1.67	0.08	1.5	15.8	193.6	10.2
			Standard Deviation	0.16	0.01	0.2	1.7	25.6	1.44
		Biodeposit Treatment (BE) (n=3)	Mean	1.47	0.10	2.5	24.6	251.8	9.9
			Standard Deviation	0.29	0.02	0.3	2.9	50.6	1.96
		Antibiotic Treatment (AB) (n=3)	Mean	1.27	0.10	2.4	20.6	198.6	8.6
			Standard Deviation	0.18	0.02	0.2	3.0	53.6	2.1
		Biodeposit: Starting t test p value		0.44	0.29	0.02	0.03	0.03	0.35
		Antibiotic +Biodeposit: Starting t test p value		0.06	0.32	0.02	0.14	0.7	0.07

Flow Exp. Biofilm Composition Report						
Biodeposit		P (µmol)	N (µmol)	C (µmol)	C:P	C:N
C (n=2)	Mean	0.05	11.76	105.01	2221.40	8.28
	Standard Deviation	0.00	8.27	79.37	1617.25	0.93
B (n=3)	Mean	0.14	3.34	21.28	154.48	6.40
	Standard Deviation	0.05	0.99	6.42	16.84	0.35
AB (n=3)	Mean	0.07	5.24	34.08	560.68	6.47
	Standard Deviation	0.02	1.49	10.96	260.71	0.51
One-way ANOVA P Value		0.09	0.31	0.26	0.18	0.08
Tukey HSD P values		NA	NA	NA	NA	NA

Appendix G: AW55 Near Mussel Bed P Concentrations Measured with Membrane Profiler

Site	Deployment period	Depth above bottom (cm)	SRP (µg/L)
AW55	7/23/18-7/31/18	35.3	1.29
AW55	7/23/18-7/31/18	30.8	2.11
AW55	7/23/18-7/31/18	26.9	1.24
AW55	7/23/18-7/31/18	22.6	1.02
AW55	7/23/18-7/31/18	18.7	1.08
AW55	7/23/18-7/31/18	15.5	0.59
AW55	7/23/18-7/31/18	7	2.10
AW55	7/23/18-7/31/18	3	2.36
AW55	8/9/18-8/16/18	29.6	0.85
AW55	8/9/18-8/16/18	27.3	0.58
AW55	8/9/18-8/16/18	23.2	0.76
AW55	8/9/18-8/16/18	20.3	0.60
AW55	8/9/18-8/16/18	15.7	0.78
AW55	8/9/18-8/16/18	11.7	0.63
AW55	8/9/18-8/16/18	7.3	0.81
AW55	8/9/18-8/16/18	3.5	1.12
AW55	8/16/18-8/23/18	32	0.69
AW55	8/16/18-8/23/18	25	0.74
AW55	8/16/18-8/23/18	16.5	0.90
AW55	8/16/18-8/23/18	11	0.77
AW55	8/16/18-8/23/18	7	1.04
AW55	8/16/18-8/23/18	31.8	0.67
AW55	8/16/18-8/23/18	25.3	0.72
AW55	8/16/18-8/23/18	21.3	0.57
AW55	8/16/18-8/23/18	13.3	0.92
AW55	8/16/18-8/23/18	9.3	0.84
AW55	8/16/18-8/23/18	5.5	1.14
AW55	8/23/18-9/4/18	30.4	0.77
AW55	8/23/18-9/4/18	26.7	0.92
AW55	8/23/18-9/4/18	22.1	0.46
AW55	8/23/18-9/4/18	18.5	0.70
AW55	8/23/18-9/4/18	14.7	0.54
AW55	8/23/18-9/4/18	10	0.59
AW55	9/11/18-9/25/18	33.3	0.00
AW55	9/11/18-9/25/18	30.8	0.89
AW55	9/11/18-9/25/18	26.8	0.23
AW55	9/11/18-9/25/18	22.8	0.23

AW55	9/11/18-9/25/18	18.9	0.70
AW55	9/11/18-9/25/18	14.8	0.56
AW55	9/11/18-9/25/18	10.8	0.66
AW55	9/11/18-9/25/18	7	2.31
AW55	7/1/19-7/11/19	21	0.80
AW55	7/1/19-7/11/19	17.1	1.24
AW55	7/1/19-7/11/19	12.6	0.91
AW55	7/1/19-7/11/19	8.4	1.99
AW55	7/1/19-7/11/19	26.7	1.38
AW55	7/1/19-7/11/19	22.7	1.14
AW55	7/1/19-7/11/19	18.4	1.41
AW55	7/1/19-7/11/19	14.4	0.82
AW55	7/1/19-7/11/19	10.1	1.92
AW55	7/1/19-7/11/19	5.7	1.51

Appendix H: AW55 Sediment Dissolved Oxygen Profiles form 7/19/18

Core 1		Core 2		Core 3		Core 4		Core 5		Core 6	
Depth (cm)	DO (ppm)	Depth (cm)	DO (ppm)	Depth (cm)	DO (ppm)	Depth (cm)	DO (ppm)	Depth (cm)	DO (ppm)	Depth (cm)	DO (ppm)
2	9.47	3	9.33	2	8.5	1.5	9.08	2	9.72	2	9.48
0.5	9.24	2	9.35	1.5	8.05	1	8.68	1.5	9.04	1	9.55
0	7.06	1.5	9.35	1	7.87	0.5	8.14	1	9.04	0.5	9.54
-0.4	5.1	1	9.17	0.5	7.8	0	6.55	0.5	8.71	0	7.99
-0.6	4.33	0.5	8.91	0	6.16	-0.4	5.35	0	8.18	-0.2	6.12
-0.7	2.1	0	7.95	-0.2	5.7	-0.6	4.69	-0.3	6.91	-0.6	4.87
-0.8	1.81	-0.2	7.26	-0.5	5.01	-0.8	4.22	-0.5	6.71	-0.9	4.45
-1	0.93	-0.4	7.16	-1	4.86	-1	3.61	-0.7	5.53	-1.3	4.07
-1.1	0.52	-0.8	5.63	-1.4	4.49	-1.2	3.29	-1	4.54	-1.8	3.9
-1.2	0.43	-1.1	4.96	-1.6	4.19	-1.4	3.14	-1.5	3.01	-2.8	3.4
-1.4	0.11	-1.3	4.61	-2	3.83	-1.6	2.76	-1.7	2.81		
-1.5	0	-1.6	4.4	-2.3	3.53	-1.8	2.61	-1.9	2.81		
		-1.8	4.23	-2.8	3.12	-2	2.41	-2.1	1.91		
		-2	4.15	-3.1	3.12	-3	1.99	-2.4	1.46		
		-2.1	4.11	-3.6	2.69	-7	1.7	-2.8	1.38		
		-2.3	4.07	-4	2.56	-8	0.95	-3	1.35		
		-2.5	3.97	-4.5	2.51	-8.5	0.74	-3.2	1.17		
		-2.7	3.84	-5	2.52	-9.5	0.41	-3.6	1.08		
		-2.9	3.73			-10	0.25	-3.8	1.03		
		-3.3	3.67			-11	0.12	-4	0.99		
		-3.5	3.34			-11.5	0.1	-4.2	0.98		
		-3.7	3.31					-4.4	0.97		
								-4.6	0.97		
								-4.8	0.95		
								-5.2	0.94		
								-5.6	0.91		
								-6	0.87		
								-6.2	0.77		
								-6.6	0.73		
								-6.9	0.72		

Appendix H: 100m Site Dissolved Oxygen Profiles from 7/23/19

Core 1		Core 2	
Depth (cm)	DO (ppm)	Depth (cm)	DO (ppm)
-4.5	12.28	-2	13.86
-4.3	12.25	-0.5	13.63
-3	12.43	0	9.86
-1.5	12.42	0.4	7.32
0	12.03	1.5	8.06
0.2	10.65	1.9	8.07
0.5	10.19	2.3	6.72
0.7	8.47	2.7	6.7
1.1	7.34	3	2.72
1.4	7.22	3.3	2.48
1.8	7.83		
2.1	7.14		
2.6	4.22		
2.8	3.11		
3.1	2.52		
3.5	2.21		

Appendix I: 100m Site Sediment Porosity, Dry Bulk Density, C and N by depth

Date collected	Site	Core	Depth (cm)	Porosity (%)	TC (mg/g)	St. Error	OC (mg/g)	St. Error	TN (mg/g)	St. Error	$\delta^{13}C/\delta^{12}C$	St. Error	$\delta^{15}N/\delta^{14}N$	St. Error
7/23/2019	100m	A	0.3	96.14	35.27	0.93	22.89	0.27	2.44	0.08	-26.74	0.03	5.53	0.03
7/23/2019	100m	A	0.5	82.27	23.60	0.49	9.47	0.25	1.42	0.03	-26.71	0.03	4.87	0.07
7/23/2019	100m	A	1.9	61.53	15.63	0.39	4.77	0.34	0.55	0.01	-27.01	0.02	3.80	0.12
7/23/2019	100m	A	2	58.16	18.75	0.87	3.70	0.18	0.55	0.01	-26.98	0.05	3.87	0.12
7/23/2019	100m	A	2.3	52.44	13.39	0.63	4.95	0.21	0.45	0.01	-27.00	0.06	3.59	0.09
7/23/2019	100m	A	2.5	51.53	17.16	0.10	4.88	NA	0.52	0.04	-27.08	NA	3.10	0.02
7/23/2019	100m	A	2.8	53.53	15.50	0.33	3.79	0.15	0.51	0.01	-26.96	0.04	3.92	0.03
7/23/2019	100m	A	3	51.96	15.47	0.37	2.83	0.18	0.43	0.00	-26.76	0.03	4.08	0.01
7/23/2019	100m	A	3.2	52.70	14.73	0.15	3.25	0.09	0.44	0.01	-26.93	0.02	3.88	0.12
7/23/2019	100m	A	3.5	50.73	15.82	0.54	3.42	0.10	0.48	0.01	-27.08	0.02	3.99	0.09
7/23/2019	100m	A	3.8	53.65	15.27	0.46	3.94	0.23	0.44	0.01	-26.89	0.09	3.81	0.02
7/23/2019	100m	A	4.3	53.10	14.84	0.28	3.71	0.20	0.48	0.02	-26.96	0.05	4.36	0.16
7/23/2019	100m	A	4.8	52.68	NA	NA	2.31	0.13	NA	NA	-27.04	0.08	NA	NA
7/23/2019	100m	A	5.2	51.49	14.29	0.18	3.69	0.12	0.45	0.02	-27.06	0.02	3.60	0.12
7/23/2019	100m	A	5.5	53.25	15.94	0.31	5.19	0.27	0.57	0.02	-27.07	0.04	4.04	0.05
7/23/2019	100m	A	5.9	54.10	16.63	0.86	4.86	0.16	0.51	0.01	-27.03	0.04	3.28	0.10
7/23/2019	100m	A	6.3	54.30	16.01	0.27	5.17	0.15	0.51	0.01	-27.06	0.08	3.02	0.17
7/23/2019	100m	A	6.7	57.08	18.26	0.51	5.48	0.10	0.59	0.02	-26.97	0.02	3.75	0.09
7/23/2019	100m	A	7	51.22	18.10	0.19	5.00	0.10	0.63	0.01	-27.09	0.01	3.84	0.07
7/23/2019	100m	A	8	56.55	16.19	0.38	5.43	0.56	0.55	0.01	-27.01	0.03	3.79	0.03
7/23/2019	100m	A	8.5	56.75	16.92	0.68	4.27	0.28	0.55	0.04	-27.09	0.05	3.69	0.01
7/23/2019	100m	A	8.8	57.78	16.84	0.28	5.53	0.06	0.56	0.01	-27.21	0.05	3.66	0.20
7/23/2019	100m	A	9.8	56.71	17.80	0.21	5.82	0.28	0.54	0.01	-27.20	0.02	3.64	0.10
7/23/2019	100m	A	10.5	59.22	20.73	0.15	5.66	0.12	0.63	0.01	-27.16	0.02	3.86	0.04
7/23/2019	100m	B	0.1	86.69	25.98	0.62	14.99	0.17	1.76	0.06	-26.74	0.02	5.25	0.03
7/23/2019	100m	B	0.2	82.71	22.53	1.66	11.49	0.24	1.54	0.12	-26.74	0.04	5.22	0.06
7/23/2019	100m	B	0.6	63.64	15.51	0.38	5.70	0.28	0.50	0.17	-26.65	0.03	4.64	0.03

7/23/2019	100m	B	0.8	57.31	16.72	0.18	4.33	0.20	0.54	0.02	-26.76	0.05	3.83	0.09
7/23/2019	100m	B	1	56.96	17.87	0.22	4.76	0.23	0.56	0.02	-26.92	0.01	3.89	0.07
7/23/2019	100m	B	1.3	54.40	14.93	0.91	3.36	0.19	0.45	0.02	-27.01	0.02	2.92	0.22
7/23/2019	100m	B	1.5	50.46	16.14	0.55	2.90	0.10	0.46	0.04	-26.73	0.06	3.02	0.14
7/23/2019	100m	B	1.9	49.62	13.47	0.11	3.14	0.07	0.40	0.01	-26.82	0.01	3.16	0.10
7/23/2019	100m	B	2.1	49.15	14.98	0.26	3.76	0.11	0.37	0.01	-26.91	0.03	3.00	0.04
7/23/2019	100m	B	2.2	49.61	15.80	0.40	3.64	0.13	0.42	0.00	-26.86	0.05	3.02	0.14
7/23/2019	100m	B	2.3	49.09	14.43	0.20	2.34	0.21	0.43	0.01	-26.96	0.04	3.64	0.21
7/23/2019	100m	B	2.7	51.92	15.04	0.44	3.42	0.16	0.46	0.02	-26.84	0.07	3.61	0.11
7/23/2019	100m	B	3	55.07	15.42	0.12	3.71	0.18	0.51	0.02	-26.91	0.00	3.65	0.15
7/23/2019	100m	B	3.5	53.27	15.63	0.60	4.69	0.26	0.48	0.02	-27.08	0.04	3.38	0.26
7/23/2019	100m	B	4	54.07	17.12	0.44	4.38	0.49	0.54	0.01	-26.91	0.03	3.57	0.05
7/23/2019	100m	B	4.4	54.98	16.73	0.31	5.26	0.16	0.57	0.01	-26.93	0.11	3.78	0.10
7/23/2019	100m	B	4.8	55.16	17.23	0.54	5.34	0.27	0.60	0.02	-26.94	0.02	3.05	0.09
7/23/2019	100m	B	5.3	56.05	19.42	0.29	6.14	0.44	0.60	0.01	-26.99	0.02	3.57	0.06
7/23/2019	100m	B	5.9	53.58	18.39	0.29	3.56	0.41	0.51	0.00	-27.12	0.00	3.58	0.04
7/23/2019	100m	B	6.6	57.27	19.16	0.37	6.10	0.40	0.51	0.01	-27.12	0.03	3.01	0.03

Appendix J: AW55 Sediment Porosity, Total Carbon, Total Nitrogen, and Total Phosphorus

Date Collected	Site	Core	Depth (cm)	# mussels	Porosity (%)	TC (mg/g)	St. Error	TN (mg/g)	St. Error	TP (mg/g)	St. Error
7/19/2018	AW55	1	0.3	7	74.06	26.64	0.94	0.79	0.026	0.33	0.005
7/19/2018	AW55	1	0.8	2	59.97	21.42	0.71	0.31	0.007	0.29	0.013
7/19/2018	AW55	1	1.4	0	46.58	22.65	0.42	0.28	0.002	0.28	0.005
7/19/2018	AW55	1	2	0	43.00	24.10	0.55	0.20	0.005	0.27	0.002
7/19/2018	AW55	1	2.8	0	39.61	23.45	0.36	0.15	0.006	0.32	0.009
7/19/2018	AW55	1	6.8	0	61.38	37.53	0.30	0.43	0.009	0.52	0.011
7/19/2018	AW55	1	8.8	0	69.82	53.22	0.17	0.74	0.009	0.51	0.003
7/19/2018	AW55	2	0.6	0	65.32	24.42	0.53	0.23	0.005	0.30	0.013
7/19/2018	AW55	2	0.7	1	51.23	21.34	0.35	0.32	0.010	0.26	0.005
7/19/2018	AW55	2	0.9	0	44.19	22.57	0.49	0.26	0.011	0.27	0.006
7/19/2018	AW55	2	1.5	0	43.58	20.54	0.24	0.22	0.002	0.29	0.008
7/19/2018	AW55	2	1.9	0	41.45	22.99	0.69	0.20	0.006	0.30	0.003
7/19/2018	AW55	2	2.9	0	38.46	25.81	0.41	0.16	0.002	0.33	0.008
7/19/2018	AW55	2	3.3	0	45.36	31.90	0.27	0.18	0.010	0.39	0.007
7/19/2018	AW55	2	3.9	0	48.22	29.66	0.55	0.24	0.004	0.45	0.009
7/19/2018	AW55	3	1	5	52.41	27.02	1.35	0.34	0.018	0.27	0.003
7/19/2018	AW55	3	1.2	1	43.90	23.18	0.80	0.23	0.012	0.29	0.004
7/19/2018	AW55	3	1.7	0	42.19	23.61	0.32	0.18	0.003	0.28	0.011
7/19/2018	AW55	3	2.2	0	38.04	23.10	0.89	0.18	0.006	0.31	NA
7/19/2018	AW55	3	2.7	0	38.55	28.27	0.79	0.15	0.001	0.32	0.007
7/19/2018	AW55	3	3.3	0	42.73	25.19	0.82	0.15	0.003	0.36	0.000
7/19/2018	AW55	3	3.5	0	44.52	28.01	0.03	0.19	0.005	0.38	0.009
7/19/2018	AW55	3	4.1	0	50.54	30.92	0.27	0.22	0.011	0.47	0.011
7/19/2018	AW55	3	4.3	0	62.60	34.01	0.32	0.43	0.006	0.62	0.003
7/19/2018	AW55	3	4.5	0	64.17	37.00	0.19	0.37	0.006	0.67	0.005
7/19/2018	AW55	4	0.2	4	59.17	17.39	0.54	0.44	0.011	0.22	0.001
7/19/2018	AW55	4	0.4	1	56.33	23.26	1.87	0.35	0.014	0.27	0.003

Date Collected	Site	Core	Depth (cm)	# mussels	Porosity (%)	TC (mg/g)	St. Error	TN (mg/g)	St. Error	TP (mg/g)	St. Error
7/19/2018	AW55	4	0.6	0	50.05	25.27	0.35	0.34	0.011	0.23	0.000
7/19/2018	AW55	4	0.8	0	49.48	22.98	0.63	0.24	0.008	0.26	0.005
7/19/2018	AW55	4	1	0	45.33	24.59	0.39	0.23	0.012	0.30	0.005
7/19/2018	AW55	4	1.2	0	43.29	24.02	0.42	0.26	0.013	0.31	0.008
7/19/2018	AW55	4	1.4	1	41.88	24.31	0.55	0.21	0.001	0.28	0.004
7/19/2018	AW55	4	1.7	0	43.49	24.40	0.42	0.20	0.007	0.27	0.005
7/19/2018	AW55	4	1.9	0	38.95	20.37	0.67	0.14	0.004	0.31	0.017
7/19/2018	AW55	4	2.1	0	38.66	25.65	0.44	0.12	0.002	0.30	0.013
7/19/2018	AW55	4	2.3	0	37.40	26.62	0.60	0.12	0.001	0.33	0.008
7/19/2018	AW55	4	2.7	0	39.10	30.09	0.06	0.15	0.000	0.33	0.006
7/19/2018	AW55	4	2.9	0	41.21	29.64	0.47	0.15	0.002	0.32	0.000
7/19/2018	AW55	4	3.3	0	51.29	30.74	0.55	0.25	0.011	0.46	0.009
7/19/2018	AW55	4	3.8	0	63.21	37.71	0.08	0.39	0.003	0.60	0.004
7/19/2018	AW55	4	4	0	62.25	39.94	0.16	0.38	0.003	0.66	0.010
7/19/2018	AW55	4	4.2	0	64.42	41.95	0.01	0.36	0.015	0.61	0.002
7/19/2018	AW55	4	5.2	0	66.41	43.43	0.05	0.47	0.011	0.60	0.002
7/19/2018	AW55	4	5.3	0	61.68	47.95	0.40	0.48	0.007	0.51	0.013
7/19/2018	AW55	4	5.5	0	65.47	36.12	0.19	0.37	0.001	0.53	0.008
7/19/2018	AW55	4	5.7	0	62.74	48.62	0.59	0.52	0.006	0.52	0.006
7/19/2018	AW55	4	6.2	0	59.92	50.56	0.40	0.47	0.005	0.46	0.000
7/19/2018	AW55	4	7.2	0	47.78	44.93	0.23	0.21	0.002	0.34	0.004
7/19/2018	AW55	5	0.1	0	57.22	16.59	0.75	0.40	0.019	0.23	0.010
7/19/2018	AW55	5	0.3	3	56.41	34.33	1.80	0.57	0.010	0.28	0.010
7/19/2018	AW55	5	0.5	0	55.29	28.00	0.63	0.45	0.018	0.29	0.001
7/19/2018	AW55	5	0.8	0	49.74	23.65	1.28	0.32	0.010	0.22	0.006
7/19/2018	AW55	5	1	0	44.92	24.92	0.95	0.31	0.008	0.27	0.008
7/19/2018	AW55	5	1.2	0	28.34	21.95	1.37	0.47	0.011	0.27	0.007
7/19/2018	AW55	5	1.4	0	41.79	24.94	0.45	0.24	0.001	0.33	NA
7/19/2018	AW55	5	1.7	0	41.87	21.29	0.15	0.18	0.005	0.30	0.005

Date Collected	Site	Core	Depth (cm)	# mussels	Porosity (%)	TC (mg/g)	St. Error	TN (mg/g)	St. Error	TP (mg/g)	St. Error
7/19/2018	AW55	5	1.9	0	40.09	22.96	0.33	0.17	0.001	0.29	0.002
7/19/2018	AW55	5	2.3	0	38.85	23.75	0.51	0.15	0.004	0.32	0.001
7/19/2018	AW55	5	2.7	0	60.67	27.77	0.40	0.13	0.005	0.32	0.000
7/19/2018	AW55	5	2.9	0	39.25	29.62	0.77	0.14	0.000	0.33	0.010
7/19/2018	AW55	5	3.4	0	46.49	32.47	0.85	0.15	0.007	0.35	0.005
7/19/2018	AW55	5	3.6	0	53.14	33.38	0.14	0.29	0.001	0.47	0.003
7/19/2018	AW55	5	3.8	0	61.34	40.31	0.31	0.39	0.005	0.54	0.010
7/19/2018	AW55	5	4	0	64.99	38.69	0.24	0.44	0.009	0.64	0.015
7/19/2018	AW55	5	4.2	0	65.21	40.16	0.43	0.44	0.005	0.58	0.004
7/19/2018	AW55	5	4.4	0	64.15	41.37	0.73	0.42	0.005	0.57	0.002
7/19/2018	AW55	5	4.9	0	63.14	42.70	0.16	0.39	0.003	0.56	0.007
7/19/2018	AW55	5	5.4	0	66.32	42.39	0.27	0.44	0.005	0.62	0.007
7/19/2018	AW55	5	5.9	0	65.75	41.39	0.14	0.50	0.003	0.60	0.003
7/19/2018	AW55	5	6.3	0	64.62	42.97	0.17	0.54	0.003	0.60	0.007
7/19/2018	AW55	5	6.9	0	67.76	43.76	0.40	0.55	0.006	0.65	NA
7/19/2018	AW55	5	7.4	0	65.69	45.20	0.18	0.52	0.009	0.61	0.007
7/19/2018	AW55	5	7.9	0	64.79	48.31	0.17	0.56	0.002	0.49	0.006
7/19/2018	AW55	5	8.4	0	65.27	49.86	0.11	0.65	0.004	0.51	0.002
7/19/2018	AW55	5	8.9	0	66.74	51.69	0.09	0.63	0.013	0.51	0.003
7/19/2018	AW55	5	9.4	0	67.42	51.50	0.52	0.69	0.008	0.51	0.006
7/19/2018	AW55	5	9.9	0	68.38	50.74	0.27	0.70	0.002	0.51	0.006
7/19/2018	AW55	5	13.1	0	37.62	28.83	0.26	0.13	0.005	0.32	0.003
7/19/2018	AW55	6	0.4	0	51.14	22.19	0.82	0.39	0.011	0.25	0.001
7/19/2018	AW55	6	0.9	1	45.58	22.98	1.26	0.24	0.012	0.29	0.007
7/19/2018	AW55	6	1.1	0	42.28	23.90	0.59	0.18	0.005	0.30	0.005
7/19/2018	AW55	6	1.3	0	40.99	25.84	0.30	0.16	0.000	0.30	0.004
7/19/2018	AW55	6	1.5	0	37.31	26.67	0.58	0.18	0.013	0.31	0.003
7/19/2018	AW55	6	1.9	0	59.23	28.56	0.68	0.14	0.004	0.32	0.004
7/19/2018	AW55	6	2.1	0	52.31	44.80	0.61	0.29	0.005	0.37	0.005

Date Collected	Site	Core	Depth (cm)	# mussels	Porosity (%)	TC (mg/g)	St. Error	TN (mg/g)	St. Error	TP (mg/g)	St. Error
7/19/2018	AW55	6	3.1	0	49.67	30.97	0.60	0.19	0.005	0.40	0.002
7/19/2018	AW55	6	3.3	0	64.70	40.50	0.42	0.41	0.008	0.64	0.001
7/19/2018	AW55	6	3.9	0	63.00	40.93	0.15	0.35	0.004	0.61	0.008
7/19/2018	AW55	6	4.1	0	62.73	40.26	0.13	0.44	0.009	0.61	0.003

Appendix K: Phosphorus Binding Fractions within the Sediment

Date Collected	Site	Core	Depth	TP (mg/g)	St. Error	IP (mg/g)	St. Error	OP (mg/g)	St. Error	NAIP (mg/g)	St. Error	AP (mg/g)	St. Error
7/23/2018	100m	A	0.3	0.630	0.012	0.373	0.005	0.242	0.002	0.093	0.006	0.234	0.001
7/23/2018	100m	A	0.5	0.381	0.003	0.217	0.003	0.140	0.001	0.049	0.001	0.144	0.005
7/23/2018	100m	A	1.9	0.261	0.001	0.200	0.003	0.075	0.002	0.028	0.001	0.121	0.002
7/23/2018	100m	A	2	0.318	0.009	0.171	0.003	0.077	0.001	0.038	0.001	0.136	0.003
7/23/2018	100m	A	2.3	0.288	0.008	0.195	0.002	0.069	0.001	0.040	0.000	0.137	0.001
7/23/2018	100m	A	2.5	0.297	0.005	0.213	0.002	0.070	0.000	0.031	0.000	0.153	0.008
7/23/2018	100m	A	2.8	0.334	0.002	0.203	0.003	0.079	0.001	0.039	0.000	0.149	0.003
7/23/2018	100m	A	3	0.305	0.015	0.189	0.003	0.071	0.000	0.035	0.000	0.155	0.002
7/23/2018	100m	A	3.2	0.305	0.006	0.206	0.004	0.074	0.001	0.032	0.000	0.166	0.006
7/23/2018	100m	A	3.5	0.290	0.003	0.205	0.007	0.064	0.000	0.032	0.000	0.155	0.003
7/23/2018	100m	A	3.8	0.352	0.006	0.218	0.004	0.081	0.001	0.038	0.001	0.166	0.006
7/23/2018	100m	A	4.3	0.337	0.006	0.247	0.004	0.075	0.001	0.040	0.002	0.159	0.001
7/23/2018	100m	A	4.8	0.311	0.007	0.205	0.001	0.075	0.001	0.036	0.001	0.162	0.004
7/23/2018	100m	A	5.2	0.365	0.003	0.247	0.006	0.086	0.001	0.069	0.001	0.173	0.006
7/23/2018	100m	A	5.5	0.436	0.010	0.356	0.012	0.088	0.003	0.098	0.001	0.202	0.008
7/23/2018	100m	A	5.9	0.566	0.016	0.403	0.007	0.078	0.001	0.136	0.001	0.221	0.004
7/23/2018	100m	A	6.3	0.735	0.032	0.620	0.001	0.089	0.002	0.216	0.007	0.293	0.010
7/23/2018	100m	A	6.7	0.907	0.021	0.757	0.012	0.108	0.002	0.338	0.006	0.369	0.008
7/23/2018	100m	A	7	0.875	0.024	0.750	0.014	0.103	0.001	0.352	0.003	0.369	0.005
7/23/2018	100m	A	8	0.583	0.000	0.466	0.012	0.094	0.005	0.145	NA	0.251	0.004
7/23/2018	100m	A	8.5	0.314	0.007	0.223	0.005	0.073	0.001	0.030	0.001	0.170	0.004
7/23/2018	100m	A	8.8	0.315	0.007	0.201	0.004	0.078	0.000	0.019	0.000	0.177	0.002
7/23/2018	100m	A	9.8	0.299	0.005	0.217	0.004	0.068	0.000	0.015	0.001	0.176	0.005
7/23/2018	100m	A	10.5	0.318	0.002	0.245	0.009	0.072	0.001	0.017	0.000	0.181	0.001
7/23/2018	100m	B	0.1	0.560	0.002	0.276	0.004	0.193	0.001	0.079	0.001	0.176	0.003
7/23/2018	100m	B	0.2	0.510	0.012	0.239	0.003	0.166	0.001	0.102	0.005	0.174	0.003

Date Collected	Site	Core	Depth	TP (mg/g)	St. Error	IP (mg/g)	St. Error	OP (mg/g)	St. Error	NAIP (mg/g)	St. Error	AP (mg/g)	St. Error
7/23/2018	100m	B	0.6	0.274	0.004	0.174	0.009	0.078	0.005	0.034	0.001	0.107	0.001
7/23/2018	100m	B	0.8	0.280	0.008	0.181	0.002	0.073	0.000	0.028	0.000	0.143	0.001
7/23/2018	100m	B	1	0.290	0.002	NA	NA	NA	NA	0.038	0.000	0.147	0.004
7/23/2018	100m	B	1.3	0.295	0.002	0.171	0.002	0.074	0.000	0.024	0.000	0.144	0.005
7/23/2018	100m	B	1.5	0.255	0.006	0.171	0.001	0.068	0.002	0.022	0.000	0.155	0.006
7/23/2018	100m	B	1.9	0.249	0.001	0.186	0.004	0.071	0.001	0.030	0.001	0.148	0.007
7/23/2018	100m	B	2.1	0.263	0.005	0.205	0.009	0.064	0.002	0.022	0.001	0.166	0.003
7/23/2018	100m	B	2.2	0.282	0.005	0.208	0.004	0.067	0.000	0.022	0.001	0.161	0.001
7/23/2018	100m	B	2.3	0.254	0.007	0.190	0.003	0.069	0.000	0.032	0.000	0.165	0.006
7/23/2018	100m	B	2.7	0.289	0.007	0.200	0.004	0.074	0.002	0.035	0.001	0.168	0.006
7/23/2018	100m	B	3	0.337	0.007	0.218	0.005	0.090	0.003	0.041	0.000	0.195	0.000
7/23/2018	100m	B	3.5	0.327	0.006	0.234	0.005	0.084	0.003	0.027	0.001	0.193	NA
7/23/2018	100m	B	4	0.334	0.011	0.227	0.002	0.091	0.002	0.043	0.000	0.188	0.002
7/23/2018	100m	B	4.4	0.702	0.018	0.594	0.003	0.101	0.001	0.299	0.010	0.271	0.006
7/23/2018	100m	B	4.8	0.911	0.018	0.709	0.035	0.101	0.002	0.326	0.004	0.381	0.004
7/23/2018	100m	B	5.3	0.497	0.004	0.425	0.010	0.091	0.002	0.172	0.006	0.278	0.004
7/23/2018	100m	B	5.9	0.311	0.009	0.192	0.005	0.072	0.001	0.021	0.000	0.191	0.001
7/23/2018	100m	B	6.6	0.293	0.007	0.207	0.004	0.068	0.001	0.016	0.000	0.196	0.003
7/19/2018	AW55	5	0.1	0.234	0.010	0.165	NA	0.071	0.003	0.032	0.001	0.126	0.008
7/19/2018	AW55	5	0.3	0.275	0.010	0.210	0.008	0.052	0.001	0.040	0.001	0.161	0.001
7/19/2018	AW55	5	0.5	0.292	0.001	0.219	0.002	0.074	0.000	0.026	0.001	0.186	0.003
7/19/2018	AW55	5	0.8	0.224	0.006	0.184	0.003	0.058	0.001	0.019	0.000	0.162	0.006
7/19/2018	AW55	5	1.7	0.304	0.005	0.253	0.002	0.045	0.001	0.027	0.001	0.214	0.005
7/19/2018	AW55	5	2.3	0.319	0.001	0.267	0.011	0.042	0.001	0.017	0.001	0.229	0.004
7/19/2018	AW55	5	2.9	0.334	0.010	0.295	0.005	0.046	0.000	0.019	0.000	0.268	0.005
7/19/2018	AW55	5	3.4	0.351	0.005	0.329	0.011	0.057	0.002	0.023	0.000	0.292	0.005
7/19/2018	AW55	5	3.8	0.536	0.010	0.465	0.006	0.075	0.001	0.056	0.001	0.388	0.007
7/19/2018	AW55	5	5.9	0.596	0.003	0.486	0.006	0.089	0.001	0.042	0.000	0.428	0.004
7/19/2018	AW55	5	6.3	0.599	0.007	0.474	0.005	0.125	0.001	0.032	0.001	0.428	0.003

Date Collected	Site	Core	Depth	TP (mg/g)	St. Error	IP (mg/g)	St. Error	OP (mg/g)	St. Error	NAIP (mg/g)	St. Error	AP (mg/g)	St. Error
7/19/2018	AW55	5	8.4	0.507	0.002	0.417	0.004	0.100	0.002	0.013	0.000	0.405	0.001
7/19/2018	AW55	5	8.9	0.508	0.003	0.428	0.001	0.093	0.000	0.015	0.000	0.414	0.013